OCRWM	MODEL COVER SHEET	1. QA: QA Page 1 of 152

2. Type of Mathematical Model

☐ Process Model ☒ Abstraction Model ☐ System Model

Describe Intended Use of Model

The purpose of this Model Report is to document the abstraction model being used in Total System Performance Assessment (TSPA) model calculations for radionuclide transport in the unsaturated zone (UZ).

3. Title

Particle Tracking Model and Abstraction of Transport Processes

4. DI (Including Rev. No. and Change No., if applicable):

MDL-NBS-HS-000020 REV00

5. Total Attachments	6. Attachment Numbers - No. of Pages in Each
3	I-10, II-8, III-16

	Printed Name	Signature	Date
7. Originator	B.A. Robinson		01/15/2004
8. CSO	V. Palciauskas		1/15/2004
9. Checker	L. Pan		1/15/2004
10. GER	K. McFall		1/16/2004
11. Responsible Manager/Lead	J.S.Y. Wang/J.E. Houseworth		1/16/2004 1/16/2004
12. Responsible Manager	P. Dixon		1-16-04

13. Remarks

Block 7. Additional contributor is C. Li.

Technical Error Report (TER) log number addressed in this Model Report:
TER-02-0058 (Currently known as Condition Report CR-153)

OFFICE OF CIVILIAN RADIOACTIVE WASTE MANAGEMENT
MODEL REVISION RECORD

2. Model Title:
Particle Tracking Model and Abstraction of Transport Processes

3. DI (including Rev. No. and Change No., if applicable):
MDL-NBS-HS-000020 REV00

4. Revision/Change No.	5. Description of Revision/Change
	This report is a revision of an Analysis/Model Report by the same title--Document Identifier ANL-NBS-HS-000026 Rev. 00 (CRWMS M&O 2000 [141418]). This revision includes the Model Validation, Section 7.
Rev. 00	In this new model report, the entire documentation was revised. Side bars are not used because the changes were too extensive to use Step 5.8d)1) per AP-SIII.10Q Rev. 2/ICN 1.

CONTENTS

Page

CONTENTS (Continued)

CONTENTS (Continued)

Page

INTENTIONALLY LEFT BLANK

FIGURES

Page

FIGURES (CONTINUED)

Page

TABLES

Page

INTENTIONALLY LEFT BLANK

ACRONYMS AND ABBREVIATIONS

1-D	one-dimensional
2-D	two-dimensional
3-D	three-dimensional
ACM	Alternative Conceptual Model
AD	advection-dispersion
AMR	analysis/model report
AFM	Active Fracture Model
CH	Calico Hills
CHn	Calico Hills nonwelded units
CHv	Calico Hills vitric units
CHz	Calico Hills zeolitic units
CRWMS M&O	Civilian Radioactive Waste Management System Management and Operating Contractor
DCPT	Dual Continuum Particle Tracking Computer Code
DIRS	Document Input Reference System
DFM	Discrete Fracture Model
dll	dynamic link library
DTN	data tracking number
Dual-K	dual permeability
EBS	engineered barrier system
FEHM	Finite Element Heat and Mass Model
FEP	feature, event, and process
f/m	fracture/matrix
LA	License Application
MINC	matrix-fracture system - multiple interactive continua
NRC	U.S. Nuclear Regulatory Commission
NSP	Nevada State Plane
OCRWM	Office of Civilian Radioactive Waste Management
PA	performance assessment
PTn	Paintbrush Tuff nonwelded
RTTF	Residence Time Transfer Function
SMT	Smeared-source, mountain-scale thermal model (part of Multiscale model)
SR	Site Recommendation
STN	software tracking number
SZ	saturated zone

ACRONYMS AND ABBREVIATIONS (Continued)

T2R3D	Transport version of TOUGH2 family of codes
TDMS	Technical Data Management System
TH	Thermal-Hydrological
THC	Thermal-Hydrological-Chemical
THM	Thermal-Hydrological-Mechanical
TSPA	Total System Performance Assessment
TSw	Topopah Spring welded units
TWP	technical work plan
UTM	Universal Transverse Mercator (map type)
UZ	unsaturated zone
V&V	verification and validation
WP	Work Package
YMRP	*Yucca Mountain Review Plan*

1. PURPOSE

The purpose of this Model Report is to document the abstraction model being used in Total System Performance Assessment (TSPA) model calculations for radionuclide transport in the unsaturated zone (UZ). The particle-tracking method of simulating radionuclide transport is incorporated into the Finite Element Heat and Mass Model (FEHM) computer code. This Model Report outlines the assumptions, design, and testing of a model for calculating radionuclide transport in the UZ at Yucca Mountain. In addition, methods for determining and inputting transport parameters are outlined for use in the TSPA analyses. Concurrently, process-level flow model calculations are being documented in another Analysis Model Report (AMR) for the UZ (BSC 2003 [163228]). Three-dimensional (3-D), dual-permeability flow fields generated to characterize UZ flow (documented in BSC 2003 [163045]; DTN: LB03023DSSCP9I.001 [163044]) are converted to make them compatible with the FEHM code, which in this abstraction model is used to simulate radionuclide transport using a particle-tracking method that is described in this report. This Model Report establishes the numerical method and demonstrates the use of the model that is intended to represent UZ transport in the TSPA. Capability of the UZ barrier for retarding the transport is demonstrated in this Model Report, and by the underlying process model (BSC 2003 [163228]).

This Model Report is a revision of an AMR. The original work was documented as a scientific analysis (ANL-NBS-HS-000026 REV00, CRWMS M&O 2000 [141418]), whereas the current report is a Model Report (MDL-NBS-HS-000020 REV00). The technical scope, content, and management of this Model Report are described in the planning document *Technical Work Plan (TWP) for: Performance Assessment Unsaturated Zone* (BSC 2002 [160819], Section 1.11, Work Package (WP) AUZM07). Deviations from the TWP are noted within the text of this Model Report, as appropriate.

Note that Section 7.3.3 provides information used to formulate the technical justification the abstraction model properly implements the active fracture model with matrix diffusion.

The particle-tracking technique presented in this Model Report, called the Residence Time Transfer Function (RTTF) particle-tracking technique, uses a cell-based approach that sends particles from node to node on a finite difference or finite element grid, after keeping each particle at the cell for a prescribed period of time. To incorporate transport mechanisms such as dispersion and matrix diffusion, the residence time of a particle at a cell is computed using a transfer function that ensures that the correct distribution of residence times at the cell is reproduced. This procedure is computationally very efficient, enabling large-scale transport simulations of several million particles to be completed rapidly on modern workstations. This requirement was needed for complex, 3-D simulation involving the simulation of multiple radionuclides. Furthermore, since the cell-based approach uses directly mass flow rate information generated from a numerical fluid flow solution, complex, unstructured computational grids and the dual-permeability flow model formulation pose no additional complications. For the present application, the technique was adapted for use in unsaturated, dual-permeability transport simulations. For such systems, numerical techniques are required to allow accurate simulation of dual-permeability systems in which there is a vast disparity in the travel times depending on whether the transport is in the fractures or the matrix. This Model Report outlines the approach and defines the proper use of that approach. Furthermore, colloid-

facilitated radionuclide transport can be simulated, and complex source terms and decay chain/ingrowth capabilities have been included in the model.

Like all numerical methods, the particle-tracking technique has limitations that must be considered when deciding whether its use is appropriate for a given application. The key physical and chemical assumptions are advection-dominated transport and linear, equilibrium sorption. Also, the accuracy of the method for dual-permeability flow systems was investigated in detail by performing comparisons to analytical solutions and alternate numerical methods, including the UZ transport process models documented in BSC 2003 [163228] and BSC 2003 [163045] and testing of the FEHM code presented in the software documentation (FEHM V2.21, LANL 2003 [166306]). Given these results, this Model Report demonstrates that the particle-tracking model can be used in 3-D radionuclide transport simulations of the Yucca Mountain UZ as long as the limits on the model are recognized and parameters and inputs are chosen accordingly. Discussion of the limits and applicability are provided in this Model Report. Inputs used in the calculations presented are believed to be representative of those to be used in TSPA model calculations, but this contention must be verified explicitly when the actual parameters to be used in TSPA multiple realization simulations become available.

2. QUALITY ASSURANCE

Development of this Model Report and the supporting modeling activities have been determined to be subject to the Office of Civilian Radioactive Waste Management's (OCRWM) quality assurance program as indicated in *Technical Work Plan for: Performance Assessment Unsaturated Zone*, TWP-NBS-HS-000003 REV 02 (BSC 2002 [160819], Section 8.2, WP AUZM07). Approved quality assurance procedures identified in the TWP (BSC 2002 [160819], Section 4) have been used to conduct and document the activities described in this Model Report. The TWP also identifies the methods used to control the electronic management of data (BSC 2002 [160819], Section 8.4, WP AUZM07) during the modeling and documentation activities.

This Model Report discusses ambient radionuclide transport through hydrogeologic units below the repository, which constitute a natural barrier that is classified in the *Q-List* (BSC 2003 [165179]) as "Safety Category" because it is important to waste isolation, as defined in AP-2.22Q, *Classification Analyses and Maintenance of the Q-List*. The results of this report are important to the demonstration of compliance with the postclosure performance objectives prescribed in 10 CFR 63.113 [156671]. The report contributes to the analysis data used to support performance assessment (PA); the conclusions do not directly impact engineered features important to preclosure safety, as defined in AP-2.22Q.

INTENTIONALLY LEFT BLANK

3. USE OF SOFTWARE

3.1 SOFTWARE TRACKED BY CONFIGURATION MANAGEMENT

The computer codes used directly in this modeling activity are summarized in Table 3-1. The computer software code on which the UZ transport abstraction model is based is FEHM V2.21, (LANL 2003 [165741]). The qualification status of this and other software is indicated in the electronic Document Input Reference System (DIRS) database. All software was obtained from Software Configuration Management and is appropriate for the application. Qualified codes were used only within the range of validation as required by AP-SI.1Q, *Software Management*. Input and output files for this Model Report are located in data tracking numbers (DTN) and identified in the respective discussions in Section 6; the outputs are listed in Section 8.2.

Table 3-1. Qualified Software Used in this Report

Software Title/Version (v)	Software Tracking Number (STN)	Code Usage	DIRS
FEHM V2.21	10086-2.21-00	Generation of transfer function curve information using a discrete fracture model. Simulation of particle tracking validation runs Abstraction model simulations	165741
GoldSim V7.50.100	10344-7.50.100-00	Abstraction model simulations	161572
ppptrk V1.0	11030-1.0-00	Post-processing of particle breakthrough curve information	165753
discrete_tf V1.1	11033-1.1-00	Post-processing of discrete fracture model results to convert results to transfer functions	165742
fehm2post V1.0	11031-1.0-00	Executes multiple FEHM simulations along with pre- and post-processing runs. Used to execute the individual simulations and generation of transfer function curves used in the TSPA UZ transport abstraction model.	165754

3.2 EXEMPT SOFTWARE

Commercial, off-the-shelf software used in support of this Model Report is listed in Table 3-2. This software is exempt from the requirements of AP-SI.1Q.

Table 3-2. Exempt Software

Software Name and Version (V)	Software Tracking Number (STN)	Description	Computer and Platform Identification
Fortner Plot	N/A	The commercial software, Fortner Plot, was used for plotting the results of breakthrough curve simulations. Only built-in standard functions in this software were used. No software routines or macros were used with this software to prepare this report. The output was visually checked for correctness.	SUN Workstation
Microsoft Excel	N/A	This standard spreadsheet package is used to perform simple spreadsheet calculations using built-in formulas and functions.	IBM PC, Window 2000 operating system

4. INPUTS

4.1 DIRECT INPUT

Data and parameters used in this Model Report as model inputs include:

- Numerical Grid for the UZ transport model
- UZ flow field for the prevailing climate
- UZ rock properties
  - Porosity
  - Fracture spacing and aperture
  - Active Fracture Model (AFM) parameter γ
  - Fracture residual saturation
  - Rock density
- UZ radionuclide transport parameters
  - Matrix diffusion coefficient
  - Radionuclide matrix adsorption coefficient
  - Colloid size distribution
  - Colloid size exclusion factor at fracture-matrix interface
  - Colloid filtration factor at Matrix Interface
  - Colloid concentration
  - Radionuclide adsorption coefficient k_d onto colloid
  - Colloid retardation factor
- Repository location

4.1.1 Data

The following data are used as inputs to FEHM for constructing the UZ transport model.

Table 4-1. Input Data

Data Name	Data Source	DTN
UZ flow model grid and nine base case flow fields. preqlA.ini, preqmA.ini, prequA.ini, monqla.ini, monqmA.ini, monqua.ini, glaqlA.ini, glaqmA.ini, glaquA.ini, fehmn.grid, and fehmn.stor	Lawrence Berkeley National Laboratory site scale flow models	LB0305TSPA18FF.001 [165625]
Repository release bin location	NEVADA_SMT_percolation_BIN_ma. txt, which contains repository node location of the thermal model	LL030610323122.029 [164513]
TOUGH2 element data	BSC 2003 [163045] *UZ Flow Models and Submodels* (MDL-NBS-HS-000006 REV01)	LB03023DSSCP9I.001 [163044]
Water saturation and permeability	BSC 2003 [163045] *UZ Flow Models and Submodels* (MDL-NBS-HS-000006 REV01)	LB03023DSSCP9I.001 [163044]

In TSPA simulations, flow fields are pre-generated and saved for use in the UZ transport abstraction model to be used in TSPA analyses. At run time, FEHM reads in the pre-generated flow fields and uses them in transport simulations. The UZ flow model grid and flow field for the prevailing climate are used in this Model Report as input to FEHM to illustrate the set-up of UZ transport model. The effects of flow field uncertainty on TSPA are investigated through multiple realizations with different climate scenarios and corresponding flow fields.

Repository location data are used to select repository nodes in the 3-D site scale model for releasing radionuclides into the UZ. There is no uncertainty related to this data.

T2R3D 3-D site-scale transport results, developed using the dual-permeability (dual-k) model, are used for benchmarking for comparison with FEHM results. Uncertainty associated with those results is described in BSC (2003 [163228]).

4.1.2 Parameters and Parameter Uncertainty

The following parameters are inputs to the FEHM UZ transport model. The values of those parameters affect the strength of the transport mechanism those parameters are related to. The values of all the parameters vary from layer to layer, as do the distributions. More detailed information regarding parameter value and discussion of uncertainty can be found in Section 6 where those parameters are discussed.

Table 4-2. Input Parameters

Parameter Name (Section discussed)	Parameter Source	DTN	Parameter Value(s)	Units	Distribution (or single value if fixed)
Fracture dispersivity Section 6.5.2	BSC 2003 [162415] *Saturated Zone In-Situ Testing* (ANL-NBS-HS-000039 REV 00)	(Table 6.3-10 of BSC 2003 [162415])	10	m	Fixed value
Matrix porosity Section 6.5.3	BSC 2003 [160240] *Calibrated Properties Model* (MDL-NBS-HS-000003 REV01)	LB0305TSPA18FF.001 [165625]	Varies from layer to layer	None	Fixed
Rock density Section 6.5.3	BSC 2003 [161773] *Analysis of Hydrologic Properties Data* (MDL-NBS-HS-000014 REV00)	LB0210THRMLPRP.001 [160799]	Varies from layer to layer	kg/m^3	Single value
Fracture porosity Section 6.5.7	BSC 2003 [161773] *Analysis of Hydrologic Properties Data* (MDL-NBS-HS-000014 REV00)	LB0205REVUZPRP.001 [159525] LB0207REVUZPRP.001 [159526]	Varies from layer to layer	None	α distribution. Layers are grouped together based on similar rock properties
Fracture frequency Section 6.5.7	BSC 2003 [161773] *Analysis of Hydrologic Properties Data* (MDL-NBS-HS-000014 REV00)	LB0205REVUZPRP.001 [159525] LB0207REVUZPRP.001 [159526]	Varies from layer to layer	1/m	Log-normal distribution
Active fracture model parameters Section 6.5.6	BSC 2003 [163045] *UZ Flow Models and Submodels* (MDL-NBS-HS-000006 REV01)	LB0305TSPA18FF.001 [165625]	Varies from layer to layer and with infiltration scenario.	None	Fixed value for a specific infiltration
Fracture residual saturation Section 6.5.6	BSC 2003 [160240] *Calibrated Properties Model* (MDL-NBS-HS-000003 REV01)	LB0302UZDSCPUI.002 [161787]	0.01	None	Fixed
Fracture spacing and aperture Section 6.5.7	BSC 2003 [161773] *Analysis of Hydrologic Properties Data* (MDL-NBS-HS-000014 REV00)	LB0205REVUZPRP.001 [159525] LB0207REVUZPRP.001 [159526]	Varies from layer to layer	m	Layers with similar rock properties are grouped together and the parameters are sampled
Colloid concentration distribution Section 6.5.12	BSC 2003 [161620] *Waste Form and Indrift Colloids-Associated Radionuclide Concentrations: Abstract and Summary* (MDL-EBS-PA-000004 REV 00)	SN0306T0504103.005 [164132]	Concentration will be sampled based on the given distribution	mg/l	Cumulative distribution
Radionuclide adsorption coefficient onto colloid Section 6.5.12	BSC 2003 [161620] *Waste Form and Indrift Colloids-Associated Radionuclide Concentrations: Abstract and Summary* (MDL-EBS-PA-000004 REV 00)	SN0306T0504103.006 [164131]	Values will be sampled based on the given distribution	ml/g	Uniform distribution parameter range depends on the type of radionuclides

Table 4-2. Input Parameters (Continued)

Parameter Name	Parameter Source	DTN	Parameter Value(s)	Units	Distribution (or single value if fixed)
Colloid size distribution Section 6.5.11	CRWMS M&O 2000 [148384] *Total System Performance Assessment Model for Site Recommendation.* (MDL-WIS-PA-000002 REV 00)	LL000122051021.116 [142973]	Parameter values are sampled at run time	None	Cumulative distribution
Colloid filtration factors Section 6.5.9	CRWMS M&O 2000 [148384] *Total System Performance Assessment Model for Site Recommendation.* (MDL-WIS-PA-000002 REV 00)	LA0003MCG12213.002 [147285]	Probability of a particle being filtered at matrix interface. Varies from layer to layer	None	Fixed values but varies with layers
Colloid size exclusion factors Section 6.5.10	CRWMS M&O 2000 [148384] *Total System Performance Assessment Model for Site Recommendation.* (MDL-WIS-PA-000002 REV 00)	LA0003MCG12213.002 [147285]	Probability of a colloid being excluded at fracture-matrix interface. Varies from layer to layer	None	Fixed values but vary from layer to layer
Fractions of colloid traveling unretarded Section 6.5.13	BSC 2003 [162729] *Saturated Zone Colloid Transport* (ANL-NBS-HS-000031 REV 01)	LA0303HV831352.003 [165624]	Varies with travel time	None	Fractions of colloids traveling unretarded are given.
Colloid retardation factor Section 6.5.13	BSC 2003 [162729] *Saturated Zone Colloid Transport* (ANL-NBS-HS-000031 REV 01)	LA0303HV831352.002 [163558]	Sampled statistical values	None	Cumulative distribution
Matrix diffusion coefficient Section 6.5.5	BSC 2003 [164889] *Drift-Scale Radionuclide Transport* (MDL-NBS-HS-000016 REV00)	LB03023DSSCP9I.001 [163044] LA0003JC831362.001 [149557]	Sampled parameter values	m^2/s	Layers are grouped together based on similar rock properties and parameters are sampled for estimating matrix diffusion coefficient
Matrix adsorption coefficient Section 6.5.4	BSC 2003 [163228] *Radionuclide Transport Models Under Ambient Conditions* (MDL-NBS-HS-000008 REV 01)	LA0302AM831341.002 [162575]	Parameter values are sampled based on the given distribution	mL/g	Distributions defined in DTN by rock type and radionuclide

Rock properties (rock density, fracture porosity, spacing, aperture, AFM parameter γ, and fracture residual saturation) are used as inputs to the FEHM UZ transport model. The validity and uncertainty of those parameters are documented in the corresponding Model Reports (*Analysis of Hydrologic Properties Data* (BSC 2003 [161773]), *Calibrated Properties Model* (BSC 2003 [160240]), and *UZ Flow Models and Submodels* (BSC 2003 [163045])). In this Model Report, we use the mean values of those parameters to demonstrate the abstraction of the UZ transport model. The influence of parameter uncertainty on system performance will be studied in TSPA multiple realization runs.

Radionuclide transport properties are used in FEHM for simulating the transport processes of radionuclides in the unsaturated fracture media from repository downward to the water table.

Colloid size distribution, concentration, adsorption coefficient, size exclusion, filtration factors, and retardation factors are input parameters to FEHM for simulating colloid-facilitated radionuclide transport in fractured media. Those data are functions of colloid and rock properties and vary from layer to layer.

The uncertainty and validity of each parameter are addressed in the corresponding documents listed in the parameter source column in Table 4.2 and are also discussed in the various subsections of Section 6.5 of this Model Report as indicated in the parameter name column of Table 4-2.

4.2 CRITERIA

Technical requirements to be satisfied by PA are based on 10 CFR 63.114 [156671] and identified in the Yucca Mountain *Project Requirements Document* (Canori and Leitner 2003 [161770]). The acceptance criteria that will be used by the U.S. Nuclear Regulatory Commission (NRC) to determine whether the technical requirements have been met are identified in the *Yucca Mountain Review Plan* (YMRP), *Final Report* (NRC 2003 [163274]). The pertinent requirements and acceptance criteria for this Model Report are summarized in Table 4-3.

Table 4-3. Project Requirements and *Yucca Mountain Review Plan, Final Report* Acceptance Criteria Applicable to This Model Report

Requirement Number[a]	Requirement Title[a]	10 CFR 63 Link	*Yucca Mountain Review Plan, Final Report* Acceptance Criteria
PRD-002/T-015	Requirements for Performance Assessment	10 CFR 63.114(a-c) [156671]	Criteria 1 to 5 for *Radionuclide Transport in the Unsaturated Zone*[b]
PRD-002/T-016	Requirements for Multiple Barriers	10 CFR 63.115(b) [156671]	Criteria 1 to 3 for *System Description and Demonstration of Multiple Barriers*[c]

NOTES: [a] from Canori and Leitner 2003 [161770]
[b] from NRC 2003 [163274], Section 2.2.1.3.7.3
[c] from NRC 2003 [163274], Section 2.2.1.1.3

The acceptance criteria identified in Sections 2.2.1.3.7.3 and 2.2.1.1.3 of the *Yucca Mountain Review Plan*, *Final Report* (NRC 2003 [163274]) are given below, followed by a short description of their applicability to this Model Report:

Acceptance Criteria for: *Radionuclide Transport in the Unsaturated Zone* (NRC 2003 [163274], Section 2.2.1.3.7.3)

- Acceptance Criterion 1, System Description and Model Integration are Adequate:

  TSPA adequately incorporates important physical phenomena and uses consistent and appropriate assumptions throughout the Radionuclide Transport in the UZ process-level model, (Section 6.3).

The description of aspects of hydrology, geology, and physical phenomena, and couplings, that may affect radionuclide transport in the unsaturated zone, is adequate, (Sections 6.3 and 6.4).

The abstraction of radionuclide transport in the unsaturated zone uses assumption, technical bases, data, and models that are appropriate and consistent with other related U.S. Department of Energy abstractions (Sections 5, 6.2, 6.3, 6.4, and 6.5).

Boundary and initial conditions used in the abstraction of radionuclide transport in the unsaturated zone are propagated throughout its abstraction approaches.

Sufficient data and technical bases for the inclusion of features, events, and processes, related to radionuclide transport in the unsaturated zone in the total system performance assessment abstraction, are provided in Section 6.2.

- Acceptance Criterion 2: Data are Sufficient for Model Justification:

  Geological, hydrological and geochemical values used in the license application are adequately justified. Adequate descriptions of how the data were used, interpreted, and appropriately synthesized into the parameters are provided, (Section 6.4).

  Sufficient data have been collected to establish initial and boundary conditions for the process-level model of Radionuclide Transport in the UZ, (Section 6.5).

- Acceptance Criterion 3: Data Uncertainty is Characterized and Propagated Through the Model Abstraction:

  Models use parameter values, assumed ranges, probability distributions, and/or bounding assumptions that are technically defensible and reasonably account for uncertainties and variabilities Section 6.5 documents the distributions and uncertainties of model parameters important for performance assessment.

- Acceptance Criterion 4, Model Uncertainty is Characterized and Propagated Through the Model Abstraction:

  Alternative modeling approaches are considered, consistent with available data and current scientific understanding, (Sections 6.6 and 6.7).

  Conceptual model uncertainties are adequately defined and documented, (Sections 6.7 and 7.1).

  Appropriate alternative modeling approaches are consistent with available data and current scientific knowledge, and appropriately consider the results and limitations, using tests and analyses that are sensitive to the processes modeled. For example, for radionuclide transport through fractures, the U.S. Department of Energy adequately considers alternative modeling approaches to develop its understanding of fracture distribution and ranges of fracture flow and transport properties in the UZ (Sections 6.6, 6.7, and 7.1).

- Acceptance Criterion 5, Model Abstraction Output is Supported by Objective Comparisons:

  The abstraction methods proposed for implementation in the TSPA-License Application (LA) are based on and consistent with output from detailed process level models, (Sections 6.4, 6.5, 7.1, 7.2, and 7.3).

  Well-documented procedures that have been accepted by the scientific community to construct and test the mathematical and numerical models are used to simulate Radionuclide Transport through the UZ, (Sections 6.1, 6.2, 6.3, 6.4, and 6.6).

  Sensitivity or bounding analyses are provided, (Sections 7.1 and 8.2).

Acceptance Criteria for: *System Description and Demonstration of Multiple Barriers*, (NRC 2003 [163274], Section 2.2.1.1.3).

- Acceptance Criterion 1, Identification of Barriers is Adequate:

  The unsaturated zone below the repository is a natural barrier important to waste isolation. This Model Report addresses the ability of the UZ geological units below the repository to limit and delay the transport of radionuclides to the saturated zone (SZ) and provides a basis for evaluating the barrier capability, (Sections 6.3 and 6.8).

- Acceptance Criterion 2, Description of Barrier Capability to Isolate Waste is Acceptable:

  The capability of the identified barriers to limit and retard the transport of radionuclides is adequately identified and described, including changes during the compliance period. The uncertainty associated with barrier capabilities is adequately described, (Sections 6.5, 6.6, 6.7, and 6.8).

- Acceptance Criterion 3, Technical Basis for Barrier Capability is Adequately Presented:

  The technical bases for this radionuclide transport abstraction are consistent with the technical basis for TSPA-LA. The technical basis for assertions of barrier capability is commensurate with the importance of the barrier's capability and associated uncertainties, (Sections, 6.3, 6.4, 6.6, and 6.8).

The criteria listed in Table 4-3 include some that were not listed in Table 3-1 of the TWP (BSC 2002 [160819]), but they are appropriate for this Model Report.

4.3 CODES AND STANDARDS

No specific formally established codes or standards have been identified as applying to this modeling activity.

INTENTIONALLY LEFT BLANK

5. ASSUMPTIONS

In this section, the assumptions taken to develop the UZ radionuclide transport abstraction model are outlined as the first step toward developing the computational and mathematical models needed in radionuclide transport calculations for the TSPA model. In Section 6.4, the mathematical basis for this algorithm is outlined, and theory is developed to incorporate the effects of sorption, dispersion, and matrix diffusion into this new particle-tracking framework. In the remainder of this section, the fundamental assumptions of the techniques itself and the specific implementation for the UZ transport abstraction model are listed and justified.

Assumption 1: Fracture frequency and permeability are log-normally distributed.

Rationale: These properties are quantities bounded at the low end by zero. Therefore, a log-normal distribution is a natural choice that can meet the measured means and standard deviations, and are constrained to be larger than zero.

Confirmation Status: This assumption does not require verification.

Where Used: Section 6.5.7

Assumption 2: The Active Fracture Model (AFM) appropriately accounts for reduced fracture/matrix interaction.

Rationale: The reduction in fracture/matrix contact area is a result of the active fracture unsaturated flow model. This reduction is justified on the basis of the desirability of maintaining consistency with the assumptions underlying the development of the flow fields developed for the UZ flow modeling effort. These assumptions are developed in Liu et al. (1998 [105729]).

Confirmation Status: This assumption does not require verification.

Where Used: Section 6.4.3

Assumption 3: The influence of matrix diffusion in a dual-permeability system can be handled with a sub-grid-block model consisting of parallel flow in a discrete fracture and connected matrix.

Rationale: Although the submodel consisting of a repeating system of parallel, equally spaced fractures and parallel flow in the fractures and matrix is an idealization, it captures one of the key features in the UZ system, namely the influence of radionuclide diffusion between fractures and matrix. Furthermore, the influence of sharp concentration gradients in the matrix is implicitly accounted for in the model by incorporating results from a Discrete Fracture Model (DFM) designed to handle these effects accurately. Therefore, systems with relatively small amounts of matrix diffusion can be simulated, in contrast to implementations of dual-permeability transport that represent the matrix with

a single grid block. In numerical modeling, this type of idealization, commonly referred to as "upscaling," is a technique for capturing the essential features of a physical system, even though it is understood that the actual system contains geometric complexities not simulated in the model. For example, Assumption 1 showed that the distribution of fracture spacings of mapped fractures is not uniform. However, the important spacing of interest for transport is the spacing of flowing fractures, which adds significant additional uncertainty. Given this situation, an appropriate assumption for the purpose of capturing the impact of matrix diffusion is to assume the model geometry of equally spaced flowing fractures.

Confirmation Status: This assumption does not require verification.

Where Used: Section 6.4.3

Assumption 4: Radionuclide sorption can be approximated with a linear, equilibrium sorption model characterized by a single parameter, the distribution coefficient K_d.

Rationale: It is well-known that the effective sorption coefficient in porous media is a function of many factors, including mineralogy, groundwater aqueous chemistry (including redox conditions), and heterogeneity at scales smaller than are considered in numerical models. Furthermore, the kinetics of the sorption reaction must be considered to ensure that the reactions are effectively at equilibrium. Despite these limitations, the K_d model is by far the most widely used sorption model in PA calculations due to its simplicity and ease of use. The factors listed above do not preclude the use of this model. However, they must be considered when establishing the parameter uncertainty distribution for K_d. As long as the range of sorption coefficients used in PA calculations takes into account uncertainties arising due to the factors listed here, then this assumption is valid for the intended use of this model.

Confirmation Status: This assumption does not require verification.

Where Used: Section 6.4.1, Eq. 6-2

Assumption 5: Dispersion of both aqueous and colloidal species can be approximated as consisting only of longitudinal dispersion, characterized by a constant value of the dispersivity α_l.

Rationale: When dispersivity is used to model solute spreading in porous media, it is introduced to capture variability in the flow velocity that exists at smaller scales than are modeled in the numerical grid. Large-scale spreading caused by features explicitly present in the flow simulation is captured directly, and are not considered to be dispersion in the sense being used here. Because the use of this model is to predict travel time distributions of radionuclides to the water table, longitudinal dispersion is potentially important to capture a dispersed solute front arriving at the water table. By contrast, transverse

dispersion, omitted in this model, will tend to allow mass to migrate short distances in the horizontal direction. However, it is unlikely that the small lateral spreading orthogonal to the direction of gravitation flow will significantly change the transit time to the water table. Therefore, transverse dispersion can be neglected. Finally, to a first approximation, this variability will act similarly on aqueous and colloidal components. Therefore, the same dispersivity should be used for both.

Confirmation Status: This assumption does not require verification.

Where Used: Section 6.4.2

Assumption 6: Radionuclide mass sorbs reversibly or irreversibly to non-diffusing colloids. The parameter used in the model to capture this behavior is the equilibrium sorption parameter $K_c = C_{coll} / C_{fluid}$, where C_{coll} is the radionuclide concentration residing on the colloids (moles radionuclide on colloid per kg fluid), and C_{fluid} is the corresponding concentration in the fluid phase (moles aqueous radionuclide per kg fluid). The value of K_c is assumed to be constant for a given radionuclide in each realization.

Rationale: Most measurements of sorption onto bulk rock and colloids are interpreted using an equilibrium sorption model such as this one. For compatibility with the data collected on sorption, this assumption is adopted in the numerical model as well. For colloids thought to be truly irreversible, the model can be used with an extremely large value of K_c for that portion of the radionuclide inventory. This approach yields a radionuclide migration behavior which exhibits no matrix diffusion.

Confirmation Status: This assumption does not require verification.

Where Used: Section 6.4.5

Assumption 7: Colloids undergo reversible filtration in the porous medium, with a colloid retardation factor of R_{coll}.

Rationale: To estimate retardation of colloids in the fracture continuum, field experiments at the C-wells complex near Yucca Mountain were examined, in which transport of microspheres was used as an analog for colloids. The microsphere breakthrough curves were fit to forward and reverse filtration rates (DTN: LA0002PR831231.003 [144462]). These rate constants were then used to calculate a retardation factor for colloid transport through saturated fractured rock (BSC 2003 [162729]; DTN: LA0303HV831352.002 [163558]). For compatibility with this analysis of field data, this assumption is adopted in the numerical model as well.

Confirmation Status: This assumption does not require verification.

Where Used: Section 6.4.5

Assumption 8: Radionuclide releases at the location of the proposed repository can be represented stochastically by identifying regions on the basis of the predicted water flux through the medium, and placing particles randomly within this region to represent the release.

Rationale: Water flux through the repository region is known to be a key factor controlling waste package degradation and waste mobilization. By partitioning the finite difference grid cells in the UZ model into groups based on flux, radionuclides will preferentially enter the system at locations where the flux is highest. This approach preserves this known relationship, and does not artificially introduce radionuclides into the model at locations where travel times are extremely long.

Confirmation Status: This assumption does not require verification.

Where Used: Section 6.5.15

Assumption 9: For the purposes of computing radionuclide transport, flow through the UZ can be approximated assuming that the system (rock mass and flow conditions) has not been influenced by repository waste heat effects or drift shadow effects. Durable changes to the rock mass hydrologic properties are also assumed to be negligible.

Rationale: It is known from numerical modeling that the flow conditions around the proposed repository will change due to thermohydrologic effects. These effects are expected to last for on the order of a few thousand years. As long as the radionuclide releases occur after the main part of this perturbation takes place, the system should have bounced back to its pre-waste-emplacement flow conditions. Regarding the potential for durable changes to the rock mass properties, a range of hydrologic flow conditions (in the form of different flow fields imported to the model) are assumed. It is assumed that this range will encompass the possibility of changes to the far-field rock conditions from repository waste heat.

Confirmation Status: This assumption does not require verification.

Where Used: Section 6.5.1

Assumption 10: Climate changes can be considered in an approximate way by imparting an instantaneous jump from one steady state flow field to another, with a corresponding rise or fall in the water table representing the bottom of the UZ model. Shorter-term transients (wet and dry years, individual storm events, etc.) are assumed to be adequately captured with a model that assumes such transients can be averaged to obtain a long-term, effective steady state.

Rationale: In simulations of system performance lasting 10,000 to 20,000 years, long-term changes in climatic conditions are expected to change the UZ flow field from its present-day condition. In the Yucca Mountain UZ, we expect water travel times of hundreds to thousands of years through the entire system, although this process is obviously uncertain. Assuming that the jump from one steady state flow field to another occurs instantaneously is a reasonable approximation, given the uncertainties and our inability to observe this process directly. When the climate changes from drier to wetter, as we expect it will within the regulatory compliance period, velocities will immediately be greater and the flow path length to the water table will be shorter: imposing both of these changes immediately will ensure that our approach will not artificially delay the imposition of the more rapid transport conditions. Regarding short-term transients, it is thought that the relatively unfractured portions of the rock, such as the Paintbrush non-welded vitric tuff (PTn) will dampen such transients, allowing a long-term steady state model to be used.

Confirmation Status: This assumption does not require verification.

Where Used: Sections 6.4.8 and 6.4.9

INTENTIONALLY LEFT BLANK

6. MODEL DISCUSSION

6.1 MODELING OBJECTIVES AND APPROACH

This Model Report documents the abstraction of UZ transport model to be used in TSPA-LA simulations. The UZ transport model studies the movement of radionuclides released from the Engineered Barrier System (EBS) into the unsaturated fractured geological media downward to the water table. Radionuclide mass flux versus time exiting the UZ is transferred to the SZ model in the TSPA system model.

Processes affecting radionuclide transport in the UZ include: advection, dispersion, fracture-matrix interaction, adsorption, colloid-facilitated transport, climate change and water table rises, and radionuclide decay/ingrowth. The numerical representation of those processes are described in Section 6.4.

To simulate radionuclide transport through the UZ, FEHM needs the following data and parameters as inputs:

- Numerical grid
- Pre-generated flow fields
- Rock density
- Fracture properties
- Spacing, porosity, aperture, residual saturation, and factor γ for Active Fracture Model (AFM)
- Radionuclide transport properties
- Dispersivity, adsorption coefficient, matrix diffusion coefficient, and fracture retardation factor
- Colloid properties
- Size exclusion factor, filtration factor, and retardation factor
- Repository release bins and water table collect bins.

The pre-generated flow fields are simulated in BSC 2003 [163228] and saved for TSPA-LA use. The use of pre-generated flow fields increases the efficiency of transport simulations.

In TSPA runs, GoldSim (BSC 2003 [161572]) initiates a call to the FEHM external dynamic link library (dll) to start UZ transport simulations (Figure 6-1). GoldSim (BSC 2003 [161572]) passes the following data to FEHM through the interface:

- Simulation time

- Flow fields to be used
- Coordinates for early failed packages and number of repository sub-regions
- Number of radionuclide species
- Radionuclide mass release from EBS to UZ in each designated sub-region for each species.

At the end of each FEHM UZ transport run, FEHM passes the simulated mass output at the water table back for input to SZ.

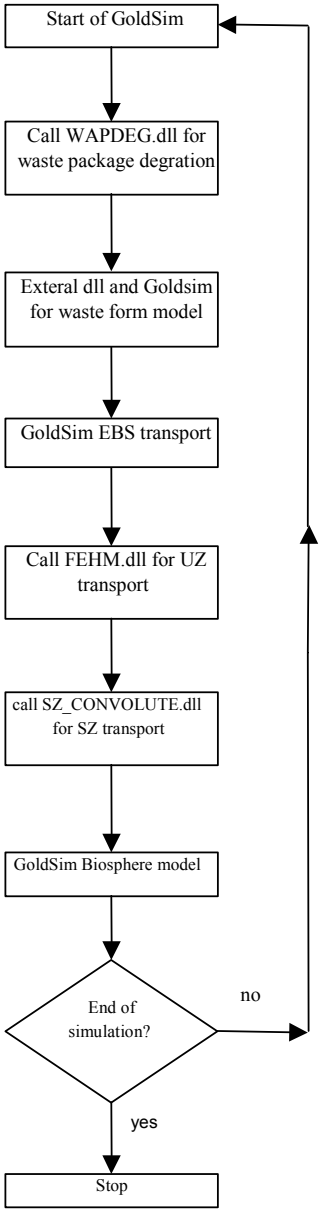

Figure 6-1. Schematic of the GoldSim-FEHM Coupling

6.2 FEATURES, EVENTS, AND PROCESSES INCLUDED IN THE MODEL

The development of a comprehensive list of features, events, and processes (FEPs) potentially relevant to post-closure performance of the Yucca Mountain repository is an ongoing, iterative process based on site-specific information, design, and regulations. The approach for developing an initial list of FEPs, in support of TSPA-Site Recommendation (SR) (CRWMS M&O 2000 [153246]), was documented in Freeze et al. (2001 [154365]). The initial FEP list contained 328 FEPs, of which 176 were included in TSPA-SR models (CRWMS M&O 2000 [153246], Tables B-9 through B-17). To support TSPA-LA, the FEP list was re-evaluated in accordance with the Enhanced FEP Plan (BSC 2002 [158966], Section 3.2).

The included FEP abstractions incorporated in the TSPA-LA model and relevant to this report, are specifically addressed in this Model Report (Table 6-1). The rationale for excluding a FEP from the TSPA-LA model is given in the UZ FEPs Scientific Analysis Report, *Features, Events, and Processes in UZ Flow and Transport* (BSC 2003 [164873]).

Table 6-1 provides a list of FEPs that are specifically addressed in this Model Report. Details of the implementation of these FEPs in TSPA-LA are summarized in Section 6.4. As noted above, as the FEPs list was re-evaluated (BSC 2002 [158966], Section 3.2), the current FEPs are not the same as those listed in the TWP (BSC 2002 [160819])

Table 6-1. Included FEPs for This Model Report and Their Disposition in TSPA-LA

FEP Number	FEP Name	Section Where FEP is Addressed	Summary of Disposition in TSPA-LA	Treatment of FEP in this Model report
1.2.02.01.0A	Fractures	Sections 6.4.3, 6.5.1, 6.5.7, and 6.6.2	Groundwater flow in the Yucca Mountain region and transport of any released radionuclides may take place along fractures. The rate of flow and the extent of transport in fractures are influenced by characteristics such as orientation, aperture, asperity, fracture length, connectivity, and the nature of any linings or infills.	Influence of fractures on radionuclide transport through UZ is investigated through the dual permeability model (Section 6.4.3). Influence of fracture characteristics on UZ flow are included in the model report through using the pre-generated flow fields (Section 6.5.1. DTN: LB0305TSPA18FF.001 [165625]). Factors (fracture aperture, porosity, and frequency. DTNs: LB0205REVUZPRP.001 [159525] and LB0207REVUZPRP.001 [159526]) affecting UZ radionuclide transport are summarized in Section 6.5.7. Simulation results for the basecase model runs are documented in Section 6.6.2. Fracture porosity and frequency data distributions are an output of this Model Report (Output-DTN: LA0311BR831371.003) and will be statistically sampled during TSPA-LA multi-realization runs.

Table 6-1. Included FEPs for This Model Report and Their Disposition in TSPA-LA (Continued)

FEP Number	FEP Name	Section Where FEP is Addressed	Summary of Disposition in TSPA-LA	Treatment of FEP in this Model report
1.2.02.02.0A	Faults	Section 6.5.1, 6.5.7 and 6.6.2.	Numerous faults of various sizes have been noted in the Yucca Mountain Region and in the repository area in specific. Faults may represent an alteration of the rock permeability and continuity of the rock mass, alteration or short-circuiting of the flow paths and flow distributions close to the repository, and represent unexpected pathways through the repository.	Influence of faults on radionuclide transport is included through the use of dual permeability model, the use of pre-generated flow fields which included the effects of faults in the 3-D model (Section 6.5.1, DTN: LB0305TSPA18FF.001 [165625]) and the characteristics of fractures within the faults (Section 6.5.7). In TSPA-LA runs, the influence of faults is included through the use of fault properties and the pre-generated flow fields under different climate conditions as described in Sections 6.5.1 and 6.5.7. Simulation results that included faults in the UZ are documented in Section 6.6.2. For this FEP, no direct data feed is generated for TSPA-LA by this Model Report.
1.3.01.00.0A	Climate change	Sections 6.4.9 and 6.6.2	Climate change may affect the long-term performance of the repository. This includes the effects of long-term change in global climate (e.g., glacial/interglacial cycles) and shorter-term change in regional and local climate. Climate is typically characterized by temporal variations in precipitation and temperature.	Climate change is included in Section 6.4.9. The effect of climate change on repository performance was studied by using pre-generated flow fields under different climates (DTN: LB0305TSPA18FF.001 [165625]). For TSPA-LA, the pre-generated flow fields are used by the FEHM model as described in Section 6.4.9. Simulations results under present day mean infiltration condition and those under the glacial mean infiltration condition are documented in Section 6.6.2. For this FEP, no direct data feed is generated for TSPA-LA by this Model Report.

Table 6-1. Included FEPs for This Model Report and Their Disposition in TSPA-LA (Continued)

FEP Number	FEP Name	Section Where FEP is Addressed	Summary of Disposition in TSPA-LA	Treatment of FEP in this Model report
1.4.01.01.0A	Climate modification increases recharge	Sections 6.5.1 and 6.6.2	Climate modification (natural or artificial) causes an increase in recharge in the Yucca Mountain region. Increased recharge might lead to increased flux through the repository, perched water, or water table rise.	The effect of climate changes in the form of increased recharge is included through the use of pre-generated flow fields (Section 6.5.1 and DTN: LB0305TSPA18FF.001 I165625]). In multi-realization TSPA-LA runs, different climate patterns are applied and the effect of climate change is included through FEHM's use of pre-generated flow fields for the corresponding climates as described in Section 6.5.1. Simulation results for present day mean and glacial mean climates are shown in Section 6.6.2. Water table rise is incorporated by processing the flow fields assuming that the water table immediately rises due to climate change – see Section 6.4.9 for details. For this FEP, no direct data feed is generated for TSPA-LA by this Model Report.
2.2.03.01 .0A	Stratigraphy	Sections 6.5.1.	Stratigraphic information is necessary information for the performance assessment. This information should include identification of the relevant rock units, soils and alluvium, and their thickness, lateral extents, and relationships to each other. Major discontinuities should be identified.	The FEP is included through the use of pre-generated flow fields (DTN: LB0305TSPA18FF.001 [165625]). The flow fields are used by FEHM in TSPA-LA multi-realization runs as described in Section 6.5.1. For this FEP, No direct data feed is generated for TSPA-LA by this Model Report. More detailed information, on implementation of this FEP for TSPA-LA can be found in document: *Development of Numerical Grids for UZ Flow and Transport Modeling* (BSC 2003 [160109]).

Table 6-1. Included FEPs for This Model Report and Their Disposition in TSPA-LA (Continued)

FEP Number	FEP Name	Section Where FEP is Addressed	Summary of Disposition in TSPA-LA	Treatment of FEP in this Model report
2.2.03.02.0A	Rock properties of host rock and other units	Sections 6.5.3, 6.5.7, and 6.6.2.	Physical properties such as porosity and permeability of the relevant rock units, soils, and alluvium are necessary for the performance assessment. Possible heterogeneities in these properties should be considered. Questions concerning events and processes that may cause these physical properties to change over time are considered in other FEPs.	Rock properties of host rock and other units are included and used in the simulations of radionuclide transport through the UZ. Sections 6.5.3 and 6.5.7 document the matrix porosity, rock density, fracture porosity, fracture spacing, and aperture data (DTN: LB0305TSPA18FF.001 [165625], LB0210THRMLPRP.001 [160799], LB0205REVUZPRP.001 [159525], and LB0207REVUZPRP.001 [159526]). Section 6.6.2 demonstrates the simulation results of radionuclide transport through the UZ using the mean rock properties. The generated distributions of fracture porosity and fracture frequency are an Output (DTN: LA0311BR831371.003) of the Model Report and will be used by TSPA-LA in multi-realization runs as described in Sections 6.5.3 and 6.5.7.
2.2.07.02.0A	Unsaturated groundwater flow in the geosphere	Section 6.5.1 and 6.6.2.	Groundwater flow occurs in unsaturated rocks in most locations above the water table at Yucca Mountain, including at the location of the repository. See related FEPs for a discussion of specific issue related to unsaturated flow.	Unsaturated groundwater flow in the UZ is the driving force for radionuclide transport through the UZ. This FEP is addressed through the use of pre-generated flow fields (Section 6.5.1, DTN: LB0305TSPA18FF.001 [165625]) for TSPA-LA multi-realization runs. The pre-generated flow fields are directly used by FEHM as described in Section 6.5.1. Simulation results of radionuclide transport through the UZ under present day mean and glacial mean infiltration conditions are documented in Section 6.6.2. For this FEP, no direct data feed is generated for TSPA-LA by this Model Report.

Table 6-1. Included FEPs for This Model Report and Their Disposition in TSPA-LA (Continued)

FEP Number	FEP Name	Section Where FEP is Addressed	Summary of Disposition in TSPA-LA	Treatment of FEP in this Model report
2.2.07.04.0A	Focusing of unsaturated flow (fingers, weeps)	Section 6.5.1 and 6.6.2.	Unsaturated flow can differentiate into zones of greater and lower saturation (fingers) that may persist as preferential flow paths. Heterogeneities in rock properties, including fractures and faults, may contribute to focusing. Focused flow may become locally saturated.	In the current model abstraction report, the effect of focusing unsaturated flow is included through the use of pre-generated flow fields (Section 6.5.1, DTN: LB0305TSPA18FF.001 [165625]) as described in Section 6.5.1. For TSPA-LA, the pre-generated flow fields are used directly by FEHM. For this FEP, no direct data feed is generated for TSPA by this Model Report. This FEP is more fully addressed in the Model Report *UZ Flow Models and Submodels* (BSC 2003 [163045]).
2.2.07.06.0A	Episodic / pulse release from repository	Sections 6.4.6, 6.4.7, 6.4.8, and 6.4.9.	Episodic or pulse release of radionuclides from the repository and radionuclide transport in the UZ may occur both because of episodic flow into the repository, and because of pulse releases from failed waste packages.	The implementation of episodic/pulse release from repository is discussed in Sections 6.4.6 through 6.4.9. For TSPA-LA, episodic/pulse release from repository is implemented by passing radionuclide mass release from GoldSim to FEHM through the GoldSim-FEHM interface (Sections 6.4.6 and 6.4.7). Episodic/pulse release caused by climate change, addressed in Sections 6.4.8 and 6.4.9 is implemented by switching from one flow field to a new flow field at time of climate change through FEHM-GoldSim interface. For this FEP, no direct data feed is generated for TSPA-LA by this Model Report.
2.2.07.06.0B	Long-term release of radionuclides from repository	Sections 6.4.6 and 6.4.7	The release of radionuclides from the repository may occur over a long period of time, as a result of the timing and magnitude of the waste packages and drip shield failures, waste form degradation, and radionuclide transport through the invert.	Long-term radionuclide release due to the failure of waste packages in the repository is addressed in Sections 6.4.6 and 6.4.7. For each TSPA-LA GoldSim-FEHM run, GoldSim passes radionuclide mass releases to FEHM and FEHM simulates the transport process through the UZ as described in Sections 6.4.6 and 6.4.7. For this FEP, no direct data feed is generated for TSPA-LA by this Model Report.

Table 6-1. Included FEPs for This Model Report and Their Disposition in TSPA-LA (Continued)

FEP Number	FEP Name	Section Where FEP is Addressed	Summary of Disposition in TSPA-LA	Treatment of FEP in this Model report
2.2.07.07.0A	Perched water develops	Section 6.5.1	Zones of perched water may develop above the water table. If these zones occur above the repository, they may affect UZ flow between the surface and the waste packages. If they develop below the repository, for example at the base of the Topopah Spring welded unit, they may affect flow pathways and radionuclide transport between the waste packages and the saturated zone.	This FEP is included through the use of pre-generated flow fields (DTN: LB0305TSPA18FF.001 [165625]). In TSPA-LA runs, pre-generated flow fields are used by FEHM and used in UZ transport simulations as described in Section 6.5.1. For this FEP, no direct data feed is generated for TSPA-LA by this Model Report. More detailed information on the treatment of fracture flow in UZ can be found in the Model Report, *UZ Flow Models and Submodels* (BSC 2003 [163045]).
2.2.07.08.0A	Fracture flow in the UZ	Section 6.5.1	Fractures or other analogous channels act as conduits for fluids to move into the subsurface to interact with the repository and as conduits for fluids to leave the vicinity of the repository and be conducted to the SZ. Water may flow through only a portion of the fracture network, including flow through a restricted portion of a given fracture plane.	In the unsaturated zone, fracture flow plays an important role in the transport of radionuclides. In TSPA-LA runs, the direct effect of fracture flow on radionuclide transport (advection) is included through FEHM's use of pre-generated flow fields (DTN: LB0305TSPA18FF.001 [165625]) in UZ transport simulations as described in Section 6.5.1. For this FEP, no direct data feed is generated for TSPA in this Model Report. More detailed information on the treatment of fracture flow in UZ can be found in the Model Report, *UZ Flow Models and Submodels* (BSC 2003 [163045]).

Table 6-1. Included FEPs for This Model Report and Their Disposition in TSPA-LA (Continued)

FEP Number	FEP Name	Section Where FEP is Addressed	Summary of Disposition in TSPA-LA	Treatment of FEP in this Model report
2.2.07.09.0A	Matrix imbibition in the UZ	Section 6.5.1	Water flowing in fractures or other channels in the unsaturated zone is imbibed into the surrounding matrix. This may occur during steady flow, episodic flow, or into matrix pores that have been dried out during the thermal period.	For TSPA-LA runs, the pre-generated flow fields (DTN: LB0305TSPA18FF.001 [165625]) are used by FEHM in UZ transport simulations as described in Section 6.5.1. For this FEP, no direct data feed is generated for TSPA-LA by this Model Report. More detailed information on the treatment of fracture flow in UZ can be found in the Model Report, *UZ Flow Models and Submodels* (BSC 2003 [163045]).
2.2.07.15.0B	Advection and dispersion in the UZ	Section 6.4.1, 6.4.2, 6.6.2, and 7.1.1.	Advection and dispersion processes may affect contaminant transport in the UZ.	Radionuclide transport through the UZ by advection is simulated using the RTTF (Residence Time Transfer Function) method documented in Section 6.4.1. Dispersion is incorporated into the RTTF algorithm through the use of a transfer function based on an analytical solution to the advection-dispersion equation (Section 6.4.2). Simulation results involving advection and dispersion under different flow conditions are shown in Section 6.6.2 and 7.1.1. In TSPA –LA runs, advection and dispersion is simulated through the use of FEHM RTTF model and the pre-generated flow fields as described in Sections 6.4.1 and 6.4.2. For this FEP, no direct data feed is generated for TSPA-LA by this Model Report.

Table 6-1. Included FEPs for This Model Report and Their Disposition in TSPA-LA (Continued)

FEP Number	FEP Name	Section Where FEP is Addressed	Summary of Disposition in TSPA-LA	Treatment of FEP in this Model report
2.2.08.08.0B	Matrix diffusion in the UZ	Section 6.4.3, 6.5.5, 6.6.2, 7.1.2, 7.1.3, and Attachment III.	Matrix diffusion is the process by which radionuclides and other species transported in the UZ by advective flow in fractures or other pathways move into the matrix of the porous rock by diffusion. Matrix diffusion can be a very efficient retarding mechanism, especially for strongly sorbed radionuclides due to the increase in rock surface accessible to sorption.	Migration of radionuclides from fast flow fracture into surrounding slow flow matrix blocks by diffusion could play an important role in delaying the transport process of radionuclides in fractures. In this report, the role of matrix diffusion is included through the development of the transfer function approach as described in Section 6.4.3. Transfer function curves (Output-DTN: LA0311BR831229.001) generated in this Model Report are a direct feed to TSPA-LA and will be used by FEHM in simulating the effect of matrix diffusion on radionuclide transport in TSPA-LA runs as described in Sections 6.4.3 and Attachment III. One important factor affecting the strength of matrix diffusion is the matrix diffusion coefficient. In this report matrix diffusion coefficient is related to matrix water content and matrix effective permeability through the relationship developed by Reimus et al. (2002 [163008]). The distributions of matrix water content and matrix effective permeability are an output of this Model Report (Section 6.5.5, Output-DTN: LA0311BR831371.003) and are used by TSPA in multiple realization runs for randomly generating matrix diffusion coefficients. Simulation results involving matrix diffusion, which are not a direct data feed to TSPA-LA, are illustrated in Sections 6.6.2, 7.7.2, and 7.7.3.

Table 6-1. Included FEPs for This Model Report and Their Disposition in TSPA-LA (Continued)

FEP Number	FEP Name	Section Where FEP is Addressed	Summary of Disposition in TSPA-LA	Treatment of FEP in this Model report
2.2.08.09.0B	Sorption in the UZ	Sections 5., 6.4.3, 6.4.5, 6.5.4, 6.5.8, and 6.6.2.	Sorption of dissolved and colloidal radionuclides in the UZ can occur on the surfaces of both fractures and matrix in rock or soil along the transport path. Sorption may be reversible or irreversible, and it may occur as a linear or nonlinear process. Sorption kinetics and the availability of sites for sorption should be considered. Sorption is a function of the radioelement type, mineral type, and groundwater composition.	Sorption in the UZ is treated as a linear process (Section 5, assumption 4). In the matrix, sorption is incorporated in the generation of transfer function curves and expressed as part of the defined dimensionless parameters (Section 6.4.3). For colloid facilitated radionuclide transport, radionuclide sorption onto colloids and its effect on transport is simulated through the colloid retardation factor, which is a function of radionuclide sorption coefficient onto colloids and the colloid retardation factor (Section 6.4.5). Radionuclide sorption coefficients used in the simulation of radionuclide transport in UZ are documented in Section 6.5.4 (DTN: LA0302AM831341.002 [162575]). Colloid concentration and radionuclide sorption coefficients onto colloids are documented in Section 6.5.12 (DTN: SN0306T0504103.005 [164132] and SN0306T0504103.006 [164131]). Simulation results involving colloid transport are demonstrated in Section 6.6.2. In TSPA-LA runs, sorption coefficients are sampled and fed into FEHM as described in the above mentioned sections. Sorption onto fracture surfaces is neglected because of few data available in supporting such a retardation mechanism in the UZ. Thus, a fracture surface retardation factor of 1 is set for use in TSPA-LA runs (Section 6.5.8.). For this FEP, no direct data feed is generated for TSPA-LA by this Model Report.

Table 6-1. Included FEPs for This Model Report and Their Disposition in TSPA-LA (Continued)

FEP Number	FEP Name	Section Where FEP is Addressed	Summary of Disposition in TSPA-LA	Treatment of FEP in this Model report
2.2.08.10.0B	Colloidal transport in the UZ	Sections 6.4.5, 6.5.9, 6.5.10, 6.5.11, 6.5.12, 6.5.13, and 6.6.2	Radionuclides may be transported in groundwater in the UZ as colloidal species. Types of colloids include true colloids, pseudo colloids, and microbial colloids.	The influence of colloid transport on radionuclide migration through the UZ is discussed in Section 6.4.5. Parameters that can impact colloid transport in the UZ include colloid size (DTN: LL000122051021.116 [142973]), colloid concentration (DTN: SN0306T0504103.005 [164132]), radionuclide sorption coefficient onto colloid (DTN: SN0306T0504103.006 [164131]), and colloid retardation factors (DTN: LA0303HV831352.002 [163558]) are documented in Sections 6.5.9 through 6.5.13. Simulation results involving colloids are documented in Section 6.6.2. In TSPA-LA runs, colloid facilitated radionuclide transport is investigated through the FEHM colloid transport model and variations of colloid transport parameters as described in the above mentioned sections. For this FEP, no direct data feed is generated for TSPA-LA by this Model Report.
2.2.11.03.0A	Gas transport in geosphere	6.4.7	Gas released from the drifts and gas generated in the near-field rock will flow through fracture systems in the near field rock and in the geosphere. Certain gaseous or volatile radionuclides may be able to migrate through the far-field faster than the groundwater advection rate.	This FEP is included on the basis that all radionuclides in TSPA are released into the aqueous phase. This is expected to bound any dose effects of gas-phase release due to the large dilution of gas-phase release in the atmosphere (*Features, Events, and Processes in UZ Flow and Transport,* BSC 2003 [164873]).

Table 6-1. Included FEPs for This Model Report and Their Disposition in TSPA-LA (Continued)

FEP Number	FEP Name	Section Where FEP is Addressed	Summary of Disposition in TSPA-LA	Treatment of FEP in this Model report
3.1.01.01.0A	Radioactive decay and ingrowth	Sections 6.4.4, 6.5.14, and 6.6.2	Radioactivity is the spontaneous disintegration of an unstable atomic nucleus that results in the emission of subatomic particles. Radioactive isotopes are known as radionuclides. Radioactive decay of the fuel in the repository changes the radionuclide content in the fuel with time and generates heat. Radionuclide quantities in the system at any time are the result of the radioactive decay and the growth of daughter products as a consequence of that decay (i.e., ingrowth). Over a 10,000-year performance period, these processes will produce daughter products that need to be considered in order to adequately evaluate the release and transport of radionuclides to the accessible environment.	In this report, decay and ingrowth are simulated through the development of an effective integration algorithm (Section 6.4.4). This algorithm can handle multiple species decay and ingrowth processes. Radionuclide half lives and daughter products considered in the UZ transport abstraction model are documented in Section 6.5.14. Simulation results involving radionuclide decay/ingrowth processes are illustrated in Section 6.6.2. In TSPA-LA runs, 36 species of radionuclides are simulated through the UZ using the FEHM decay/ingrowth model over a specified time period as described in the above mentioned sections in this Model Report. For this FEP, no direct data feed is generated for TSPA-LA by this Model Report.

6.3 THE UZ TRANSPORT ABSTRACTION MODEL

The UZ transport component of the total system model tracks the movement of radionuclides released from the EBS down to the water table (Figure 6-2).

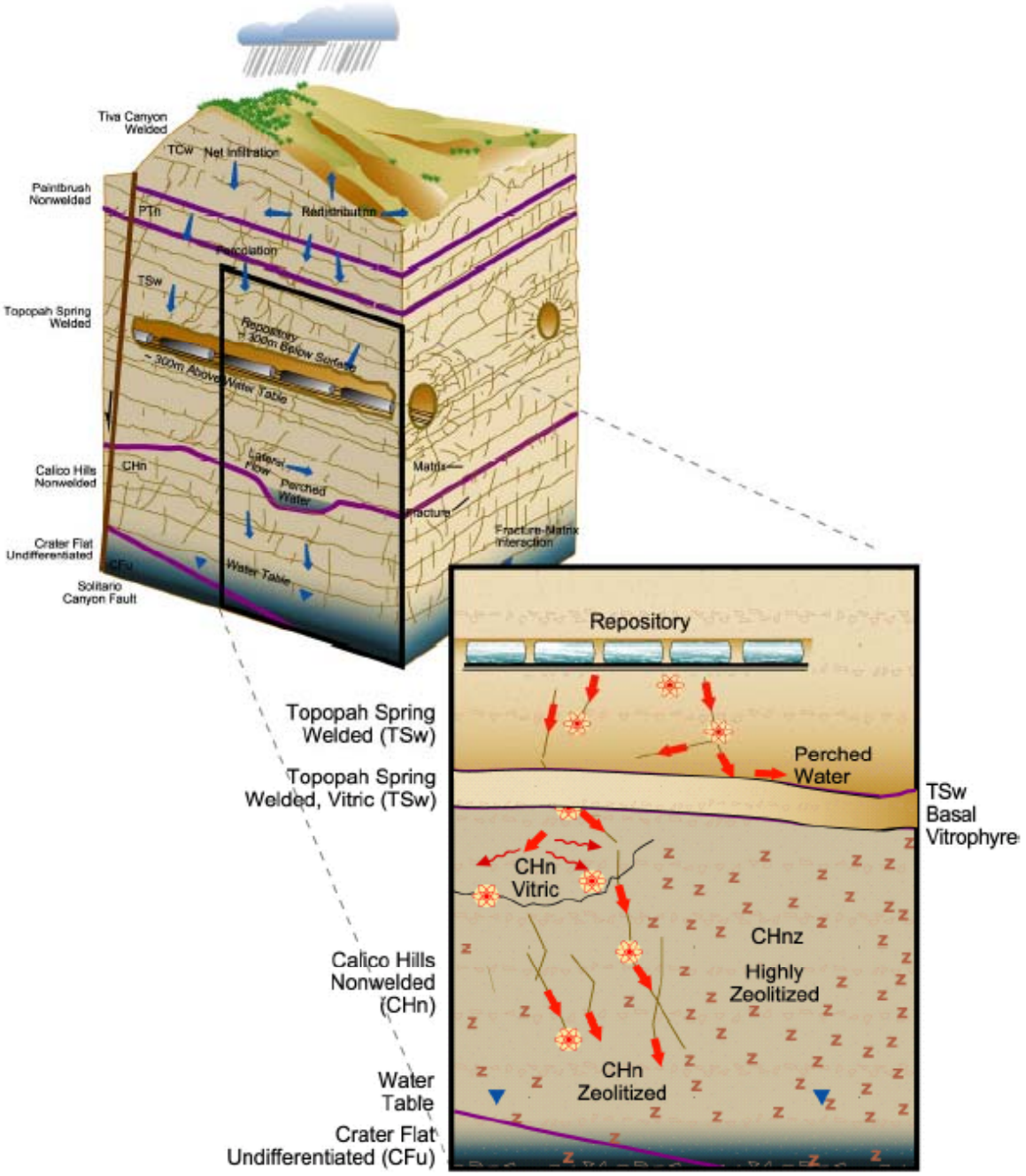

Figure 6-2. Schematic of Water Movement and Radionuclide Transport through the UZ

The top boundary of the UZ flow model is the ground surface, with prescribed infiltration rates, and the bottom boundary is the water table. The side boundaries are no flow.

The UZ flow fields are pregenerated and saved for use by FEHM. During TSPA simulation runs, the FEHM dll reads in the pregenerated flow fields and then carries out transport simulations. The impact of climate change is investigated by using the UZ flow fields corresponding to different climate scenarios. The FEHM-compatible flow field files developed for the TSPA-LA model are in DTN: LB0305TSPA18FF.001 [165625].

The UZ transport model is based on the dual permeability formulation for fluid flow, with additional transport considerations to incorporate the influence of sorption and fracture-matrix interactions on radionuclide transport. The influence of spatial variability is included through a 3-D model that incorporates the appropriate geometry and geology.

For the UZ transport model, radionuclides are released the repository where failed waste packages release radionuclides into the system. Any radionuclide that reaches the water table is removed from the UZ transport system and put into the SZ system.

Once a radionuclide particle is released from the EBS into UZ, the particle is carried by water traveling through the fractured media downward to the water table. The following transport mechanisms can affect the movement of a radionuclide particle and are considered in the UZ transport model:

- Advection
- Dispersion
- Adsorption
- Fracture-matrix interaction including matrix diffusion
- Colloid-facilitated transport
- Radioactive decay/ingrowth
- Climate change and water table rise.

Implementation of the above transport mechanisms inside FEHM are described in Section 6.4 of this Model Report. The abstraction model is designed to facilitate parameter uncertainty analyses in TSPA. This is done by running multiple realizations with different parameter values based on parameter distributions.

Performing multiple realizations (numbering in the hundreds) for such a complex system requires that the software used for simulating radionuclide transport in the system be efficient while also being able to handle complex physical and chemical processes with sufficient accuracy. FEHM (Zyvoloski et al. 1997 [100615]) was selected for simulating radionuclide transport in the system because of the efficiency of the particle tracking method and its ability to handle advection, dispersion, sorption, matrix-diffusion, and multiple-species radionuclide decay/ingrowth in the system.

6.4 THE NUMERICAL REPRESENTATION OF THE UZ TRANSPORT MODEL

This section outlines the development of the general transport methods used for the Residence Time/Transfer Function (RTTF) particle-tracking model and issues specific to the use of this model to simulate radionuclide transport for the Yucca Mountain UZ.

Prediction of solute transport is a critical element of many groundwater flow studies, including contaminant transport and the movement of dissolved species in solution. Modeling efforts typically are motivated by the need to predict the movement of a pollutant or dissolved chemical in the subsurface to answer practical questions concerning the rate and direction of contaminant movement and the predicted concentration in solution. In a typical solute transport simulation, a dissolved chemical is introduced into a steady-state or time-varying flow field, and the fate of the chemical is tracked while undergoing physical and chemical processes such as advection, dispersion, chemical and biological reaction, or diffusion into dead-end pore space. Often, a concentration front is established that must be tracked accurately. In addition, many field investigations employ natural or introduced tracers to study the flow and transport system. These studies also require models to simulate the movement of dissolved species.

Traditional solutions to the advection-dispersion (AD) equation, such as those used in most finite-element or finite-difference flow and transport codes, are versatile and allow the simultaneous solution of multiple interacting species. One drawback of a finite-difference or finite-element solution to the AD equation is that significant numerical dispersion may arise in the portion of a computational domain occupied by a front of rapidly varying concentration. Reducing the numerical dispersion requires either increased grid resolution or higher-order approximation methods, both of which may lead to prohibitive computational costs. Numerical dispersion is identical in character to actual dispersion, so it is difficult to separate numerical from actual dispersion in complex transport simulations.

Approaches to cope with this problem include front-tracking algorithms with multiple grids (e.g., Yeh 1990 [101501]; Wolfsberg and Freyberg 1994 [101498]), the method of characteristics (e.g., Chiang et al. 1989 [101384]), hybrid Eulerian-Lagrangian solution techniques (Neuman 1984 [101463]), and particle-tracking techniques (e.g., Tompson and Gelhar 1990 [101490]). Front-tracking algorithms solve the AD equation in integrated form on a numerical grid while tailoring the mesh to increase the resolution of the calculation at fronts. In contrast, an Eulerian-Lagrangian technique casts the AD equation using the total derivative, so that the advection portion of transport can be solved accurately using particle-tracking techniques or the method of characteristics, while the dispersion component of transport is solved on a finite-difference or finite-element grid using standard techniques.

Particle-tracking transport models take a fundamentally different approach. The trajectory of individual molecules or packets of fluid containing molecules are tracked through the model domain. When the fluid path lines are the model result of interest (Pollack 1988 [101466]; Lu 1994 [101413]), a relatively small number of particles can be used to trace the streamlines. Particle tracking is also used to simulate solute transport, such as the migration of a contaminant plume (Akindunni et al. 1995 [101378]) or the prediction of breakthrough curves in interwell tracer experiments (Johnson et al. 1994 [101400]). For these applications, a relatively large number of such particles must be used to obtain accurate solutions to the transport problem.

Particle tracking has also been used to solve the advective portion of complex reactive transport models that simulate chemical reactions among multiple species (Fabriol et al. 1993 [101387]).

In a typical particle-tracking algorithm, a particle is sent to a new position assuming that the magnitude and direction of the velocity vector are constant during a time step. If small enough time steps are taken, particle pathways can be tracked accurately. Dispersion is treated as a random process that diverts the particle a random distance from its dispersion-free, deterministic path. In these so-called "random walk" models (e.g., Kinzelbach 1988 [101402]), dispersion is usually calculated stochastically subject to a Gaussian model to reproduce the specified dispersion coefficient. The technique has also been extended by employing non-Gaussian random walk functions to represent scale-dependent dispersion (Scheibe and Cole 1994 [101477]). Linear equilibrium sorption can be handled through the use of a retardation factor to correct the magnitude of the particle velocity.

A crucial component of most random-walk particle-tracking algorithms developed to date is the need to accurately estimate the velocity at every position in the model domain. In the context of a finite-difference or finite-element numerical code, this means that velocities at positions other than the node points of the fluid flow grid must be computed using an interpolation scheme. Many studies have proposed and studied the accuracy of different interpolation schemes, including methods developed for regular, two- or three-dimensional finite difference grids (Schafer-Perini and Wilson 1991 [101476]; Zheng 1993 [101502]), for two- and three-dimensional finite-element grids (Cordes and Kinzelbach 1992 [101385]), and for codes that employ the boundary element method for computing fluid flow (Latinopoulos and Katsifarakis 1991 [101408]). Special techniques have been developed to handle complexities such as point fluid sources and sinks and abrupt changes in the conductivity of the medium (Zheng 1994 [101503]).

Unfortunately, many of the velocity interpolation schemes used in conventional particle-tracking techniques are computationally intensive, thus limiting the number of particles that can practically be used. Another drawback to traditional particle-tracking approaches is that spatial and temporal discretization often results in numerical inaccuracy in the fluid flow solution upon which velocity determinations are based. Thus, precise and time-consuming velocity interpolation schemes may not be justified in finite-difference or finite-element models. Finally, and most important for the simulation of transport in the UZ at Yucca Mountain, dual-permeability models employ overlapping continua to represent fracture and matrix flow (Zyvoloski et al. 1992 [101026]; Zimmerman et al. 1993 [100614]). To develop a streamline-based particle-tracking method for dual-permeability models, velocity interpolations on each continuum would have to be coupled to a transfer term that allows particles to move from one medium to the other. This additional complexity, along with the inherent approximations associated with the dual-permeability method itself, may make precise velocity interpolation calculations of limited validity.

In this model, a particle-tracking technique is employed that can be used for transient, multi-dimensional finite-difference or finite-element codes. The algorithm is designed for computing solute concentration fields quickly and easily with structured or unstructured numerical grids of arbitrary complexity. Both continuum and dual-permeability formulations can be simulated. This flexibility is accomplished by extending the cell-based strategy of

Desbarats 1990 [101386] for mapping out the path of the particle. In this method, the calculation of an "exact" pathline is replaced with a cell-to-cell migration of the particle. The mass flux from cell to cell is used directly, and no velocity interpolations are required. Since numerical solutions for fluid flow are typically mass-conservative (though not necessarily accurate) the particle-tracking method automatically conserves mass.

6.4.1 Basic Methods

The particle-tracking method developed in the present study views the fluid flow computational domain as an interconnected network of fluid storage volumes. Particles travel only from cell to cell, requiring no greater resolution of the particle pathways. In this sense, the method is similar to the node-to-node routing method of Desbarats (1990 [101386], p. 156). This simple starting point has been extended to include many different transport submodels and complex flow domains. Even though some aspects of the development that follows would appear to be applicable for steady-state, single-porosity flow fields, the extensions to the method for treating transient flow systems and dual-porosity model formulations are discussed in Section 6.4.3. The two steps in the particle-tracking approach are: 1) determine the time a particle spends in a given cell; and 2) determine which cell the particle travels to next. These two steps are detailed below.

The residence time for a particle in a cell is governed by a transfer function describing the probability of the particle spending a given length of time in the cell. Thus, this particle-tracking approach is called the RTTF method. The schematic plots shown in Figures 6-3 and 6-4 illustrate the basis of the RTTF approach. For a cumulative probability distribution function of particle residence times, the residence time of a particle in a cell is computed by generating a random number between 0 and 1 to determine the corresponding residence time from the distribution function. In the simplest case, advective transport through the cell, there is only one possible travel time through the cell, and the function illustrated in Figure 6-4 is the Heaviside function. However, dispersion and diffusion give rise to a distribution of travel times through the cell that must be reproduced in order to simulate these mechanisms. In this example, the advection-dispersion (AD) equation was used to generate the RTTF curve, but other transport mechanisms can be incorporated as well, as demonstrated below.

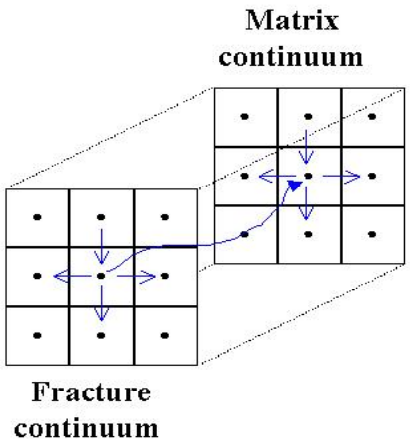

Figure 6-3. Schematic of the Cell-Based Particle-tracking Technique

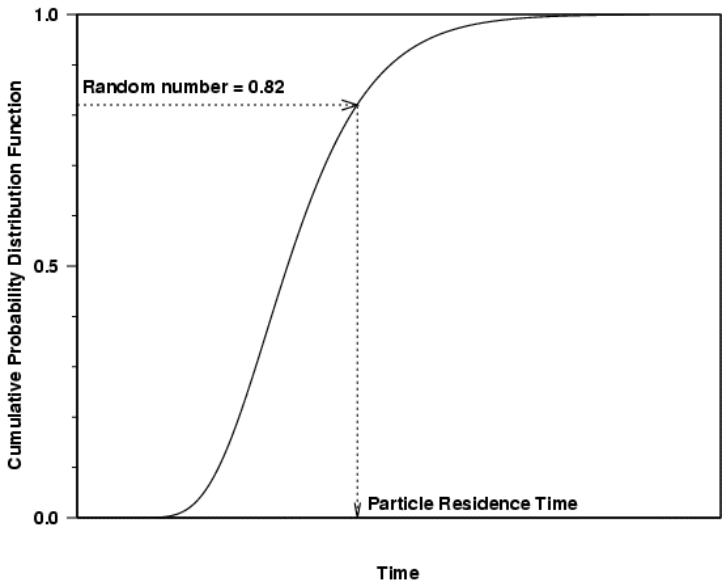

Figure 6-4. Schematic of the RTTF Technique for Determining Particle Residence Time in a Cell. The time axis represents the probabilistically determined residence time of a particle in the cell.

If a large number of particles pass through the cell, the cumulative residence time distribution of particles in the cell will be reproduced. Particle-tracking models of single-fracture transport (Yamashita and Kimura 1990 [101499]) have employed this approach to simulate fracture transport with diffusion into the rock matrix. From the solution of the flow field in a numerical model, the mass of fluid in the computational cell and the mass flow rate to or from each adjacent cell is computed. In the simplest case, the residence time of a particle in a cell, τ_{part}, is given by

$$\tau_{part} = \tau_{fl} = \frac{M_{fl}}{\sum \dot{m}_{out}} \qquad \text{(Eq. 6-1)}$$

where M_{fl} is the fluid mass in the cell and the summation term in the denominator refers to the outlet fluid mass flow rates from the cell to adjacent cells. In the absence of dispersion or other transport mechanisms, the transfer function describing the distribution of particle residence times is a Heaviside function (unit step function) that is unity at the fluid residence time τ_{fl}, because for this simple case, all particles entering the cell will possess this residence time. Equilibrium, linear sorption is included by correcting the particle residence time by a retardation factor R. Thus, $\tau_{part} = R\,\tau_{fl}$, and R is given by

$$R = 1 + \frac{\rho_b K_d}{\theta_{fl}} \qquad \text{(Eq. 6-2)}$$

where

K_d is the equilibrium sorption coefficient (ml fluid/g rock)

ρ_b is the bulk rock density (g rock/ml total)

θ_{fl} is the volumetric water content (ml fluid/ml total)

Once again, in the absence of other transport processes, the transfer function is a Heaviside function. Note that the method is applicable for either liquid or gas phase transport, so the generic term "fluid" is used in the definition above. However, in this Model Report, only liquid phase transport is simulated.

Before discussing more complex transfer functions for the RTTF method, the method for determining which cell a particle travels to after completing its stay at a given cell is discussed. The approach that is consistent with the RTTF method is that the probability of traveling to a neighboring cell is proportional to the mass flow rate to that cell. Only outflows are included in this calculation; the probability of traveling to an adjacent node is 0 if fluid flows from that node to the current node. A uniform random number from zero to one is used to make the decision of which node to travel to. In summary, the particle-tracking algorithm is: 1) compute the residence time of a particle at a cell using the RTTF method; and 2) at the end of its stay, send the particle to an adjacent cell randomly, with the probability of traveling to a given cell proportional to the mass flow rate to that cell.

6.4.2 Dispersion

Transport processes such as dispersion can be incorporated into the RTTF particle-tracking algorithm through the use of transfer functions. For dispersion, within a computational cell, the equation for one-dimensional, axial dispersion is applied. The solution desired is the concentration-time breakthrough curve at the outlet of the one-dimensional (1-D) model for a unit step change in inlet concentration. This solution represents the cumulative distribution of travel times for transport with dispersion, which is what is desired for the transfer function. The transport equation and boundary conditions for the 1-D, advective-dispersion equation are (from Eq. 9.9 of Freeze and Cherry 1979 [101173]):

$$R\ \frac{\partial C}{\partial t} = D_{eff}\ \frac{\partial^2 C}{\partial z^2} - v\frac{\partial C}{\partial z} \qquad \text{(Eq. 6-3)}$$

$$C(z,t) = 0, \qquad t = 0 \qquad \text{(Eq. 6-4)}$$

$$C(0,t) = C_0, \qquad z = 0 \qquad \text{(Eq. 6-5)}$$

$$C(z \to \infty, t) = 0, \qquad z \to \infty \qquad \text{(Eq. 6-6)}$$

where

C is the concentration (moles/kg fluid)

C_0 is the injection concentration (moles/kg fluid)

v is the flow velocity (m/s)

D_{eff} is the effective dispersion coefficient (m^2/s), given by $D_{eff} = \alpha v$, where α is the dispersivity of the medium (m).

Here the molecular diffusion coefficient is ignored, since in general it is much smaller than the flow dispersion component of D_{eff}. A non-dimensional version of Equation 6-3 can be obtained by the following transformations: $\hat{C} = C / C_0$, $\hat{z} = z / L$, and $\hat{t} = vt / R\,L$, where L is the flow path length. The solution to Equations 6-3 to 6-6 is obtained after manipulation of Freeze and Cherry (1979 [101173], p. 391, Equation 9.5), yielding:

$$\hat{C} = \frac{1}{2}\left[erfc\left(\frac{\sqrt{Pe}\left(1-\hat{t}\right)}{2\sqrt{\hat{t}}} \right) + e^{Pe}\, erfc\left(\frac{\sqrt{Pe}\left(1+\hat{t}\right)}{2\sqrt{\hat{t}}} \right) \right] \qquad \text{(Eq. 6-7)}$$

where Pe is the Peclet number (dimensionless), $Pe = vL / D_{eff} = L / \alpha$. This solution was obtained from Freeze and Cherry by substituting the definitions of Pe and $\hat{t}$ into the corresponding terms of the Freeze and Cherry equation and performing the needed algebra.

The use of this solution in the RTTF particle-tracking method requires that the transport problem be advection-dominated, such that during the time spent in a computational cell, solute would not tend to spread a significant distance away from that cell. Then, the approximate use of a distribution of times within a single cell will be adequate. Quantitatively, the criterion for applicability is based on the grid Peclet number $Pe_g = \Delta x / \alpha$, where Δx is the characteristic length scale of the computational cell. Note that in contrast to conventional numerical solutions of the advective-dispersion equation, coarse spatial discretization is helpful for satisfying this criterion. Of course, the mesh spacing must still be small enough to provide an accurate flow solution. Highly dispersive transport invalidates the assumptions of the RTTF particle-tracking technique. When dispersion coefficients are large, accurate solutions to the advective-dispersion equation are easily obtained by conventional finite-difference or finite-element techniques, so these techniques should be used instead under these circumstances.

For multi-dimensional flow systems, the dispersion model developed for 1-D systems can be extended to include dispersion coefficient values aligned with the coordinate axes. For this case, the flow direction is determined by the vector drawn from the nodal position of the previous cell to the current cell, and the dispersivity for this flow direction is computed from the equation for an ellipsoid:

$$\alpha = \frac{L}{\sqrt{\Delta x^2 / \alpha_x^2 + \Delta y^2 / \alpha_y^2 + \Delta z^2 / \alpha_z^2}} \quad \text{(Eq. 6-8)}$$

where L now represents the distance from the previous cell to the current cell, Δx, Δy, and Δz are the distances from one grid point to the other in the three coordinate directions, and α_x, α_y, and α_z are the longitudinal dispersivities in the three coordinate directions. The RTTF particle-tracking technique cannot be simply formulated with a longitudinal and transverse dispersion coefficient model, with the tensor aligned with the flow direction, because the flow rates between cells are defined rather than the actual flow velocity at a position. For a dispersion model aligned with the flow direction, a random-walk particle-tracking method such as that of Tompson and Gelhar (1990 [101490]), also implemented in the SZ particle-tracking algorithm of FEHM, or a conventional finite-element or finite-difference solution to the AD equation, such as the reactive transport solution module in FEHM, should be used instead.

The numerical implementation of this technique requires the determination of the dimensionless time $\hat{t}$ in Equation 6-7 for a randomly determined value of the dimensionless concentration $\hat{C}$. This determination is accomplished numerically in the particle-tracking code by fitting Equation 6-7 at selected values of Pe between 1 and 1000 using a piecewise continuous series of straight lines spanning the entire range of values. Then, the value of $\hat{t}$ at an arbitrary value of Pe is computed by linear interpolation between values determined at the Peclet numbers that bracket the actual value. This technique, involving a simple search for the correct type curves, followed by the calculation of two values of $\hat{t}$ and an interpolation, is much more computationally efficient (about a factor of two in cpu time) and robust than an iterative approach to the exact solution using Newton's method. Solutions of adequate accuracy (less than 1% RMS error: see LANL 2003 [166306], Verification and Validation (V&V) Report, tests titled "Tests of Cell-Based Particle Tracking Model") are easily obtained using this linear-interpolation method. This error is trivial compared to the uncertainties being propagated through the model. Therefore, this implementation is adequate for the purposes of the model.

6.4.3 Fracture-Matrix Interaction Submodel

In a dual-permeability system, the transfer of solute mass between fractures and matrix can occur via advection, where fluid movement carries solute from one medium to the other, and matrix diffusion, where molecular diffusion transports mass. Matrix diffusion has been recognized as an important transport mechanism in fractured porous media (e.g., Neretnieks 1980 [101148]; Robinson 1994 [101154]). For many hydrologic flow systems, fluid flow is dominated by fractures because of the orders-of-magnitude larger permeabilities in the fractures compared to the surrounding rock matrix. However, even when fluid in the matrix is completely stagnant, solute can migrate into the matrix via molecular diffusion, resulting in a physical retardation of solute compared to pure fracture transport. This effect has recently been demonstrated on the laboratory scale by Reimus (1995 [101474]) and on the field scale both by Maloszewski and Zuber (1991 [146957]) and in the SZ at Yucca Mountain by Reimus et al. (1999 [126243]). In the UZ at Yucca Mountain, dual-permeability models allow fluid to migrate in both the fractures and the matrix. An additional process that allows solute to transport between the continua is

molecular diffusion. The distribution of travel times through such a system is a complex function of the relative velocities in the two media, the advective flux between the media, the spacing between flowing fractures, matrix diffusion coefficients, and sorption. In this section, we describe the submodel developed to obtain transfer functions suitable for use in dual-permeability systems.

For transport in a dual-permeability system at the field scale, it is important to recognize that the flow model consists of one matrix grid cell for each fracture cell. However, important processes associated with flow and transport occur at scales smaller than those considered in the mountain-scale UZ model, particularly in the immediate region of the matrix adjacent to each flowing fracture. Therefore, the incorporation of fracture-matrix interactions into the model is in essence an upscaling problem. The goal of this development is to utilize a suitable idealized system that captures, at the small scale, important transport processes, and allows this small-scale behavior to be simply upscaled for inclusion in the large-scale model. As we will demonstrate, this upscaling method will allow us to test alternate conceptual models for the fracture/matrix (f/m) interaction model for transport.

To accomplish the upscaling within the particle tracking transport model, we continue to use the transfer function approach, constructing an idealized transport model at the small scale that allows the transfer functions to be tabulated. In a dual-permeability system, transport behavior is vastly different depending on whether solute starts in the fracture or in the matrix. Therefore, the transfer function method is adapted in the UZ transport model to accommodate dual-permeability behavior. The approach consists of using transfer functions to determine both the residence time in a cell, and to determine whether the particle enters the next cell in the fractures or the matrix. In this way, the combined fracture and matrix system will be treated as a unified medium in which there is a distribution of travel times depending on whether the particle enters the cells in the fracture versus the matrix. The transfer functions themselves (described below and in Attachment III) are computed based on an idealized f/m transport model with parallel flow in the fractures and matrix. The steps of the algorithm are as follows (note that the algorithm starts with a known particle location , either in the fracture or matrix continuum):

Step 1. Determine probabilistically whether the particle should move to the other medium due to advective flux to that medium

Step 2. Determine probabilistically whether the particle will leave this cell via the current medium or the other medium

Step 3. Use the conditional transfer function to determine probabilistically the residence time of the particle

Step 4. Determine probabilistically using the relative total flux to adjacent nodes which cell the particle moves to next (whether it starts in the fracture or matrix continuum in the next cell has been determined previously in Step 2).

This approach handles the combined fracture and matrix continua as a single porous medium through which mass travels, and apportions the particles to each continuum according to the diffusive and advective fluxes defined by the flow field and the transport parameters. In the

most general case, the dual-permeability flow model at the mountain scale prescribes a net flow through the fracture continuum, a net flow through the matrix continuum, and a fracture to matrix (or matrix to fracture) fluid flux. To implement this algorithm and allow the transfer function to be computed readily, Step 1 takes the fracture-matrix advective flux term and applies it immediately when the particle enters the cell. Then, after potentially shifting the particle from one medium to the other via advection (with no increase to the travel time), the subsequent transfer functions are based on parallel flow in the two continua with no flux between the continua. This approach, which amounts to a form of upwinding of the fracture-matrix fluid flux term, simplifies the transfer function process by eliminating the need for an additional variable, the fracture-matrix advective flux, in the construction of the transfer function curves. Instead, we assign a probability p_{fm} of the particle transferring to the other medium (Step 1) as

$p_{fm} = 0$ if the fracture-matrix flux term f_{fm} is into the medium in which the particle already resides, or

$p_{fm} = f_{fm}/(f_{fm} + f_{in})$, where f_{in} is the total flux into the continuum in which the particle currently resides.

Step 2 accounts for the fact that there is a finite probability that, due to matrix diffusion, the particle will leave the cell through the other medium regardless of where it starts. In the transfer function approach, we introduce solute mass in the model system (the 2-D Discrete Fracture Model [2DFM]) in either the fracture fluid or the matrix fluid. For the general case of water flow through both the fracture and matrix, mass leaves the DFM via either medium. Therefore, conditional transfer functions must be generated to obtain the probabilities in Step 2. That is, for mass injected with the fracture fluid entering the discrete fracture submodel, there is a breakthrough curve for mass leaving the model via the fracture fluid, and a similar breakthrough curve for mass leaving via the matrix fluid. Similarly, there are two breakthrough curves for mass injected with the matrix fluid. The plateau values attained for a given transfer function curve represents the probability of leaving via a particular medium in Step 2. In other words, the probability of a particle leaving via a given continuum equals the steady state solute mass flux (the plateau of the transfer function curve) divided by the total mass flux through the DFM. This step provides a way to assign probabilities for moving particles between the media via diffusion in a system in which water flows through both continua.

Once Step 2 is completed using the steady state solute mass flux derived from the conditional transfer functions, we now know which transfer function to apply to obtain the residence time for Step 3. This part of the method is identical to that described previously, which is to generate a random number between 0 and 1 and determine the particle residence time from the transfer function.

Finally, Step 4 routes the particle to the appropriate connecting cell in the finite volume domain, as described earlier. If the particle is determined to enter an adjoining cell via the fracture continuum, then the internodal fluxes associated with the fractures are used to define the probabilities of traveling to each connected fracture cell. Similarly, for transport to an adjoining matrix cell, matrix fluxes are used.

The process employed in this model to obtain the transfer functions for the dual permeability transport submodel consists of a series of numerical simulations on the idealized model system shown in Figure 6-5. Because each grid block in the mountain-scale model possesses different hydrologic and transport parameters, a procedure for deriving a non-dimensional form of the submodel is required to make the method practical. Attachment III presents the derivation of the non-dimensional model, and presents the method for generating the transfer function curves. In summary, there are three non-dimensional groups that, if specified, fully capture the range of behavior of the submodel:

$$p_1 = \frac{D_m \tau_f R_f}{B^2 R_m} \quad \text{(Eq. 6-9)}$$

$$p_2 = \frac{D_m \tau_f \theta_m}{bB\theta_f} \quad \text{(Eq. 6-10)}$$

$$p_3 = \frac{\tau_f R_f}{\tau_m R_m} \quad \text{(Eq. 6-11)}$$

In these equations, D_m is the effective diffusion coefficient, τ_f and τ_m are the fluid travel times in the fracture and matrix, respectively, R_f and R_m are the retardation factors in the fracture and matrix, respectively, B is the half-spacing between flowing fractures, b is the fracture half-aperture, and θ_f and θ_m are the volumetric water contents of the fracture and matrix, respectively. For a given parameter vector (p_1, p_2, p_3), there is a unique set of conditional transfer function curves of the form $\hat{C}$ versus $\hat{t}$, where $\hat{C}$ is the normalized breakthrough curve for the non-dimensional time $\hat{t}$ given by

$$\hat{t} = \frac{t}{R_f \tau_f} \quad \text{(Eq. 6-12)}$$

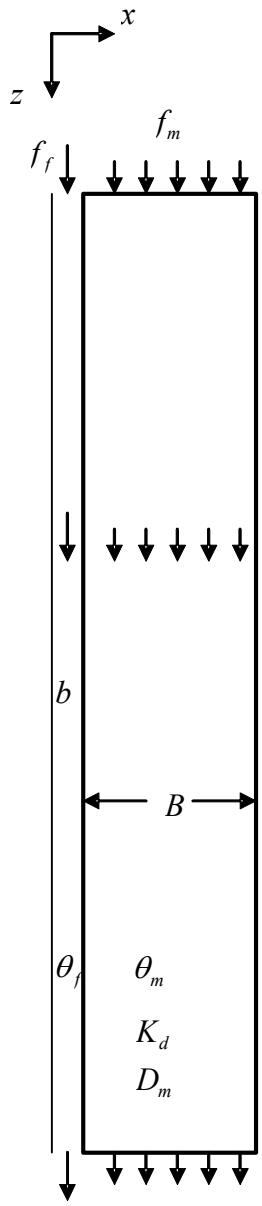

Figure 6-5. Schematic of the Fracture Transport Submodel

The set of conditional transfer function curves consists of a total of four normalized curves for each (p_1, p_2, p_3): mass input in fracture, output in fracture; mass input in fracture, output in matrix; mass input in matrix, output in fracture; and mass input in matrix, output in matrix. This capability for sampling conditional transfer functions associated with the fracture-matrix interaction dual permeability submodel of the UZ transport abstraction model has been implemented and documented in FEHM V2.21 (LANL 2003 [165741]). For details on the generation of the transfer function curves and other important implementation details, see Attachment III.

The final issue associated with implementing the transfer function approach is the means by which the idealized model of Figure 6-5 is simulated. In this abstraction model, we implement

two Alternate Conceptual Models (ACMs) to simulate different types of fracture/matrix (f/m) interaction conceptualizations. In the first ACM, called the DFM formulation, a two-dimensional numerical grid is used with fine discretization in the matrix close to the fracture. This allows sharp gradients in concentration close to the fracture to be captured. The second ACM, called the dual-k formulation, uses a numerical grid with one finite volume cell that is paired with each fracture grid cell. This type of discretization is identical to that used in the dual-k transport formulation of the T2R3D process model. It could be argued that the DFM formulation more accurately captures the small-scale transport processes. However, the dual-k formulation has the advantage of consistency with the model formulation on which the flow simulations are based. Furthermore, as a practical matter, the 3-D process model uses a dual-k formulation for transport, so for benchmarking purposes the dual-k approach is more likely to yield comparable results. The advantage of the transfer function approach used in the particle tracking abstraction model is that both conceptualizations can be implemented easily by using either the DFM or dual-k model grid to generate the transfer function curves. Then, when running the abstraction model, the user selects one or the other set of transfer function curves, and all other input remains the same. Additional details on the behavior of these two f/m interaction submodels are presented in Attachment III.

6.4.4 Multiple Radionuclides With Decay/Ingrowth

The FEHM code (Zyvoloski et al. 1997 [100615]) allows particles to decay with or without the production of the daughter product. For multiple species with decay chains, the code uses the approach outlined below to determine the number of decayed particles, and the code performs the bookkeeping needed to keep track of the locations and numbers of each type of radionuclide. These multiple species can each have their own transport parameters such as sorption and diffusion coefficients.

For decay-ingrowth simulations with time-dependent release of tracer particles, the computational burden increases dramatically with the number of particles in the field. For example, the decay-ingrowth calculation for species *i* decaying into species *j* at a decay rate λ is:

$$N_j = \sum_{m=1}^{N_i} \{1 - \exp[-\lambda(t - t_m)]\} \qquad \text{(Eq. 6-13)}$$

where N_j is the number of particles of species *j* decayed from species *i*, N_i is the number of particles of species *i,* and t_m is the time at which the *m th* particle is injected into the system. If 500,000 particles of species *i* are injected into the system, then at each time step, the number of mathematical operations for ingrowth calculations alone are around 2.5 million. For a simulation time period of 1 million years, the typical calculation requires about 100 time steps. Therefore, the total number of operations for ingrowth calculations will reach 0.25 billion. Therefore, for site-scale simulations, the use of Equation 6-13 would be extremely inefficient.

To reduce the computational burden in simulations, the decay-ingrowth calculation in Equation 6-13 is approximated with an integral by assuming that particles are injected into the system uniformly in time domain. Multiplying both sides of Equation 6-13 by Δt, the average injection time interval between particles, and approximating Equation 6-13 with respect to $t - t_m$:

$$N_j \approx \left\{ (\tau_1 - \tau_2) + \frac{1}{\lambda} \bullet [\exp(-\lambda\tau_1) - \exp(-\lambda\tau_2)] \right\} \Big/ \Delta t \qquad \text{(Eq. 6-14)}$$

where $\tau_1 = t - t_1$ and $\tau_2 = t - t_{Ni}$, t_1 is the time at which particle injection starts, t_{Ni} is the time of the Nth injected particle, and t is the time at which the decay-ingrowth calculation is carried out. The use of Equation 6-14 reduces the number of operations within one time step from millions of operations to just 10, which greatly increases the speed of simulations. Validity of this approach is demonstrated in Figure 6-6.

The accuracy of the integral approach depends on the number of particles and their release history. In general, the use of a greater number of particles increases the accuracy. With respect to release, for the same number of particles, a simulation with a constant release rate will exhibit less error than a time-varying release such as a shorter pulse. If the release rate changes with time, the release period is divided into segments so that within each segment the release rate can be treated as a constant.

Validity of this approach was demonstrated in detail in LANL (2003 [166306]). A FEHM test run from the cited document is summarized in this report to demonstrate the capability of FEHM decay-ingrowth model. Simulation results from the FEHM particle tracking model with decay and ingrowth were verified against results from a semi-analytical solutions for a 4 species chain decay-ingrowth model, CHAIN (van Genuchten 1985 [146961]) The method of comparison for the run is a visual comparison of the plotted results.

For all comparisons of FEHM with the semi-analytical solution for decay-ingrowth simulations, a flow system was developed with the following attributes LANL (2003 [166306]):

- Saturated steady state flow in a 1-D system
- Porosity of 0.3
- Average pore-water velocity was 1.05192×10^{-4} m/year
- Solute with constant injection concentration of 1.0 mol/l released from 0 to 5,000 years at origin x=0. Breakthrough data were collected at x=1 m down stream.
- FEHM grid resolution: 0.005 m
- Longitudinal dispersivity of 0.005 m.

In the test case, a pseudo sequential decay chain is simulated with species $1 \rightarrow 2 \rightarrow 3 \rightarrow 4$, with half lives for species 1 through species 4 of 10,000, 3,000, 10,000, and 4,000 years, respectively. The transport process was dominated by advection and dispersion only with a grid Peclet number of 1.0. In the FEHM simulations, the 5,000 year release period was divided into 50 segments so that each segment corresponding to 100 years. Within each segment, 10,000 particles were injected into the system uniformly over the 100 year period for species 1. There was no source release for the other species, which are generated by the decay-ingrowth model. The retardation factors for species 1 through species 4 were 1.0, 1.0, 1.9, and 1.001, respectively.

The FEHM and CHAIN breakthrough curves are plotted in Figure 6-6. In general, good agreement was observed between FEHM and CHAIN curves. Combined with the suite of validation runs documented in Section 7 of this Model Report, this simulation demonstrates that the particle tracking model accurately handles decay chains and, thus, is suitable for use in simulating multiple radionuclides in the UZ transport model.

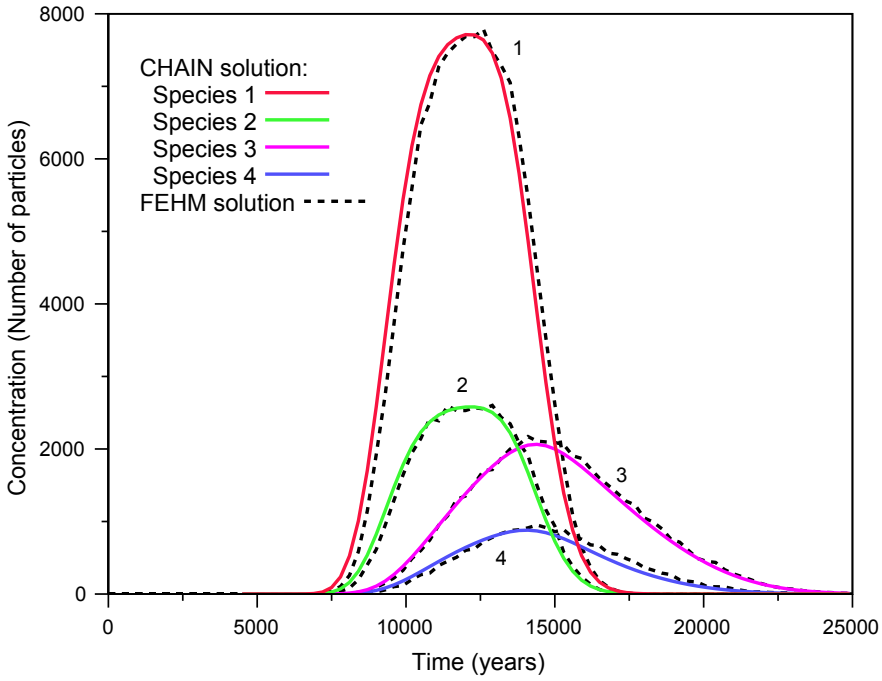

Figure 6-6. Comparison of Software CHAIN and FEHM Transport Results for a Case with a 4-Member Decay-Ingrowth CHAIN and a Retardation Factor of 1.9 for Species 3. Peclet Number = 1.0 (used for comparative purposes only; taken from Fig. 59 of LANL 2003 [166306]).

6.4.5 Colloid Transport

For colloid-facilitated transport, the transport equations for matrix diffusion, with either the semi-infinite or finite fracture spacings, can be simply revised. Given the assumptions listed in Section 5, the expression for transport for contaminant on colloids is analogous to Eq. 6-3 earlier (from Eq. 9.9 of Freeze and Cherry 1979 [101173]):

$$R_{coll}\frac{\partial C_{coll}}{\partial t} = D_{eff}\frac{\partial^2 C_{coll}}{\partial z^2} - v\frac{\partial C_{coll}}{\partial z} \qquad \text{(Eq. 6-15)}$$

where D_{eff} is the same as for an aqueous solute and R_{coll} is the colloid retardation factor. The governing equation for the corresponding dissolved contaminant moving in fractures with interactions with matrix blocks but without decay can be derived from Equation (1) of Sudicky and Frind (1982 [105043]) and re-written as:

$$R_f\frac{\partial C}{\partial t} = D_{eff}\frac{\partial^2 C}{\partial z^2} - v\frac{\partial C}{\partial z} - \frac{q}{b} \qquad \text{(Eq. 6-15a)}$$

where R_f is the retardation factor of the dissolved contaminant, b is half of the fracture aperture, and q (mass per time per unit area) is the mass exchange rate through fracture-matrix interface.

Combining Equations 6-15 and 6-15a, and making use of the relation $K_c = C_{coll} / C$:

$$\left(\frac{R_f + K_c R_{coll}}{1 + K_c} \right) \frac{\partial C}{\partial t} = D_{eff} \frac{\partial^2 C}{\partial z^2} - \nu \frac{\partial C}{\partial z} - \frac{q}{b(1 + K_c)} \quad \text{(Eq. 6-16)}$$

This equation can be recognized as being analogous to the matrix diffusion model of Sudicky and Frind (1982 [105043], Eq. 1), with the exception of a different term preceding the time derivative and a modified denominator of the term involving diffusive flux q. Mathematically, this implies that the transport equation for matrix diffusion can be revised to include colloid facilitated transport by replacing the half-aperture b by

$$b_{coll} = (1 + K_c) b \quad \text{(Eq. 6-17)}$$

And the retardation factor in the fracture by

$$R_{f,coll} = \frac{R_f + K_c R_{coll}}{1 + K_c} \quad \text{(Eq. 6-18)}$$

These relationships are built into the FEHM particle-tracking code, so that the additional terms K_c and R_{coll} are provided as inputs. Note that to simulate a radionuclide irreversibly attached to colloids, one should set a large value of K_c (say, 1.e20) so that the radionuclide essentially travels without diffusion. Then, either a retarded or unretarded colloidally bound radionuclide is simulated by setting R_{coll} to a number greater than or equal to 1.

In addition to the transport of radionuclides bound to colloids, there are several mechanisms related to the migration of the colloids themselves that can be simulated in the model. Above, the reversible retardation factor for colloid migration R_{coll} was introduced. In addition, the model parameterization provides a means for accounting for colloid size and surface charge effects. When the colloid size and/or surface properties preclude their transport into a porous medium, size exclusion and/or filtration can occur. In the particle-tracking module, models have been implemented for these processes. For advective flow from fracture to matrix in the dual-permeability model, a size-exclusion model is implemented whereby colloids can remain in the fracture in proportions greater than the relative flow rate entering the matrix. A size exclusion parameter $f_{coll} \leq 1$ is defined such that the probability of particles entering the matrix due to advective transport is multiplied by this factor. Therefore, complete exclusion from the matrix is obtained by setting $f_{coll} = 0$, whereas aqueous solute behavior is retained by setting $f_{coll} = 1$. Filtration, resulting in complete immobilization of the particle, can also be simulated at specified interfaces within either the fracture or matrix continua. To invoke this mechanism, a filtration factor f_{filt} at an interface (the finite element connections between two specified zones in an FEHM simulation) is defined. If a particle is slated to pass from one zone to the other via

advective transport, f_{filt} is the probability the particle continues moving, $(1 - f_{filt})$ is the probability that it is irreversibly removed by filtration).

When using the filtration option, a word of caution is warranted. Colloid simulations are typically used to provide a mechanism for radionuclides to travel in the water bound to colloids. Filtration renders the colloids immobile, which, in reality, only renders the radionuclide immobile if it is irreversibly bound to the colloid. When the radionuclide is only weakly sorbed to the colloid, the filtration option will artificially remove radionuclide mass from the system, resulting in a non-conservative simulation. Therefore, the filtration option should only be invoked for irreversibly bound radionuclides or when simulating colloid tracer experiments. The reversible model, using R_{coll} to delay the migration, should be used instead for colloid-facilitated transport of radionuclides.

6.4.6 Particle Sources and Sinks

There are two methods for introducing particles into the flow system: particles are (1) either injected with the source fluid entering the model domain or (2) released at a particular cell or set of cells. The first method is used to track source fluid as it passes through the system. The number of particles entering with the source fluid at each cell is proportional to the source flow rate at that cell, which is equivalent to injecting fluid with a constant solute concentration. For Method 2, an arbitrary number of particles are released at each specified cell, regardless of the source flow rate. In the present application, Method 2 is used to input particles, which are used to represent radionuclide mass into the system at the repository level.

Within Method 2, there are various ways to input a time-varying source of particles. For stand-alone simulations, the particles are inserted at a constant rate for a specified duration. There is also an option, used when the FEHM code is coupled with GoldSim (BSC 2003 [161572]), to input a time-varying and spatially varying source mass flux into the model. The details of the method for accepting complex sources of multiple radionuclides from the EBS model are discussed in the next section.

When fluid exits the model domain at a sink, the model treats this flow as another outlet flow from the cell. The decision of whether the particle leaves the system or travels to an adjacent cell is then made on a probabilistic basis, just as though the fluid sink were another connected cell. Thus, the complexities discussed by Zheng (1994 [101503]) for handling a so-called weak sink are avoided in the RTTF particle-tracking model.

6.4.7 EBS Random Release Model for Radionuclide Source Terms

If waste packages containing high level radionuclide material in the repository eventually fail due to corrosion, the process will almost certainly be variable in both space and time. At early times, a few packages may fail, releasing radionuclides into the UZ. At later times, a greater number of packages may fail. In Viability Assessment calculations (DOE 1998 [100547], Figure 4-10), releases from the EBS to UZ were spread over the entire repository sub-regions. Such treatment of the EBS release could result in significant artificial dilution of the UZ transport source term. In reality, waste packages may not fail uniformly in space and time. Rather, a few waste packages may fail at early times, while others may fail gradually over longer

time periods. An EBS random release model was developed in FEHM to allow the model to simulate early failed packages and time- and spatially variable radionuclide releases.

To begin, a repository is defined consisting of N_large sub-regions. Each sub-region contains certain number of waste packages. Initially, M_fine packages fail at locations designated by package x-y locations (x,y). The M_fine failed packages release radionuclides at a mass flow rate of M_flux_i, where i is the ith failed package.

With time, packages fail in the sub-regions of the repository. At each time step, there are a certain number of failed packages in each sub-region i. The mass flux released from those packages is denoted as N_large_flux for the i^{th} sub-region. In this model, the release nodes in the numerical grid for the failed packages are randomly selected from the available repository nodes within that sub-region to mimic the failure process of the waste packages. The mass release of M_fine packages is separated from those of the other failed packages.

To simulate the impact of the EBS random release on system performance at the Yucca Mountain site, the FEHM EBS random release model was developed to perform the following tasks:

- Locate the M_fine early failed package nodes in repository sub-regions based on given failed package coordinates. If no node matches a given coordinate, then select the nearest node to the given coordinate. Note that in the current version of the TSPA model, the M_fine user option is not used. However, because it is still in the code, the GoldSim (BSC 2003 [161572]) calling program passes M_fine = 0 to FEHM.

- Randomly select the failed package nodes in the designated sub-region i.

- Release particle into the selected fracture or matrix nodes based on the fracture flow fraction data passed from EBS.

For a species, a particle can be released into a fracture node or a matrix node. The probability of the particle being released into the fracture node is proportional to the fracture fractional flow data from EBS. At run time, a random number is generated for each particle, if the random number is smaller than the fracture fractional flow data, then the particle will be released into the selected fracture node. Otherwise, the particle will be injected into the matrix node corresponding to the selected fracture node.

From FEHM particle-tracking subroutine *part_tr*ack, subroutine *getrip* is called to determine the particle release locations. First, the subroutine obtains information passed by GoldSim (BSC 2003 [161572]) in an input 1-D array called in[ ]. The structure of the in[ ] array is shown in Figure 6-7.

time	flow field index	parameter index	M_fine, # of early failed packages	(x,y) coordinates of early failed packages (M_fine)	N_large, # of repository sub-regions	List # of failed packages in each sub-region (N_large)	Number of species or the product of number of species and N_large	Optional input. default value: 1. Fracture fractional flow data for each species (N_large x #_of_species)	Mass input flag. 0: no mass input 1: there is mass input	# of in put buffers, M_fine+N_large	# of output buffers	Mass release for each species during the current time step. Values are passed first for the early failed packages for all species from the first releasing node to the M_fine th node. Then, from the first sub-region to the N_large th sub-region (M_fine+N_large) x number_of_species

Figure 6-7. The Structure of the in [ ] Array Passed to FEHM from GoldSim

The algorithm used in FEHM EBS random release model is summarized in Figure 6-8, the flow chart of the EBS random release model.

Starting with the M_fine early failed packages, *getrip* extracts the (x,y) coordinates of the early failed packages and loops through each repository sub-region node to select the one that is closest to the given coordinates. To prevent a node being selected more than once for two or more given coordinates, getrip checks the selected nodes for overlapping. If overlapping is found, *getrip* prints out error messages to the error file fehmn.err, then stops the program.

When the selection of M_fine nodes is complete, *getrip* extracts the number of failed packages in each sub-region for the N_large sub-regions. The number of failed packages at the current time step is compared with the values at the previous time step to determine the number of newly failed packages, N_newly_failed, within the current time step in each sub-region. Then, *getrip* randomly selects N_newly_failed nodes within the corresponding sub-region. The selected failed nodes are stored in the memory for use in releasing radionuclides and are removed from the base of available repository nodes. If the number of failed packages is larger than the number of nodes in a sub-region, then radionuclide will be released from all nodes within the sub-region. Once all nodes of failed packages are determined, *getrip* allocates the number of released particles proportionally to the mass flux values of each failed package. Then, subroutine *setmptr* is called to inject particles into the system for each species.

When the locations/coordinates of M_fine early failed packages are unknown, the user can simulate the effect of early failed packages on UZ transport by passing the number of early failed packages in the N_large sub-regions to FEHM. FEHM then randomly selects the locations of the early failed packages and releases particles into the UZ as described in the paragraph above. Using this option, the user will pass M_fine=0 to FEHM and omit the coordinates of the early failed packages (the 5th data block in Figure 6-7 is not needed).

To investigate the influence of matrix diffusion on UZ transport behavior, a radionuclide can be released from either a fracture node or a matrix node. The probability of the particle to be released from a fracture node is proportional to the fracture fractional flow data passed from GoldSim to FEHM in the input array in[ ] (Figure 6-7). At run time, a random number is generated, when the generated random number is smaller than the given fracture fraction flow, the particle is released from a selected fracture node. Otherwise, the particle is released through a selected matrix node.

In the case of radionuclide release as gas phase and transport through geosphere, TSPA treats the released mass as aqueous phase. This is expected to bound any dose effects of gas-phase release due to the large dilution of gas-phase release in the atmosphere (*Features, Events, and Processes in UZ Flow and Transport,* BSC 2003 [164873])

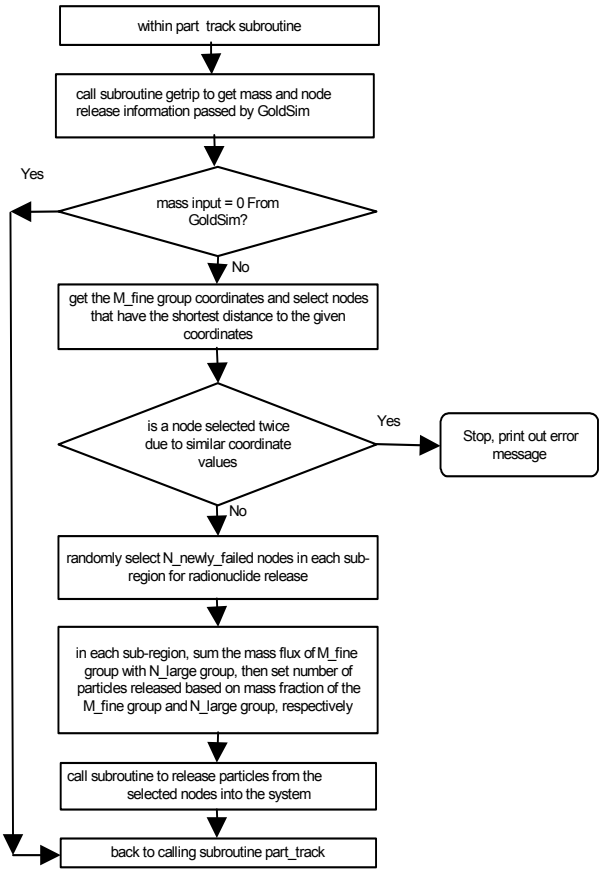

Figure 6-8. Flow Chart of EBS Random Release Model

6.4.8 Transient Fluid Flow

When the RTTF particle-tracking method is implemented for a time-varying fluid flow system, the approach is somewhat more complex but still tractable. Consider a numerical simulation in which a discrete time step is taken at time t and a new fluid flow field is computed. In this model, the new fluid flow time $t_{new} = t + \Delta t$ is treated as an intermediate time at which the particle-tracking calculation must stop. The time is intermediate because if the flow field is at steady state, there is no reason to stop at any time before the end of the simulation except to record particle information for output or processing purposes. The fate of all particles is tracked from time t to time t_{new} assuming that the flow field is constant over this time interval. When the simulation reaches t_{new}, the position (cell number) of the particle is recorded, along with its fractional time remaining at the cell and the randomly generated y-coordinate of the transfer function used for that particle in the cell. When the new fluid flow solution is established, the remaining residence time for a particle is determined from the following steps:

1. Compute a new fluid residence time τ_f.

2. Using the *y*-coordinate of the transfer function previously computed and the new transfer function, calculate a new particle residence time.

3. Multiply this time by the fractional time remaining in the cell to obtain the remaining time in the cell.

This method approximates the behavior in a transient system, while reducing to the behavior that would be obtained in an unchanging flow field had the calculation not been forced to stop at the intermediate time.

Another transient effect that must be considered is that the sum of the outlet mass flow rates $\sum \dot{m}_{out}$ in Equation 6-1 does not necessarily equal the sum of the inlet mass flow rates. When there is net fluid flow into a cell, the particle-tracking algorithm uses the sum of the inlet flow rates in Equation 6-1, whereas Equation 6-1 itself is used when there is net outflow from a cell. Finally, with respect to the transfer function methodology outlined in Section 6.4.3, when the climate changes, the code redefines the parameters in Equations 6-9, 6-10, and 6-11, and uses these parameters and the new flow field to continue the transport simulation.

6.4.9 Climate Change and Water Table Rise

One important factor that could affect the performance of the repository is future climate changes. As it is difficult and time consuming to simulate the transition of flow fields from one climate to another, in TSPA several pre-generated flow fields are used to represent the corresponding climates. These flow fields are developed in BSC 2003 [163045], and are converted to FEHM-compatible flow fields in DTN: LB0305TSPA18FF.001 [165625]. This approach treats flow in the system as a sequence of steady states (CRWMS M&O 2000 [153246], Section 3.2.3.1). For TSPA simulations, those pre-generated flow fields are read in by FEHM at run time and whenever the GoldSim (BSC 2003 [161572]) model signals to FEHM that the climate is changing. From that point until the climate changes again, the flow field is assumed to be steady. Section 6.4.8 details the numerical approach for handling varying flow fields.

It is expected that the water table will be higher in future climates (CRWMS M&O [153246], Section 3.7.2). One issue related to climate change is water table rise. In the UZ transport model abstraction, water table is switched instantaneously from one climate to another when climate changes. Any radionuclides (in the form of particles in the particle tracking model) below the new water table are immediately removed from the UZ and sent to SZ. This approach is conservative as both the flow field and water table are immediately switched to the wetter climate at time of climate change, which not only accelerates the movement of radionuclides in the system but also tends to result in instantaneous pulses of radionuclides into the SZ.

To set the water table elevation to a higher value than that used for the development of the flow fields in DTN: LB0305TSPA18FF.001 [165625], the flow field files must be post-processed using the software WTRISE (LBNL 2003 [163453]). This has not been done in this abstraction model because the calculations presented are being compared to process model results that assumed the present-day water table for the future climate modeling. For TSPA-LA model calculations, this processing step has been performed for all flow fields of future, wetter climates. The use of WTRISE requires the specification of a water table elevation under the future climate scenarios. The code adjusts the flow field for all grid blocks beneath this elevation to force particles to immediately leave when reaching any of these grid blocks. Therefore, an

elevation for the higher water table must be selected. Forester et al. (1999 [109425], p. 56) suggests that site data are consistent with past water table elevations up to 120 m higher than present day elevations. Because the water table is not flat, a nominal elevation for the present-day water table must be selected and the future water table must then be based on that selection. For the typical water table elevation under present day conditions beneath the repository of 730 m (BSC 2003 [162649], Section 6.4.5.1), a rise of 120 m results in an elevation of 850 m. As a comparison, note that BSC 2003 [162649], Section 6.4.5.1 performed an analysis in which the water table was assumed to be 100 m higher than present-day, but processed the water table to parallel the present-day water table at all locations. Figure 6.4-8 of BSC 2003 [162649] shows that for the future water table analysis used to investigate the impact on SZ processes, the 850 m elevation contours passes through the repository footprint. Therefore, choosing an elevation of 850 m for processing the UZ flow fields for the future climate cases is consistent with available site data, and is consistent with SZ studies. Furthermore, since there is no site data or numerical modeling available to form a basis for selecting different water table elevations for the various future climate states, the 850 m elevation should be used for all future climate flow fields. With respect to UZ transport to the water table, this approximation should be conservative because a reasonable maximum elevation, resulting in a minimum for the UZ flow path length, is used for all future climates. The flow fields processed to incorporate the higher water table for the future, wetter climates are available in DTN: LB0312TSPA06FF.001 [166671].

6.4.10 Interface With GoldSim

The interface between GoldSim and FEHM establishes a protocol for defining the radionuclide sources to the UZ transport model (provided by GoldSim (BSC 2003 [161572]), the definition of a particular flow field for FEHM to use, and exit mass fluxes of radionuclides from the UZ model (from FEHM to GoldSim based on the particle-tracking simulation). This protocol is quite flexible, allowing an arbitrary number of source regions, radionuclides, exit regions, and flow fields to be defined and passed between GoldSim and FEHM through the FEHM subroutine call statement. Figure 6-9 shows a simplified flow chart of the GoldSim-FEHM coupling.

During a GoldSim simulation, FEHM cedes control of the time step to GoldSim. At each time, GoldSim provides a flag defining the flow field and the mass flux inputs of radionuclides. By changing the flow field during a simulation, the model can simulate the impact of a climate-induced change in the UZ system. When this occurs, FEHM reads in the new flow field and proceeds with the transport simulation (see Section 6.4.8). Since each flow field is a steady state flow field, the implicit assumption is a quasi-steady one, that is, the system establishes a new steady state rapidly in comparison to transport velocities through the UZ. At the end of each time step, FEHM passes back to GoldSim the exiting mass flux values from the UZ model.

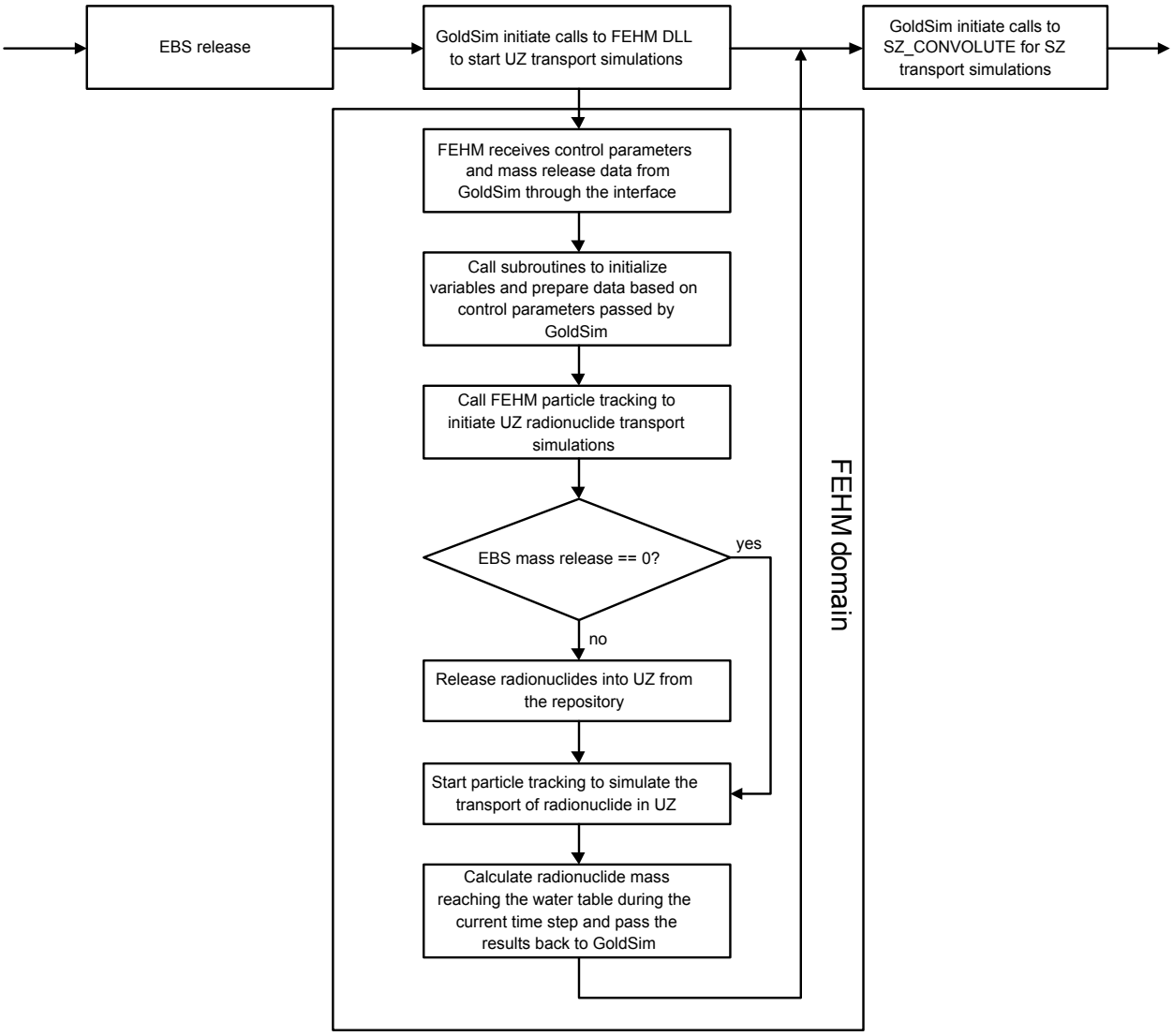

Figure 6-9. Schematic Flow Chart of GoldSim-FEHM Coupling

6.5 TRANSPORT MODEL INPUTS

The top boundary of the transport model is the repository where radionuclides are released from the EBS into the system. The strength of the source release varies with time and depends on the failure rate of the waste packages.

At the bottom boundary (the water table), radionuclides are removed from the UZ system and become the source term for the SZ model.

The side boundaries of the transport model are no-flow boundaries.

The initial condition of the transport model is set to a concentration of zero for all radionuclides.

Strength of the different transport mechanisms depends on the values of their corresponding parameters that are inputs to the transport model. Parameters read in by FEHM as input to the transport model include

- Dispersivity (m)
- Matrix porosity and rock density (kg/m^3)
- Matrix adsorption coefficient (mL/g)
- Matrix diffusion coefficient (m^2/sec)
- Fracture residual saturation and fracture gamma parameters (unitless)
- Fracture porosity, fracture spacing (m), and fracture aperture (m)
- Fracture surface retardation factor (unitless)
- Colloid size distribution, colloid Kc, colloid Rc, and colloid filtration factor
- Radionuclide half lives (years) and daughter products.

For layers above the repository, placeholder values for these transport parameters are used in the input files for the model, but these values are not germane to the model results because radionuclide particles do not pass through these units. Beyond the above transport parameters, at run time, FEHM also reads in the pre-generated flow fields and property zone data. Those data are inputs from UZ flow model to the transport model.

The sub-sections below give a more detailed discussion about each parameter.

6.5.1 Pre-generated Flow Fields

In TSPA runs, a total of 9 base case flow fields corresponding to 9 climate scenarios, present day [low, mean, and high], glacial transition [low, mean, and high], and monsoon [low, mean, and high], are pre-generated and fed into FEHM.

The flow fields are based on the dual permeability/dual porosity model formulation that allows water flow in both fractures and the corresponding matrix blocks. A total of 120,711 physical nodes are used to discretize the Yucca Mountain Project site. For the dual permeability/dual porosity model, at any physical node, there is a fracture node and a corresponding matrix node. Thus, the flow model has a total of 241,422 flow nodes (DTN: LB0305TSPA18FF.001 [165625]).

The UZ flow model is characterized by potential lateral flow in the PTn unit, the occurrence of perched water within low-permeability zeolites in the CHn or the densely welded basal vitrophyre of the TSw unit, and the effects of faults on the UZ flow system (BSC 2003 [163045]).

In TSPA-LA runs, all the 9 base case flow fields will be used in the corresponding climates. The name of the flow fields and corresponding files are listed in Table 4-1.

6.5.2 Dispersivity

Yucca Mountain site-scale flow models have indicated that flow in the fractured rock system is dominated by fast fracture flow (CRWMS M&O 2000 [134732], Section 6.2.2, Figure 8). In

such a system, radionuclide transport is primarily advection dominated, and the influence of dispersion on radionuclide transport is not important (CRWMS M&O 2000 [148384], Section 6.3.6).

There are few data available on dispersivity distributions at Yucca Mountain site. (Neuman 1990 [101464]) showed that field dispersivity varied with the scale of study. Field tracer tests at the C-holes at Yucca Mountain also showed that on a 100 m scale, field dispersivity had a range of approximately 3 to 63 m (BSC 2003 [162415], Table 6.3-10).

In past simulations (CRWMS M&O 2000 [148384], Section 6.3.6), the dispersivity values of all units had a value of 20 m.

Sensitivity studies from TSPA-SR, using flow conditions and dispersivity values representative of the UZ at Yucca Mountain, showed that transport of radionuclides is not sensitive to variations in dispersivities within the UZ. Use of a dispersivity greater than 20 m does not show any significant effect on radionuclide peak concentration or arrival time (CRWMS M&O 2000 [148384], Section 6.3.6, Figures 6-156 and 6-157).

In TSPA-LA, the fracture dispersivity is set at 10 m. This is toward the lower end of the value from field studies (BSC 2003 [162415], Table 6.3-10). Although the impact of dispersivity should be very small, the value chosen should be conservative, as higher dispersivity tends to spread the radionuclide plume and reduce the peak value. While it can be argued that for a decaying species, higher dispersivity can allow a greater fraction of the mass to arrive downstream before decaying, the point here is that in comparison to diffusion and large scale heterogeneities, dispersivity effects have a very small influence on the breakthrough curves.

Table 6-2. Dispersivity Used in UZ Transport Model

Input Name	Input Description	Input Sources	Value (units)	Type of Uncertainty
Fracture dispersivity	Input to FEHM for simulating dispersion effect	BSC 2003 [162415], Table 6.3-10 *Saturated Zone In-Situ Testing*.	10 m	Fixed value

Because the dual permeability abstraction model treats the combined fracture-matrix system as a unified continuum, this dispersivity applies to the medium as a whole. Therefore, the model does not distinguish between fracture dispersivity and matrix dispersivity.

6.5.3 Matrix Porosity and Rock Density

Matrix porosity is used to calculate the matrix pore volume associated with each matrix block. The pore volume data are then multiplied by the corresponding water saturation data to determine the fluid volume in a cell.

Matrix porosity and rock density values combined with rock adsorption coefficient and water saturation are used for calculating matrix retardation factors used in simulating the adsorption effect on radionuclide transport.

Values of matrix porosity are from the Technical Data Management System (TDMS) (DTN: LB0305TSPA18FF.001[165625]) and listed in Table 6-3.

Table 6-3. Matrix Porosities Used in the Transport Model

Matrix Layer	Matrix Porosity	Input Description	Input Source	Type of Uncertainty
tcwm1	2.41E-01	Matrix porosity values is used in determining matrix pore volume, simulating matrix diffusion effect, and calculating matrix adsorption coefficient	LB0305TSPA18FF.001 [165625] *"Eighteen 3-D Site Scale UZ Flow Fields Converted from TOUGH2 to T2FEHM format." TOUGH2 file: glaq_uA.dat*	Fixed values for each layer but varies from layer to layer
tcwm2	8.80E-02			
tcwm3	2.00E-01			
ptnm1	3.87E-01			
ptnm2	4.38E-01			
ptnm3	2.54E-01			
ptnm4	4.11E-01			
ptnm5	4.99E-01			
ptnm6	4.92E-01			
tswm1	5.40E-02			
tswm2	1.57E-01			
tswm3	1.55E-01			
tswm4	1.11E-01			
tswm5	1.31E-01			
tswm6	1.03E-01			
tswm7	1.03E-01			
tswm8	4.30E-02			
tswmv	2.29E-01			
tswmz	2.75E-01			
ch1mv	3.31E-01			
ch2mv	3.46E-01			
ch3mv	3.46E-01			
ch4mv	3.46E-01			
ch5mv	3.46E-01			
ch6mv	3.31E-01			
ch1mz	2.85E-01			
ch2mz	3.22E-01			
ch3mz	3.22E-01			
ch4mz	3.22E-01			
ch5mz	3.22E-01			
ch6mz	2.71E-01			
pp4mz	3.21E-01			
pp3md	3.18E-01			
pp2md	2.21E-01			

Table 6-3. Matrix Porosities Used of the Transport Model (Continued)

Matrix Layer	Matrix Porosity	Input Description	Input Source	Type of Uncertainty
pp1mz	2.97E-01			
bf3md	1.75E-01			
bf2mz	2.34E-01			
tr3md	1.75E-01			
tr2mz	2.34E-01			
pcm38	4.30E-02			
pcm39	2.75E-01			
pcm1z	2.85E-01			
pcm2z	3.22E-01			
pcm5z	3.22E-01			
pcm6z	2.71E-01			
pcm4p	3.21E-01			

Rock density values are from the TDMS (DTN: LB0210THRMLPRP.001 [160799]) and are listed in Table 6-4 below.

Table 6-4. Matrix Rock Density Values

Matrix Layer	Rock Density (kg/m^3)	Input Description	Input Source	Type of Uncertainty
tcwm1	2514.	Rock density data are used by FEHM in the calculation of matrix adsorption coefficient	LB0210THRMLPRP.001 [160799] *"Thermal Properties of UZ Model Layers: Data Summary"*	Fixed values for each layer but varies from layer to layer
tcwm2	2514.			
tcwm3	2274.			
ptnm1	2288.			
ptnm2	2288.			
ptnm3	2288.			
ptnm4	2288.			
ptnm5	2288.			
ptnm6	2283.			
tswm1	2274			
tswm2	2514.			
tswm3	2358.			
tswm4	2466.			
tswm5	2325.			
tswm6	2473.			
tswm7	2473.			
tswm8/pcm38	2274.			
tswm9/pcm39/tswmv/tswmz	2274.			
ch1mv	2288.			
ch2mv	2256.			
ch3mv	2256.			
ch4mv	2256.			

Table 6-4. Matrix Rock Density Values (Continued)

Matrix Layer	Rock Density (kg/m^3)	Input Description	Input Source	Type of Uncertainty
ch5mv	2256.			
ch6mv	2256			
ch1mz/pcm1z	2288.			
ch2mz/pcm2z	2256.			
ch3mz	2256.			
ch4mz	2256.			
ch5mz/pcm5z	2256.			
ch6mz/pcm6z	2256.			
pp4mz/pcm4p	2103.			
pp3md	2103			
pp2md	2385.			
pp1mz	2038.			
bf3md	2106.			
bf2mz	2012.			
tr3md	2371.			
tr2mz	2224			
Fault Zone Rock Density Data				
tcw	2394			
ptn	2286			
tsw	2368			
chn	2198			

6.5.4 Matrix Adsorption Coefficient (mL/g)

Dissolved radionuclide waste traveling through the matrix can be retarded due to adsorption on to the surface of the porous matrix material. In TSPA-LA runs, the linear adsorption model is used to describe the partitioning of radionuclides between the solute and the matrix through the UZ system. Matrix adsorption coefficients can be read in by FEHM at run time. The values are then used to calculate matrix rock retardation factors of different radionuclides. The validity of the linear equilibrium assumption (Section 5, assumption 4) and the derivation of adsorption coefficient distributions based on laboratory experiment data are documented in Model Report, *Radionuclide Transport Models Under Ambient Conditions* (BSC 2003 [163228]).

The strength of matrix adsorption depends on the properties of the rock material and the radionuclides. Matrix adsorption coefficients for different rock types (zeolitic, devitrified, and vitric) are taken from the TDMS (DTN: LA0302AM831341.002 [162575]). Values of the adsorption coefficient are divided into three groups based on rock type (e.g., devitrified, vitric, and zeolitic). Table 6-5 lists the statistical distribution of matrix adsorption coefficient for different radionuclide types.

To address the influence of adsorption coefficient uncertainty on system performance, the matrix adsorption coefficients of each species are pre-sampled for each rock type (based on the listed

distribution values in Table 6-5) for each TSPA realization. For a discussion on the method of correlating sorption coefficients to one another in the stochastic sampling of parameters, see Attachment II of BSC (2003 [163228]).

Table 6-5. Sorption-Coefficient Distributions for Unsaturated Zone Units

Species	Rock Type	Type of Uncertainty	Coefficients describing distribution (Kd: mL/g)	Input Description
U	Zeolitic	Cumulative	(Kd value, probability) (0, 0) (0.5, 0.5) (30., 1.0)	The matrix adsorption coefficient data are read in at run time by FEHM for simulating the effect of matrix adsorption on radionuclide transport.
	Devitrified	Cumulative	(Kd value, probability) (0, 0) (0.2, 0.5) (4., 1.0)	
	Vitric	Cumulative	(Kd value, probability) (0, 0) (0.2, 0.5) (3., 1.0)	
Np	Zeolitic	Cumulative	(Kd value, probability) (0, 0) (0.5, 0.5) (6., 1.0)	
	Devitrified	Cumulative	(Kd value, probability) (0, 0) (0.5, 0.5) (6., 1.0)	
	Vitric	Cumulative	(Kd value, probability) (0, 0) (1.0, 0.5) (3., 1.0)	
Pu	Zeolitic	Cumulative	(Kd value, probability) (10., 0) (100., 0.5) (200., 1.0)	
	Devitrified	Cumulative	(Kd value, probability) (10., 0) (70., 0.5) (200., 1.0)	
	Vitric	Cumulative	(Kd value, probability) (10., 0) (100., 0.5) (200., 1.0)	
Am	Zeolitic	Uniform	range= 100 - 1000	
	Devitrified	Uniform	range= 100 - 2000	
	Vitric	Cumulative	(Kd value, probability) (100., 0) (400., 0.5) (1000., 1.0)	
Pa	Zeolitic	Uniform	range= 1000 – 20,000	
	Devitrified	Uniform	range= 1000 – 20,000	
	Vitric	Uniform	range= 1000 – 20,000	
Cs	Zeolitic	Cumulative	(Kd value, probability) (425., 0) (5,000., 0.5) (20,000., 1.0)	
	Devitrified	Uniform	range = 1 - 15	
	Vitric	Cumulative	(Kd value, probability) (0., 0) (2., 0.5) (100., 1.0)	
Sr	Zeolitic	Uniform	range = 50 - 2000	
	Devitrified	Uniform	range = 10 - 70	
	Vitric	Uniform	range = 0 - 50	
Ra	Zeolitic	Uniform	range = 1000 - 5000	
	Devitrified	Uniform	range = 100 - 1000	
	Vitric	Uniform	range = 50 - 600	
Th	Zeolitic	Uniform	range = 1000 - 30,000 mL/g	
	Devitrified	Uniform	range = 1000 - 10,000 mL/g	
	Vitric	Uniform	range = 1000 - 10,000 mL/g	

DTN: LA0302AM831341.002 [162575]

6.5.5 Matrix Diffusion Coefficient (m^2/sec)

It has been shown that matrix diffusion combined with matrix adsorption can play an important role in slowing the movement of radionuclides in fractured rocks (Sudicky and Frind 1982 [105043]).

A matrix diffusion coefficient is used in FEHM for simulating the effect of matrix diffusion on radionuclide transport in the fractured media. Values of matrix diffusion coefficient affect the strength of fracture-matrix interaction due to diffusion of radionuclides.

In the Radionuclide Transport Process Model documented in BSC 2003 [163228], the diffusive flux is defined in terms of the concentration gradient and the effective diffusion coefficient, which is the product of the free diffusion coefficient and the tortuosity. BSC 2003 [163228] show, based on work by Grathwohl (2000 [141512]) that it is a reasonable approximation to set tortuosity equal to the matrix porosity. The abstraction model calls for the effective diffusion coefficient as a direct parameter input, rather than separately defining tortuosity and free diffusion coefficient. In the development below, correlations between effective diffusion coefficient, water content, and matrix permeability are proposed based on available experimental data. The end result of this development is a range of effective diffusion coefficients that in effect capture the uncertainty in the mechanisms associated with diffusion through tortuous pore spaces. Therefore, even though the tortuosity is not a direct model input, its impact on matrix diffusion, and the correlation between diffusion and matrix porosity, is implicitly captured in the abstraction model.

In current TSPA simulations, unsaturated matrix diffusion coefficients are based on the correlation between matrix diffusion, porosity, and saturated permeability developed for the SZ (Reimus et al. 2002 [163008]). To adapt the relationship for the UZ, the porosity is replaced with water content and the permeability is replaced with effective permeability. The equation is re-written as

$$\log\left(D_m\right) = -3.49 + 1.38\theta_m + 0.165\log\left(k_m\right) \qquad \text{(Eq. 6-19)}$$

where D_m is the matrix diffusion coefficient in cm^2/s, θ_m is the matrix water content, and k_m is the effective permeability to water in m^2.

The data from Reimus et al. (2002 [163008]) suggests that the range of diffusion coefficients for tritium, bicarbonate, and pertechnetate individually are roughly similar to the range of mean values for each. This suggests that a single broad distribution scaled by the range of values between cations and anions from DTN: LA0003JC831362.001 [149557] would provide a better representation of the uncertainty in matrix diffusion. To capture this with the correlation given by Reimus et al. (2002 [163008]), consider the following transformation:

$$X = \log\left(\frac{D_0}{D_m}\right) \qquad \text{(Eq. 6-20)}$$

where D_0 is the limiting upper value for D_m. This value is given in DTN: LA0003JC831362.001 [149557] as 10^{-9} m^2/s. The average for X is

$$\mu_X = \log(D_0) - \overline{\log(D_m)} \quad \text{(Eq. 6-21)}$$

where the second term on the right hand side is the mean of $\log(D_m)$. If we stipulate that the variable X ranges from 0 to infinity, then D_m is constrained to be less than 10^{-9} m^2/s.

Given the semi-infinite range for X, it can be sampled as a lognormal distribution. This introduces the second logarithmic transformation, Y,

$$Y = \ln(X) \quad \text{(Eq. 6-22)}$$

The mean for Y is taken to be

$$\mu_Y = \ln(\mu_X) \quad \text{(Eq. 6-23)}$$

such that the mean for the Reimus correlation is unchanged by the transformation to a lognormal distribution. In this case, note that μ_x is the median of X, not the mean. Distribution parameters may be obtained by setting $\overline{\log(D_m)}$ to be the log of the geometric mean of the mean values in DTN: LA0003JC831362.001 [149557] and then adjust the standard deviation for Y such that it covers the range of values represented by cations and anions in DTN: LA0003JC831362.001 [149557]. The standard deviation of 0.3 for Y results in a spread for the distribution that is representative of the spread of values in DTN: LA0003JC831362.001 [149557], as shown in Figure 6-10.

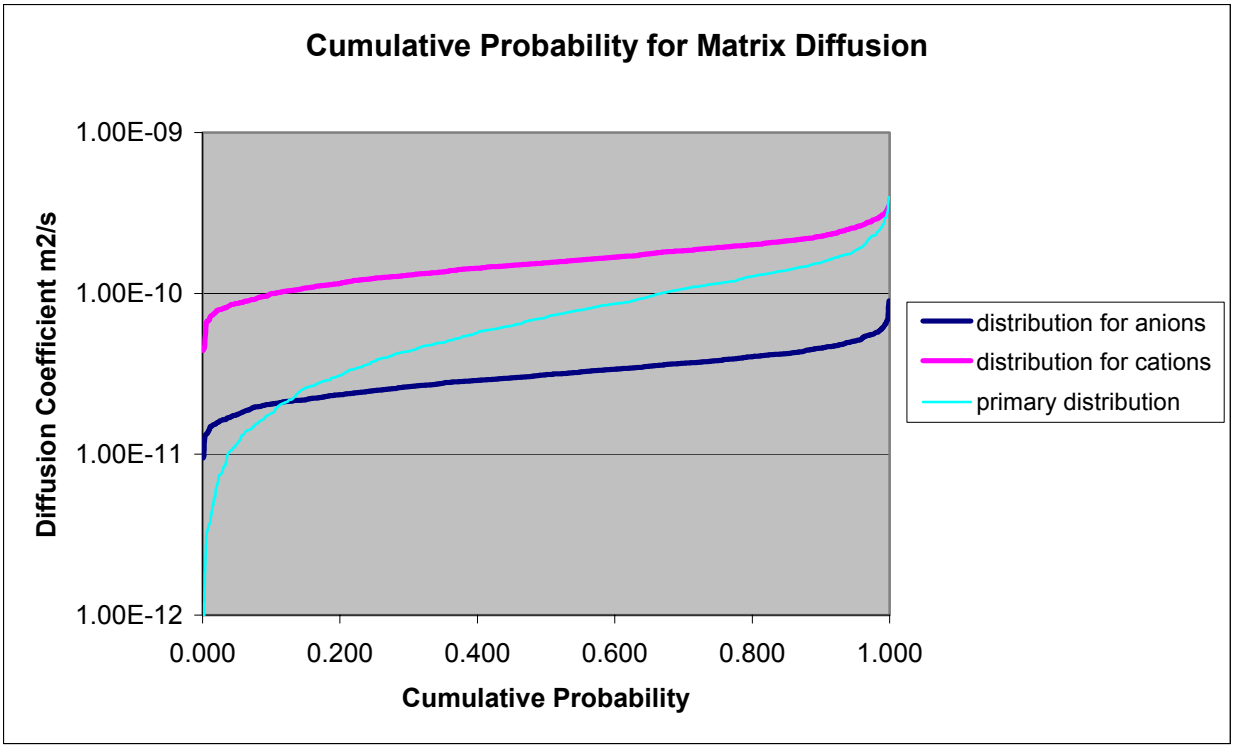

Output DTN: LA0311BR831371.003

Figure 6-10. Cumulative Probability for Matrix Diffusion Under Saturated Conditions

The range of values for the UZ may be examined using 5th and 95th percentile values for water content and effective matrix permeability. Doing this, the "low" distribution may be computed based on the Reimus correlation (Reimus et al. 2002 [163008]) by assigning the mean using the 5th percentile water content and effective matrix permeability and a "high" distribution based on the 95th percentile of values of these quantities. The results are shown in Figure 6-11.

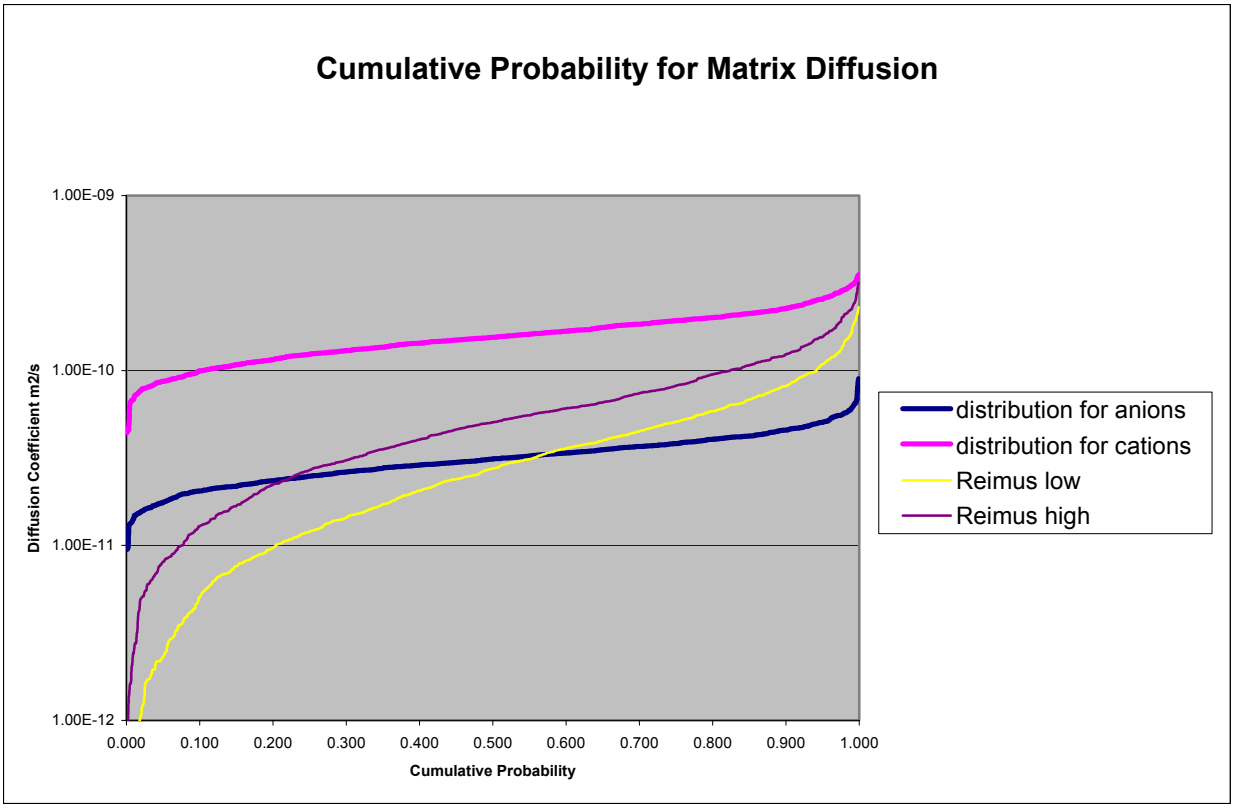

Output DTN: LA0311BR831371.003

Figure 6-11. Comparison of Cation/Anion Distributions with Reimus High/low Distributions for Unsaturated Conditions

Figure 6-11 shows that most of the matrix diffusion coefficients estimated using Equation 6-19 will fall within the range of the "Reimus low" and "Reimus high" curves. The data used to develop the distributions in DTN: LA0003JC831362.001 [149557] were from diffusion measurements under saturated conditions. Therefore, the generally lower values represented by the Reimus distributions are expected. The comparison with measured diffusion coefficients for tritium, technetium, and carbon is given in Figure 6-12. Again, the correlations for the UZ are lower than the measured values, which were all performed under saturated conditions.

The groups of model units for sampling matrix diffusion shown in Table 6-6 were selected based on similarity in properties of porosity, permeability, and water content. Distributions for the water content and (log) effective permeability to water for each group are derived from the 9 flow fields used for TSPA calculations (Source: BSC 2003 [163045]; DTN: LB03023DSSCP9I.001 [163044]).

The influence of matrix diffusion coefficient uncertainty on radionuclide transport is investigated by independently sampling water content and permeability for each rock group (Table 6-6). The water content and (log) effective permeability are independently sampled from these cumulative distributions. A matrix diffusion coefficient is then computed from equation Equation 6-19.

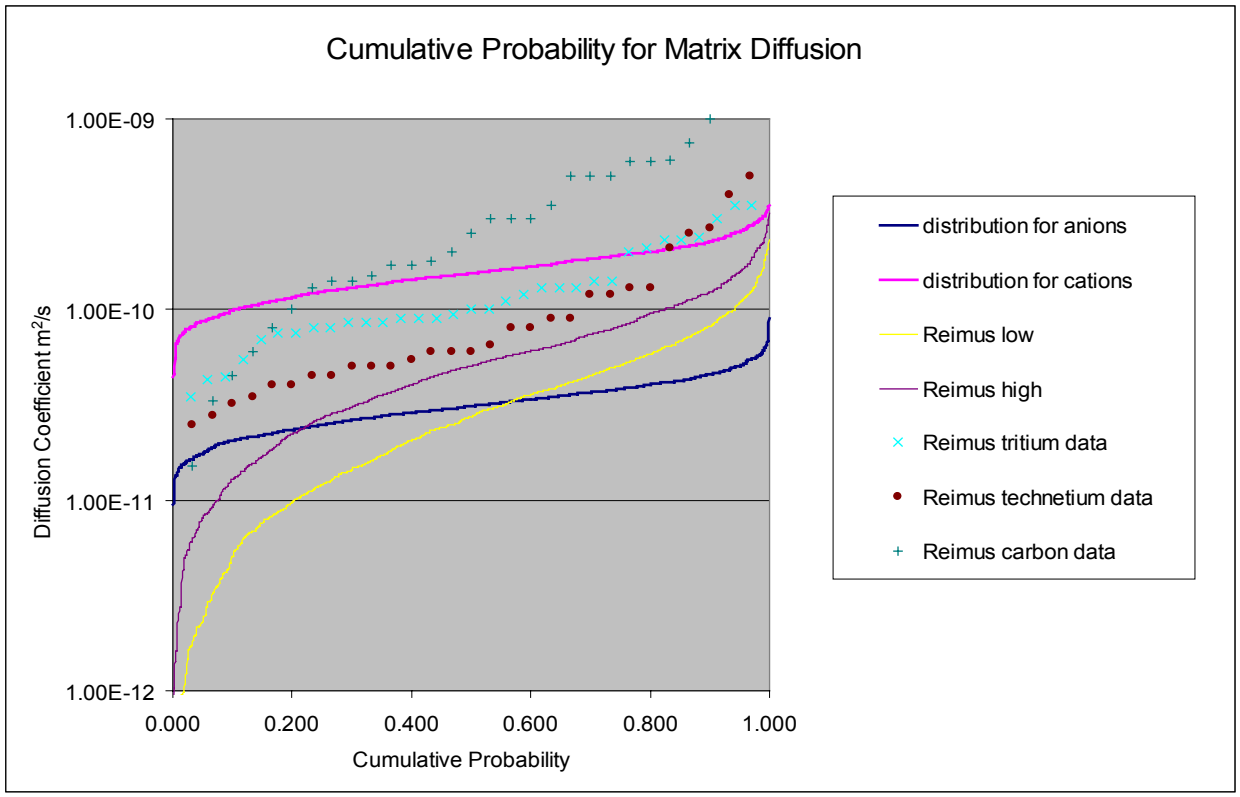

Output DTN: LA0311BR831371.003

Figure 6-12. Comparison of the Distributions With Diffusion Data

Table 6-6. Distribution of Water Content and Effective Permeability

Group Index	Unit	Mean Water Content (-)	Standard Deviation Water Content	Maximum Water Content	Minimum Water Content	Mean Log Effective Permeability (m^2)	Standard Deviation Log Effective Permeability (m^2)	D_m calculated using listed mean values and Eq. 6-19 (m^2/s)
1	bf2mz, ch1mz, ch[1,2,3,4,5, 6]mv, tswmv, tswmz, , pp3Md, pp2Md, pp1Mz, pp4Mz, bf3Md, tr3Md	2.06E-01	8.41E-02	5.33E-01	6.81E-03	-1.62E+01	5.50E-01	1.33E-10
2	ch[2,3,4,5,6]mz, pcm[1,2,5,6]mz, pcm39, pcm4p,	3.00E-01	5.12E-02	5.78E-01	7.73E-02	-1.83E+01	4.20E-01	8.10E-11
3	tswm[3,4,5,6,7,8], pcM38	1.12E-01	3.43E-02	3.19E-01	7.75E-5	-1.89E+01	4.62E-01	3.47E-11

DTN: LA0311BR831371.003

NOTE: A Beta distribution was used for the matrix water content, and a lognormal distribution was used for the matrix effective permeability.

In all TSPA simulations, colloid matrix diffusion (diffusion of a colloid from the fracture to the matrix) is neglected because of lack of data and because diffusion coefficients for colloidal particles are expected to be small. This is conservative with respect to the dose rates calculated by the TSPA model.

6.5.6 Fracture Residual Saturation and Active Fracture Model Gamma Parameters (Unitless)

Fracture residual saturation and fracture γ parameter values are used by FEHM to calculate the fracture spacing based on the Active Fracture Model (Liu et al. 1998 [105729]).

In TSPA-LA, a constant fracture residual saturation of 0.01 is used for all layers (DTN: LB0302UZDSCPUI.002 [161787]). Currently, there are no data from Yucca Mountain that could be used to assess the uncertainty in residual fracture saturation.

Table 6-7. Fracture Residual Saturation Values

Input Name	Input Value	Input Description	Input Source	Type of Uncertainty
Fracture residual saturation	0.01	Fracture residual saturation is used to calculate active fracture spacing	LB0302UZDSCPUI.002 [161787]	Fixed value. The fracture residual saturation is constant over all layers and does not change with climate

Values of fracture γ parameter vary with infiltration rates in each rock layer. Tables 6-8 through 6-10 list the fracture γ parameter values used in TSPA-LA for different infiltration scenarios (DTN: LB0305TSPA18FF.001 [165625]).

The influence of γ parameter uncertainty on radionuclide transport is investigated using sensitivity analyses in Section 7.3.3.

Table 6-8. Fracture γ Parameter for Lower-Bound Infiltration Scenario

Rock Layer	Fracture γ	Rock Layer	Fracture γ	Input Description	Input Source	Type of Uncertainty
tcwf1	0.4834	ch1fz	0.2759	This value is read in by FEHM and used in calculating fracture spacing values based on the active fracture model.	LB0305TSPA18FF.001 [165625] *"Eighteen 3-D Site Scale UZ Flow Fields Converted from TOUGH2 to T2FEHM format."* File : glaq_lA.dat.	Fixed value for each layer but varies from layer to layer. The values also depends on climate.
Tcwf2	0.4834	ch2fz	0.2759			
tcwf3	0.4834	ch3fz	0.2759			
ptnf1	0.1032E-01	ch4fz	0.2759			
ptnf2	0.1032E-01	ch5fz	0.2759			
ptnf3	0.1032E-01	ch6fz	0.2759			
ptnf4	0.1032E-01	pp4fz	0.2759			
ptnf5	0.1032E-01	pp3fd	0.2476			
ptnf6	0.1032E-01	pp2fd	0.2476			
tswf1	0.3741E-01	Pp1fz	0.2776			
tswf2	0.5284	bf3fd	0.2476			
tswf3	0.5284	bf2fz	0.2759			
tswf4	0.4764	tr3fd	0.2476			
tswf5	0.4764	tr2fz	0.2759			
tswf6	0.4764	pcf38	0.00			
tswf7	0.4764	pcf39	0.00			
tswf8	0.4764	Pc1fz	0.00			
tswfz	0.2759	Pc2fz	0.00			
tswfv	0.2500	Pc5fz	0.00			
ch1fv	0.2500	Pc6fz	0.00			
ch2fv	0.2500	pc4fp	0.00			
ch3fv	0.2500	tcwff (fault)	0.4000			
ch4fv	0.2500	ptnff (fault)	0.1138			
ch5fv	0.2500	tswff (fault)	0.3000			
ch6fv	0.2500	chnff (fault)	0.3000			

Table 6-9. Fracture γ Parameter for Mean Infiltration Scenario

Rock Layer	Fracture γ	Rock Layer	Fracture γ	Input Description	Input Source	Type of Uncertainty
tcwf1	0.5866	ch1fz	0.3704	This value is read in by FEHM and used in calculating fracture spacing values based on the active fracture model.	LB0305TSPA18FF.001 [165625] *"Eighteen 3-D Site Scale UZ Flow Fields Converted from TOUGH2 to T2FEHM format". File :* glaq_mA.dat	Fixed value for each layer but varies from layer to layer. The values also depends on climate.
Tcwf2	0.5866	ch2fz	0.3704			
tcwf3	0.5866	ch3fz	0.3704			
ptnf1	0.9051E-01	ch4fz	0.3704			
ptnf2	0.9051E-01	ch5fz	0.3704			
ptnf3	0.9051E-01	ch6fz	0.3704			
ptnf4	0.9051E-01	pp4fz	0.3704			
ptnf5	0.9051E-01	pp3fd	0.1989			
ptnf6	0.9051E-01	pp2fd	0.1989			
tswf1	0.1289	pp1fz	0.3704			
tswf2	0.6000	bf3fd	0.1989			
tswf3	0.6000	bf2fz	0.3704			
tswf4	0.5686	tr3fd	0.1989			
tswf5	0.5686	tr2fz	0.3704			
tswf6	0.5686	pcf38	0.00			
tswf7	0.5686	pcf39	0.00			
tswf8	0.5686	pcf1z	0.00			
tswfz	0.3704	pcf2z	0.00			
tswfv	0.2500	pcf5z	0.00			
ch1fv	0.2500	pcf6z	0.00			
ch2fv	0.2500	pcf4p	0.00			
ch3fv	0.2500	tcwff (fault)	0.4000			
ch4fv	0.2500	ptnff (fault)	0.1138			
ch5fv	0.2500	tswff (fault)	0.3000			
ch6fv	0.2500	chnff (fault)	0.3000			

Table 6-10. Fracture γ Parameter for Upper-Bound Infiltration Scenario

Rock Layer	Fracture γ	Rock Layer	Fracture γ	Input Description	Input Source	Type of Uncertainty
tcwf1	0.5000	ch1fz	0.5000	This value is read in by FEHM and used in calculating fracture spacing values based on the active fracture model.	LB0305TSPA18FF.001 [165625] *"Eighteen 3-D Site Scale UZ Flow Fields Converted from TOUGH2 to T2FEHM format".* File : glaq_uA.dat.	Fixed value for each layer but varies from layer to layer. The values also depend on climate.
Tcwf2	0.5000	ch2fz	0.5000			
tcwf3	0.5000	ch3fz	0.5000			
ptnf1	0.8319E-01	ch4fz	0.5000			
ptnf2	0.8319E-01	ch5fz	0.5000			
ptnf3	0.8319E-01	ch6fz	0.5000			
ptnf4	0.8319E-01	pp4fz	0.5000			
ptnf5	0.8319E-01	pp3fd	0.5000			
ptnf6	0.8319E-01	pp2fd	0.5000			
tswf1	0.1000	pp1fz	0.5000			
tswf2	0.5606	bf3fd	0.5000			
tswf3	0.5606	bf2fz	0.5000			
tswf4	0.5700	tr3fd	0.5000			
tswf5	0.5700	tr2fz	0.5000			
tswf6	0.5700	pcf38	0.0000			
tswf7	0.5700	pcf39	0.0000			
tswf8	0.5700	pcf1z	0.0000			
tswfz	0.5000	pcf2z	0.0000			
tswfv	0.2500	pcf5z	0.0000			
ch1fv	0.2500	pcf6z	0.0000			
ch2fv	0.2500	pcf4p	0.0000			
ch3fv	0.2500	tcwff (fault)	0.4000			
ch4fv	0.2500	ptnff (fault)	0.1138			
ch5fv	0.2500	tswff (fault)	0.3000			
ch6fv	0.2500	chnff (fault)	0.3000			

6.5.7 Fracture Porosity, Fracture Spacing (M), and Fracture Aperture (M)

Fracture porosity is used in FEHM to calculate the fracture pore volume of the corresponding fracture node block for determining the resident time of radionuclides within each fracture cell.

Fracture spacing and aperture data are used by FEHM in estimating the effect of matrix diffusion on radionuclide transport. In the abstraction model, aperture and spacing based on geometric considerations are adjusted before use in the transport calculations to conform to the assumptions of the AFM of Liu et al. (1998 [105729]). This section describes the geometric parameters. For a discussion of how the model implements the AFM for transport, see Attachment III, Section III-5.

The fracture porosity and fracture spacing data are sampled to address the uncertainty of fracture properties on radionuclide transport in TSPA calculations. The data sets (DTN: LB0205REVUZPRP.001 [159525] and DTN: LB0207REVUZPRP.001 [159526]) list fracture spacing data in terms of fracture frequency, defined as the inverse of fracture spacing.

Thus, the fracture frequency is first sampled, and the inverse of the sampled data are taken to derive sampled fracture spacing data.

Table 6-11 lists the uncalibrated fracture porosity and frequency data based on field information. Among them, data for the fault zone are from DTN: LB0207REVUZPRP.001 [159526]. Those are the uncalibrated properties as developed in BSC 2003 [160240]. However, fracture porosity and frequency data are not subject to adjustment in the calibration in BSC 2003 [160240], therefore, these properties are carried forward into the calibrated property set without modification.

Among the listed geological rock layers only those that below the repository could affect the transport of radionuclides downward toward the water table are sampled. Rock layers below the repository are grouped together based on similarity in the fracture porosity and frequency characteristics. The 9 groups identified are shown in Table 6-12. For groups with multiple units having different parameter values, an arithmetic average value is used for the group. There is only one standard deviation for fracture porosity, so the other groups are assigned a fracture porosity standard deviation such that the ratio of the standard deviation to the mean is constant for all the groups. Group 9 (tswf3) has its own standard deviation for fracture frequency, which is used. For the other groups, the standard deviation is set equal to 0.831 times the mean. This is based on the relationship between fracture frequency and the standard deviation of fracture frequency found for model units above the proposed repository (see Figure 6-13). In this way, the mean and standard deviation for each parameter in each group was computed.

As porosity must lie within the finite range of 0 to 1, a beta distribution with these bounds is suitable for studying the influence of porosity uncertainty on radionuclide transport, Table 6-13 lists the distribution data for fracture porosity.

Table 6-11. Fracture Porosity and Frequency Data

Rock Layer	ϕ_f	Std.	*f* (1/m)	σ_f	Input Description	Input Source	Type of Uncertainty
tcwf1	2.4E-2	-	0.92	0.94	θ_f is the fracture porosity and *f* is fracture frequency. Data are uncalibrated. However, the fracture porosity and fracture frequency data are not subject to adjustment in calibration; therefore, those properties are carried forward into the calibrated property set without modification.	LB0205REVUZPRP.001 [159525] Fault zone fracture porosity data are from LB0207REVUZPRP.001 [159526]	As porosity must fall in the range of 0 and 1, a beta distribution is suitable to describe the uncertainty of the porosity values.
tcwf2	1.7E-2	-	1.91	2.09			
tcwf3	1.3E-2	-	2.79	1.43			
ptnf1	9.2E-3	-	0.67	0.92			
ptnf2	1.0E-2	-	0.46	-			
ptnf3	2.1E-3	-	0.57	-			
ptnf4	1.0E-2	-	0.46	0.45			
ptnf5	5.5E-3	-	0.52	0.6			
ptnf6	3.1E-3	-	0.97	0.84			
tswf1	5.0E-3	-	2.17	2.37			
tswf2	8.3E-3	-	1.12	1.09			
tswf3	5.8E-3	-	0.81	1.03			
tswf4	8.5E-3	2.50E-03	4.32	3.42			
tswf5	9.6E-3	-	3.16	-			
tswf6	1.3E-2	-	4.02	-			
tswf7	1.3E-2	-	4.02	-			
tswf8/pcf38	1.1E-2	-	4.36	-			
tswf9/pcf39/ tswfz/tswfv	4.3E-3	-	0.96	-			
ch1fv	6.1E-4	-	0.10	-			
ch2fv	7.7E-4	-	0.14	-			
ch3fv	7.7E-4	-	0.14	-			
ch4fv	7.7E-4	-	0.14	-			
ch5fv	7.7E-4	-	0.14	-			
ch6fv	7.7E-4	-	0.14	-			
ch1fz/pcf1z	1.6E-4	-	0.04	-			
ch2fz/pcf2z	3.7E-4	-	0.14	-			
ch3fz	3.7E-4	-	0.14	-			
ch4fz	3.7E-4	-	0.14	-			
ch5fz/pcf5z	3.7E-4	-	0.14	-			
ch6fz/pcf6z	1.6E-4	-	0.04	-			
pp4f/pcf4p	3.7E-4	-	0.14	-			
pp3f	9.7E-4	-	0.20	-			
pp2f	9.7E-4	-	0.20	-			
pp1f	3.7E-4	-	0.14	-			
bf3f	9.7E-4	-	0.20	-			
bf2f	3.7E-4	-	0.14	-			
tr3f	9.7E-4	-	0.20	-			
tr2f	3.7E-4	-	0.14	-			
tcw fault	2.9E-2	-	1.90	-			
ptn fault	1.1E-2	-	0.54	-			
tsw fault	2.5E-2	-	1.70	-			
chn fault	1.0E-3	-	0.13	-			

Table 6-12. Grouping of Rock Layers Below the Repository

Group	Units	Porosity	Frequency (m^{-1})
1	chnf	1.0E-03	0.13
2	tswf	2.5E-02	1.7
3	ch[2,3,4,5]fz	3.7E-4	0.14
	pc[2,5]fz	3.7E-4	0.14
	pp4fz/pcf4p	3.7E-4	0.14
	pp1fz	3.7E-4	0.14
	bf2fz	3.7E-4	0.14
	tr2fz	3.7E-4	0.14
4	pp3fd	9.7E-4	0.20
	pp2fd	9.7E-4	0.20
	bf3fd	9.7E-4	0.20
	tr3fd	9.7E-4	0.20
5	ch1fz/pcf1z	1.6E-4	0.04
	ch6fz/pcf6z	1.6E-4	0.04
6	ch1fv	6.1E-4	0.10
	ch[2,3,4,5,6]fv	7.7E-4	0.14
7	tswf9/pcf39/ tswfz/tswfv	4.3E-3	0.96
8	tswf4	8.5E-3	4.32
	tswf5	9.6E-3	3.16
	tswf[3,6,7]	1.3E-2	4.02
	tswf8/pcf38	1.1E-2	4.36
9	tswf3	5.8E-3	0.81

Source DTNs: LB0205REVUZPRP.001 [159525] and LB0207REVUZPRP.001 [159526]

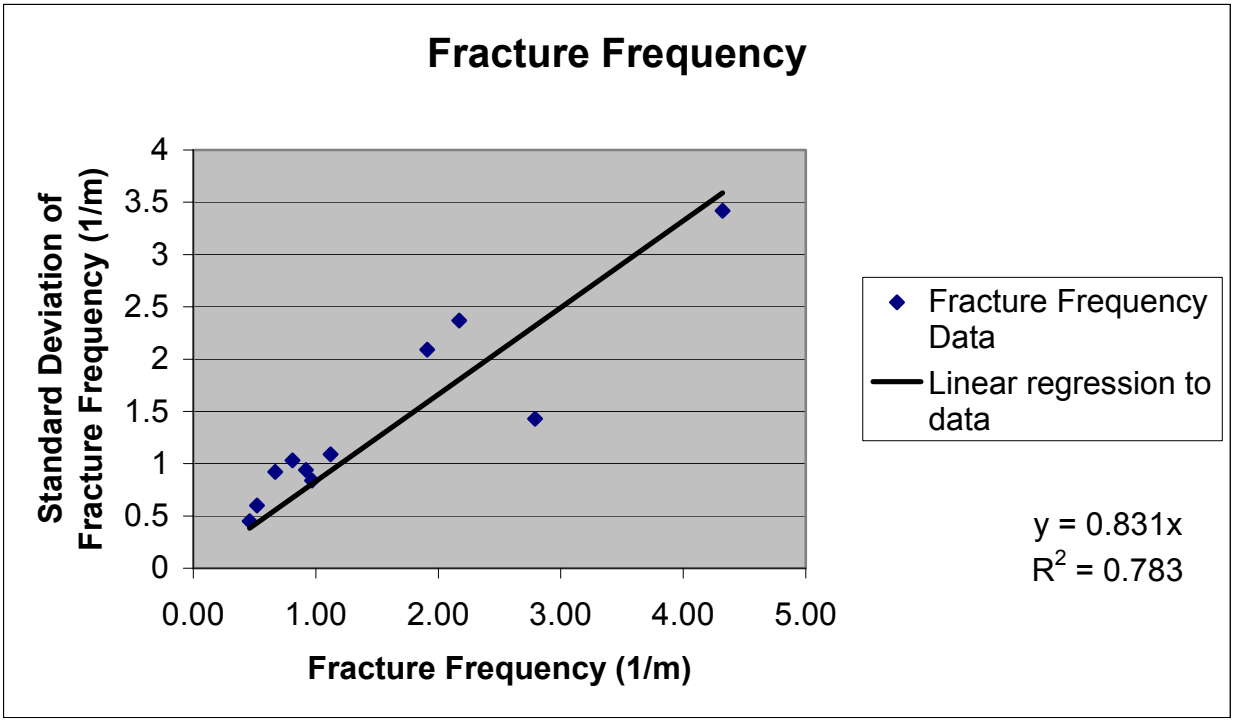

Output DTN: LA0311BR831371.003

Figure 6-13. Relationship between Fracture Frequency and Standard Deviation

Given that fracture frequency can theoretically span values from zero to infinity, the lognormal distribution is suitable. The mean and standard deviation for $\ln(f)$ are given in terms of the mean and standard deviation for f by the following relationships from Hogg and Craig (1978 [163236], pp. 180 and 432):

$$\mu_{\ln(f)} = \ln(\mu_f) - \frac{1}{2}\ln\left(1 + \frac{\sigma_f^2}{\mu_f^2}\right) \quad \text{(Eq. 6-24)}$$

$$\sigma_{\ln(f)} = \sqrt{\ln\left(1 + \frac{\sigma_f^2}{\mu_f^2}\right)} \quad \text{(Eq. 6-25)}$$

For further information on this derivation, see Attachments I and XI of BSC 2003 [164889], Equations I-1, I-2, and XI-4 through XI-7. Values for $\mu_{\ln(f)}$ and $\sigma_{\ln(f)}$ are given in Table 6-13.

Table 6-13. Fracture Porosity and Frequency Distribution Data

		Porosity (-) Beta Distribution min = 0; max = 1		Fracture Frequency (m^{-1})		Fracture Frequency (m^{-1}) Lognormal Distribution		Aperture (m) 2b derived from Eq. 6-26: $2b = \frac{\phi_f}{f}$
						Mean	Std	
Group	**Units**	**Mean**	**Std**	**Mean**	**Std**	**For ln (f)**	**For ln (f)**	
1	chnf	1.0E-03	3.09E-04	1.26E-01	1.05E-01	-2.42E+00	7.24E-01	7.94E-03
2	tswf	2.5E-02	7.25E-03	1.75E+00	1.45E+00	2.11E-01	7.24E-01	1.43E-02
3	ch[2,3,4,5]fz	3.7E-4	1.09E-04	1.40E-01	1.16E-01	-2.31E+00	7.24E-01	2.64E-03
	pcf[2,5]z							
	pp4fz							
	pp1fz							
	bf2fz							
	tr2fz							
4	pp3fd	9.7E-4	2.85E-04	2.00E-01	1.66E-01	-1.96E+00	7.24E-01	4.85E-03
	pp2fd							
	bf3fd							
	tr3fd							
5	ch1fz/pcf1z ch6fz/pcf6z	1.6E-4	4.71E-05	4.00E-02	3.32E-02	-3.57E+00	7.24E-01	4.00E-03
6	ch[1,2,3,4,5,6]fv	6.9E-4	2.03E-04	1.20E-01	9.96E-02	-2.47E+00	7.24E-01	5.75E-03
7	tswf9/pcf39 /tswfv/tswfz	4.3E-3	1.26E-03	9.60E-01	7.97E-01	-3.87E-01	7.24E-01	4.48E-03
8	Tswf[4,5]	1.05E-02	3.10E-03	3.97E+00	3.29E+00	1.03E+00	7.24E-01	2.64E-03
	tswf[6,7]							
	tswf8/pcf38							
9	tswf3	5.8E-3	1.71E-03	8.10E-01	1.03E+00	-6.92E-01	9.81E-01	7.16E-03

DTN: LA0311BR831371.003

In TSPA-LA calculations, the fracture porosity and fracture frequency are sampled independently. The basis for this approximation is that there is only a very weak correlation between fracture porosity and frequency (Figure 6-14). Therefore, correlating these two parameters is not warranted.

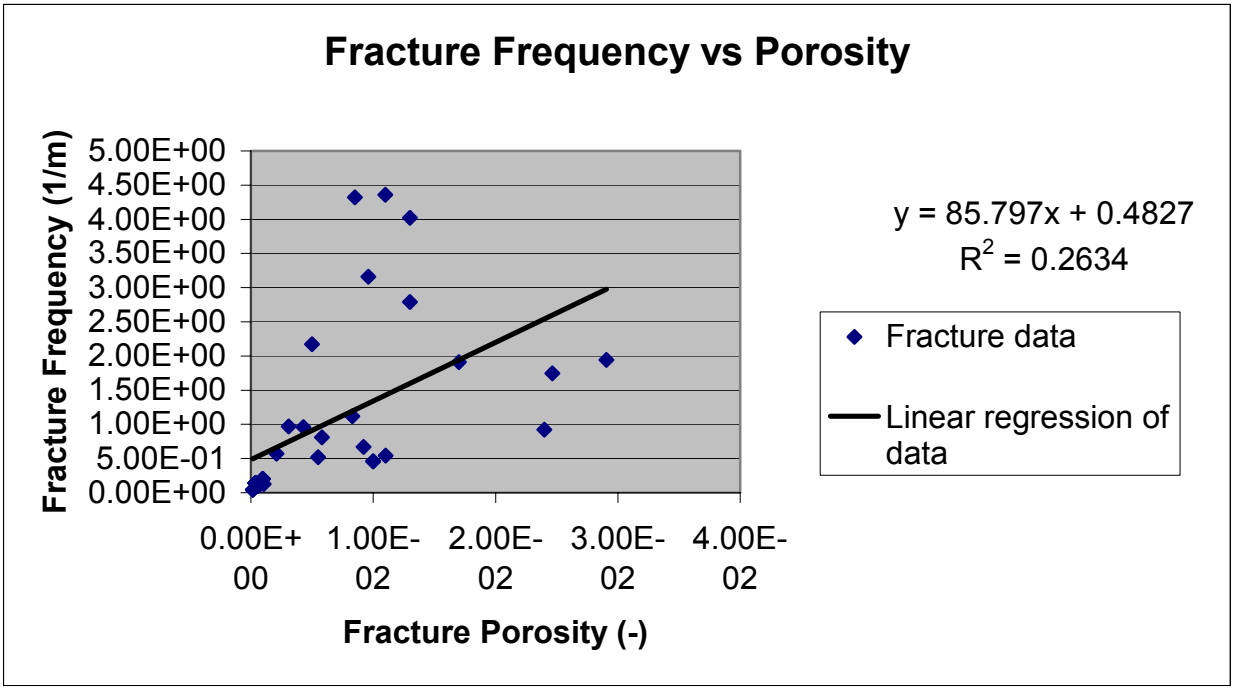

Output DTN: LA0311BR831371.003

Figure 6-14. Relationship between Fracture Porosity and Frequency

The sampled fracture porosity and frequency data are used in deriving the fracture spacing and aperture based on the following relationship:

$$\phi_f = (2b)f \qquad \text{(Eq. 6-26)}$$

where $2b$ is the fracture aperture (m), f is the fracture frequency (m^{-1}), and ϕ_f is the fracture porosity (-). Fracture frequency is the inverse of the fracture spacing.

6.5.8 Fracture Surface Retardation Factor (Unitless)

Because few data are available on fracture surface retardation factors, no fracture surface retardation is simulated in the TSPA model. In current TSPA simulations, all the fracture surface retardation factors are set to 1.0 (no fracture surface retardation) to be conservative. Values of fracture surface retardation factors are included in FEHM input data file and are read in at run time.

Table 6-14. Fracture Surface Retardation Factor

Rock Layers	Fracture Surface Retardation Factor	Input Description	Input Source	Type of Uncertainty
All layers	1.0	Parameter used to simulate the effect of fracture surface retardation on radionuclide transport.	CRWMS M&O 2000 [148384]	Fixed value

6.5.9 Colloid Filtration at Matrix Interface

Matrix pore size distribution combined with colloid size distribution is used in FEHM for determining colloid filtration at the interfaces between matrix units. Each time step, at a matrix unit interface FEHM compares a colloid's size against the sampled pore size of the matrix unit it is entering. If the colloid size is bigger than the pore size, then the colloid cannot enter the matrix and is removed from the simulation (permanently filtered). In TSPA simulations the cumulative probabilities for colloid transport between one matrix unit and another are taken from DTN: LA0003MCG12213.002 [147285] and listed in Table 6-15 (only colloid size data beneath the repository level are listed). In FEHM the matrix pore size data are sampled based on the cumulative colloid transport probability data in Table 6-15 and the sampled data are used in simulating colloid filtration at matrix interfaces.

Table 6-15. Cumulative Probabilities for Colloid Transport at Matrix Interfaces

	Colloid Size (nm)						
Units	2000	1000	450	200	100	50	6
TMN/TSW4	1.00	0.92	0.87	0.81	0.71	0.55	0.31
TLL /TSW5	1.00	0.80	0.79	0.70	0.61	0.51	0.19
TM2/TSW6	1.00	0.94	0.90	0.82	0.65	0.51	0.21
TMN1/TSW7	1.00	0.99	0.99	0.99	0.93	0.68	0.36
PV3 /TSW8	1.00	0.98	0.96	0.94	0.90	0.89	0.68
PV2/TSW9	1.00	0.72	0.57	0.47	0.39	0.35	0.22
BT1a/CH1	1.00	0.91	0.89	0.87	0.85	0.83	0.53
CHV	1.00	0.58	0.49	0.43	0.39	0.36	0.07
CHZ	1.00	0.79	0.76	0.73	0.68	0.56	0.30
BT/CH6	1.00	0.95	0.94	0.92	0.92	0.85	0.40
PP1	1.00	0.79	0.68	0.63	0.57	0.48	0.21
PP2	1.00	0.91	0.86	0.81	0.65	0.53	0.22
PP3	1.00	0.49	0.34	0.26	0.21	0.16	0.07
PP4	1.00	0.99	0.99	0.98	0.98	0.96	0.32
BF2	1.00	0.98	0.97	0.96	0.96	0.83	0.25
BF3	1.00	0.97	0.94	0.83	0.74	0.66	0.14
Input Description	Data are used by FEHM in combination with colloid size distribution data for simulating the effect of colloid filtration at matrix interface.						
Input Source	DTN: LA0003MCG12213.002 [147285].						
Type of Uncertainty	Fixed values.						

6.5.10 Colloid Size Exclusion

Due to flow exchange between fractures and the corresponding matrix block, colloids may be carried into matrix from fractures by advection. The amount of colloids that can enter into matrix depends on the size of the colloids and the size of the matrix pores. At the fracture-matrix interface, when a colloid's size is larger than the matrix pore size, this colloid will stay in the fracture. On the other hand, when a particle size is smaller than the matrix pore size, the colloid will enter into the matrix through advection. The colloid size exclusion effect in the current FEHM model is simulated with a size exclusion factor f_c based on the percentage of the pores that are greater than the expected colloid size of 100 nm (DTN: LA0003MCG12213.002 [147285]). Table 6-16 lists the values used in FEHM. There is no site-specific transport data available to validate this aspect of the colloid transport model. The incorporation of this feature is intended to avoid a non-physical situation in which colloids are allowed to enter the matrix even when they are larger than the typical pore size. This aspect of the model is conservative, in that it will tend to exclude some colloids from the slower moving matrix fluid and keep them in the fractures.

Table 6-16. Colloid Size Exclusion Factor Used in FEHM

Rock Units	Size Exclusion Factor	Input Description	Input Source	Type of Uncertainty
TMN (TSW4)	0.29	Parameters are used by FEHM for simulating the effect of colloid size exclusion on radionuclide transport at the fracture-matrix interface.	LA0003MCG12213.002 [147285]	Fixed value. In TSPA-LA simulations, a random number generator is used to determine the probability of a colloid entering into matrix from the corresponding fractures.
TLL (TSW5)	0.39			
TM2 (TSW6)	0.35			
TMN1 (TSW7)	0.07			
PV3 (TSW8)	0.10			
PV2 (TSW9)	0.61			
BT1a (CH1)	0.15			
CHV	0.61			
CHZ	0.27			
BT (CH6)	0.08			
PP4	0.02			
PP3	0.79			
PP2	0.35			
PP1	0.43			
BF3	0.26			
BF2	0.04			

6.5.11 Colloid Size Distribution

A colloid size distribution is used by FEHM to get the interpolated colloid size of each colloid particle. The colloid size information is then combined with pore size data to simulate filtration effects at matrix unit interfaces.

The colloid size range of 6 nm to 450 nm is based on CRWMS M&O (2001 [154071], Section 6.3); DTN: LL000122051021.116 [142973]. However, because a specific distribution was not available, the following distribution (Table 6-17) was chosen (not developed) to be

consistent with Figure 23 of CRWMS M&O (2001 [154071]); DTN: LA0007MCG12213.001 [153251].

The same colloid size distribution data are used in this abstraction model. FEHM data files contain the colloid size input data under the macro "size."

Table 6-17. Colloid Size Distribution

Colloid Size (nm)	Cumulative Probability	Input Description	Input Source	Type of Uncertainty
1	0	Colloid size distribution data are used in simulating colloid filtration effect at matrix interface.	LL000122051021.116 [142973]	FEHM read in the cumulative distribution data at run time. Random colloid size data are generated on the fly to address the effect of colloid size uncertainty on filtration.
6	0.2			
50	0.4			
100	0.6			
200	0.8			
450	1.0			

6.5.12 Colloid Concentration and Colloid K_c

The colloid equilibrium sorption parameter K_c is defined as $K_c=C_{coll}/C_{fluid}$, where C_{coll} is the radionuclide concentration residing on colloids and C_{fluid} is the radionuclide concentration in fluid. Colloid K_c is used in FEHM as an input parameter for calculating the retardation factors for colloid facilitated radionuclide transport in the media.

Radionuclide sorption to colloids can be categorized into reversible and irreversible categories. When sorption to colloids is treated as an irreversible process, a very large number (1.0E20) is assigned for K_c (see Table 6-18).

Table 6-18. K_c for Irreversible Colloid

Irreversible Colloids	K_c	Input Description	Input Source	Type of Uncertainty
Irreversible colloids	1.0E20	Simulating the effect of irreversible sorption to colloid.	A large value that ensures the adsorption process to colloids be irreversible.	Fixed value

NOTE: This input value is not data: rather it is a recommended input value to allow irreversible sorption to colloids to be simulated in the abstraction model.

For reversible radionuclide sorption to colloids, the K_c values are calculated by multiplying the adsorption coefficient, K_d, of radionuclide to colloid by colloid concentrations in the water.

Field data and laboratory experiments have shown that colloid concentration in groundwater can vary several order of magnitudes and is also a function of ionic strength and groundwater pH (BSC 2003 [161620]; DTN: SN0306T0504103.005 [164132]). To address the uncertainty of colloid concentration on colloid facilitated radionuclide transport, in TSPA-LA, the colloid concentration is sampled at run time and provided to FEHM for the calculation of reversible colloid K_c. Table 6-19 lists the distribution of colloid concentration used in TSPA-LA.

Table 6-19. Colloid Concentration Distribution

Colloid Concentration (mg/l)	Cumulative Probability	Input Description	Input Source	Type of Uncertainty
0.001 to 0.1	50	Ionic strength less than 0.05. Data are used in the estimation of reversible colloid K_c.	BSC 2003 [161620], Section 6.3.2.2.2, Figure 31, and Table 6. SN0306T0504103.005 [164132]	The cumulative distribution data listed in this table will be used to generated random colloid concentrations at TSPA-LA run time to address the influence of colloid concentration uncertainty of radionuclide transport.
0.1 to 1.0	75			
1.0 to 10	90			
10 to 50	98			
50 to 200	100			
1.E-6	100	Ionic strength >= 0.05		

NOTE: The probability of occurrence values listed in the source Table 6 are summed up to generate the cumulative probability in this table.

The strength of radionuclide adsorption onto colloid is determined by the adsorption coefficient K_d. In TSPA-LA, the following K_d distribution is used (Table 6-20). Among them, K_d ranges and distributions for Th and Pa are assumed to be those of Am primarily because of limited data on Th and Pa (BSC 2003 [161620]; DTN: SN0306T0504103.006 [164131]).

Table 6-20. Radionuclide Adsorption Coefficient (mL/g) Onto Colloids

Radionuclide	Colloid	Values (-)	Type of Uncertainty	Input Description	Input Source
Pu	Iron-(hydr)oxide	10^4 to 10^6	Uniform	Parameters are used in the calculation of colloid K_c values by FEHM.	BSC 2003 [161620], Section 6.3.2.3.1, Table 7, and Section 6.5.3, Table 15. SN0306T0504103.006 [164131]
	Smectite	10^3 to 10^6	Uniform		
Am	Iron-(hydr)oxide	10^5 to 10^7	Uniform		
	Smectite	10^4 to 10^7	Uniform		
Th	Iron-(hydr)oxide	10^5 to 10^7	Uniform		
	Smectite	10^4 to 10^7	Uniform		
Pa	Iron-(hydr)oxide	10^5 to 10^7	Uniform		
	Smectite	10^4 to 10^7	Uniform		
Cs	Iron-(hydr)oxide	10^1 to 10^3	Uniform		
	Smectite	10^2 to 10^4	Uniform		

In TSPA-LA calculations, to reflect the influence of reversible colloid facilitated radionuclide transport on system performance, colloid K_d values $K_{d,coll}$ are sampled at run time and used in the calculation of K_c. The sampled radionuclide adsorption coefficients are then multiplied by the colloid concentration C_{coll} to calculate the colloid K_c values:

$$K_c = C_{coll} K_{d,coll} \quad \text{(Eq 6-27)}$$

6.5.13 Fractions of Colloids Traveling Unretarded and Colloid Retardation Factor

Colloid retardation factor, R_c, is used in FEHM to study the impact of colloid retardation in the fractured media on irreversibly sorbed radionuclide transport. Field experiments have shown that a small percentage of colloids transport through the groundwater system essentially without

retardation (BSC 2003 [162729]). The fractions of unretarded colloids have been developed based on field data and are listed in Table 6-21.

This table, derived in BSC 2003 [162729], postulates that the fraction of colloids escaping retardation due to physical and chemical processes is a function of the residence time of the colloid: progressively fewer colloids migrate unretarded with time. This poses a difficulty in simulating transport for the unretarded colloids – the travel times are not known a priori. Therefore, it is recommended that the fraction be chosen for a travel time that can be reasonably expected to be conservative, such as 100 yr in the UZ. If simulations suggest that a different residence time is more representative, then this time should be changed, and a new unretarded fraction should be selected from Table 6-21. It should be noted that this aspect of the colloid transport model is relatively uncertain, so parameter sensitivity studies are advisable if it is determined that a colloidal radionuclide may be important to performance.

Colloids traveling unretarded will be given a retardation factor of 1.

Table 6-21. Fractions of Colloids Traveling Unretarded

Travel Time (Years)	Fraction of Colloids Unretarded	Input Description	Input Source	Type of Uncertainty
1	0.011	This parameter is used in determining fractions of colloids traveling unretarded in the UZ.	BSC 2003 [162729] LA0303HV831352.003 [165624]	Fixed value
5	0.005702			
10	0.004297			
20	0.003238			
30	0.002744			
40	0.00244			
50	0.002227			
75	0.001888			
100	0.001678			
300	0.001072			
600	0.000808			
1000	0.000656			
2000	0.000494			
5000	0.00034			
10000	0.000256			

For colloids that are delayed relative to a conservative species, the retardation of colloids in groundwater system depends on colloid type; colloid size; groundwater PH, Eh, and ionic strength; and rock properties, etc. Field (C-wells complex near Yucca Mountain and Nevada Test Site) and laboratory experiments were carried out under saturated conditions to estimate colloid retardation factors (BSC 2003 [162729]). As there is no data are available on colloid retardation factors in the UZ, the distribution of retardation factors from the SZ are used to represent colloid retardation through unsaturated fractures. Table 6-22 lists the cumulative distribution data of colloid retardation factors.

Table 6-22. Colloid Retardation Factors

Colloid Retardation Factor	Cumulative Probability	Input Description	Input Source	Type of Uncertainty
10	0.240831	Colloid retardation factor is used by FEHM in simulation the effects of colloid retardation in fractured rock on colloid facilitated radionuclide transport.	BSC 2003 [162729] LA0303HV831352.002 [163558]	A cumulative distribution is used to describe the distribution of colloid retardation factor. In TSPA-LA, the colloid retardation factor will be sampled at runtime and used by FEHM in TSPA calculations.
12	0.268609			
14	0.296387			
14	0.324165			
20	0.351942			
20	0.37972			
21	0.435276			
22	0.463053			
24	0.490831			
30	0.518609			
32	0.546387			
40	0.574165			
40	0.601942			
40	0.62972			
46	0.657498			
50	0.685276			
50	0.713053			
53	0.740831			
60	0.768609			
60	0.796387			
200	0.835276			
280	0.890831			
410	0.918609			
600	0.972232			
800	1			

In TSPA-LA calculations, to investigate the uncertainty of colloid retardation factors on radionuclide transport, colloid retardation factors are sampled for each realization at run time based on the given cumulative distribution in Table 6-22.

6.5.14 Radionuclide Half Lives (Years) and Daughter Products

FEHM needs the radionuclide half life and daughter products information to simulate the influence of radionuclide decay and ingrowth on system performance. The radionuclide half life and daughter products for the following species are used in FEHM as input parameters (see Table 6-23).

Table 6-23. Radionuclide Half-Life and Daughter Products used in TSPA

Radionuclide	Half-Life (yr)	Daughter Product	Input Description	Input Source	Type of Uncertainty
C^{14}	5.715E+03		Radionuclide half-lives and daughter products. Those data will be used by FEHM in radionuclide decay and ingrowth calculations.	Parrington et al. 1996 [103896] DTN: N/A accepted data	Fixed values
Cs^{135}	2.3E6				
Cs^{137}	3.007E+1				
I^{129}	1.57E+7				
Sr^{90}	2.878E+1				
Tc^{99}	2.13E+5				
Am^{243}	7.37E+3	Pu^{239}			
Pu^{239}	2.410E+4	U^{235}			
U^{235}	7.04E+8	Pa^{231}			
Pa^{231}	3.28E+04				
Am^{241}	4.327E+2	Np^{237}			
Np^{237}	2.14E+06	U^{233}			
U^{233}	1.592E+5	Th^{229}			
Th^{229}	7.3E+3				
Pu^{240}	6.56E+3	U^{236}			
U^{236}	2.342E+7	Th^{232}			
Th^{232}	1.40E+10				
U^{232}	6.98E+1				
Pu^{242}	3.75E+5	U^{238}			
Pu^{238}	8.77E+1	U^{234}			
U^{238}	4.47E+9	U^{234}			
U^{234}	2.46E+5	Th^{230}			
Th^{230}	7.54E+4	Ra^{226}			
Ra^{226}	1.599E+3				
Irreversible and reversible colloid facilitated radionuclide has the same half-life and daughter products as corresponding dissolved species.					
Pu^{242}	3.75E+5				
Pu^{240}	6.56E+3				
Pu^{239}	2.410E+4				
Pu^{238}	8.77E+1				
Am^{243}	7.37E+3				
Am^{241}	4.327E+2				

6.5.15 Repository Radionuclide Release Bins

Radionuclides will be released from nodes corresponding to the repository location. These nodes were grouped into bins (zones) that shared common infiltration ranges, to be compatible with a conceptual model for radionuclide release in which releases are a strong function of the percolation rates at the repository horizon. This would help to categorize release points according to high or low percolation rates. Five bins were chosen based on the cumulative probability of percolation for the glacial climate period. The glacial period was selected to perform this binning because the majority of the simulation is performed under this climate state. The definition of the 5 bins is listed in Table 6-24.

Table 6-24. Definition of Repository Release Bins

	Bin 1	Bin 2	Bin 3	Bin 4	Bin 5
Range of Cumulative Probability	0 – 0.05	0.05 – 0.30	0.30 – 0.70	0.70 – 0.95	0.95 – 1.00
Range of Percolation Glacial Climate (mm/year)	0.73 – 6.71	6.71 – 11.77	11.77 – 21.22	21.22 – 38.48	38.48 – 76.67

NOTE Binning data are from BSC 2001 [158204], Attachment VIII, "Binning Calculations".

Node coordinates within each bin are given in the multiscale thermohydrological model (DTN: LL030610323122.029 [164513]). As the grid resolution of the thermohydrological model is much finer (file: NEVADA_SMT_percolation_BIN_ma.txt. DTN: LL030610323122.029 [164513]) than the site scale FEHM transport model, the node coordinates of the thermohydrological model are mapped onto the FEHM grid to derive the corresponding FEHM nodes.

The mapping was done using FEHM V2.21 (LANL 2003 [165741]) and Microsoft Excel. The SMT (Smeared-sources Mountain-scale Thermal model) node coordinates from the thermohydrological model were read in by FEHM using the "zone" macro. FEHM did a search to find the closest node to a given SMT coordinate. Once FEHM nodes corresponding to the given SMT coordinates are found, Excel was used to get the frequency of FEHM node within each bin (data to be submitted). The following rules are applied during the mapping using Excel.

- As the FEHM grid is coarser than the thermohydrological model grid, it is possible that some nodes in the thermohydrological model within different bins may map onto a single FEHM node in the corresponding bins. In this case, the FEHM node with the most frequent appearance prevails. For example, FEHM 36189 appeared two times in bin 1 and four times in bin 4. Based on the rule, FEHM node 36189 was assigned to bin4.

- When a FEHM node appeared equal number of times in different bins, this node will be assigned to the highest bin number to be conservative. For example, FEHM node 39316 appeared three times in bin2 and bin3, respectively. Thus, node 39316 was assigned to bin3.

A file containing a listing of these bins and the associated nodes was created and named *repository_bins*. The bin data are incorporated into FEHM zone files in TSPA simulations and used to release radionuclides from the repository.

Figures 6-15 and 6-16 are plots showing the location of SMT repository release nodes and the transformed FEHM repository release nodes, respectively. It is clear that the transformed FEHM release nodes corresponding to the SMT release nodes closely. But, because of the much coarser FEHM grid and the lack of a one-to-one transformation from one grid to the other, the FEHM repository release nodes does not capture the detail depicted in the SMT grid. Nevertheless, the transformation is sufficient for the purposes of depicting the role of percolation variability on radionuclide releases and transport.

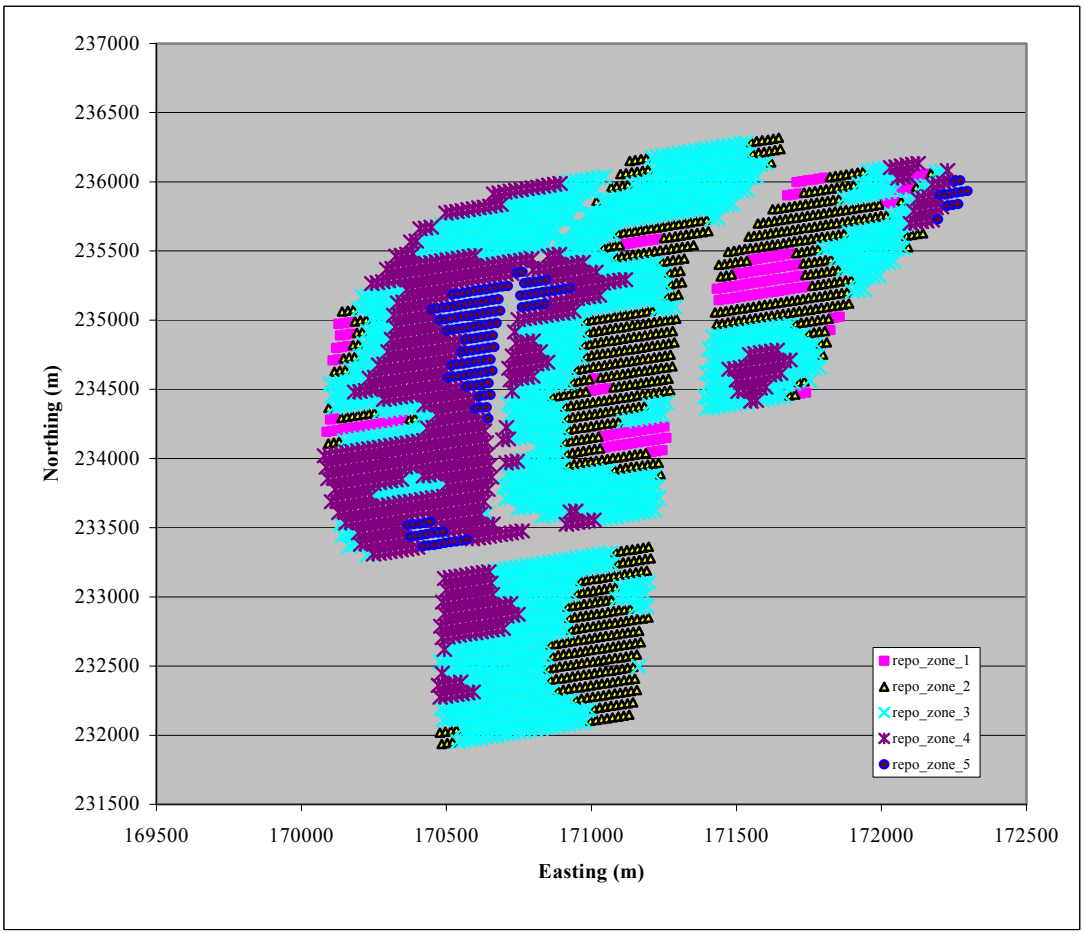

Output-DTN: LA0311BR831371.003

Figure 6-15. SMT Repository Release Nodes.

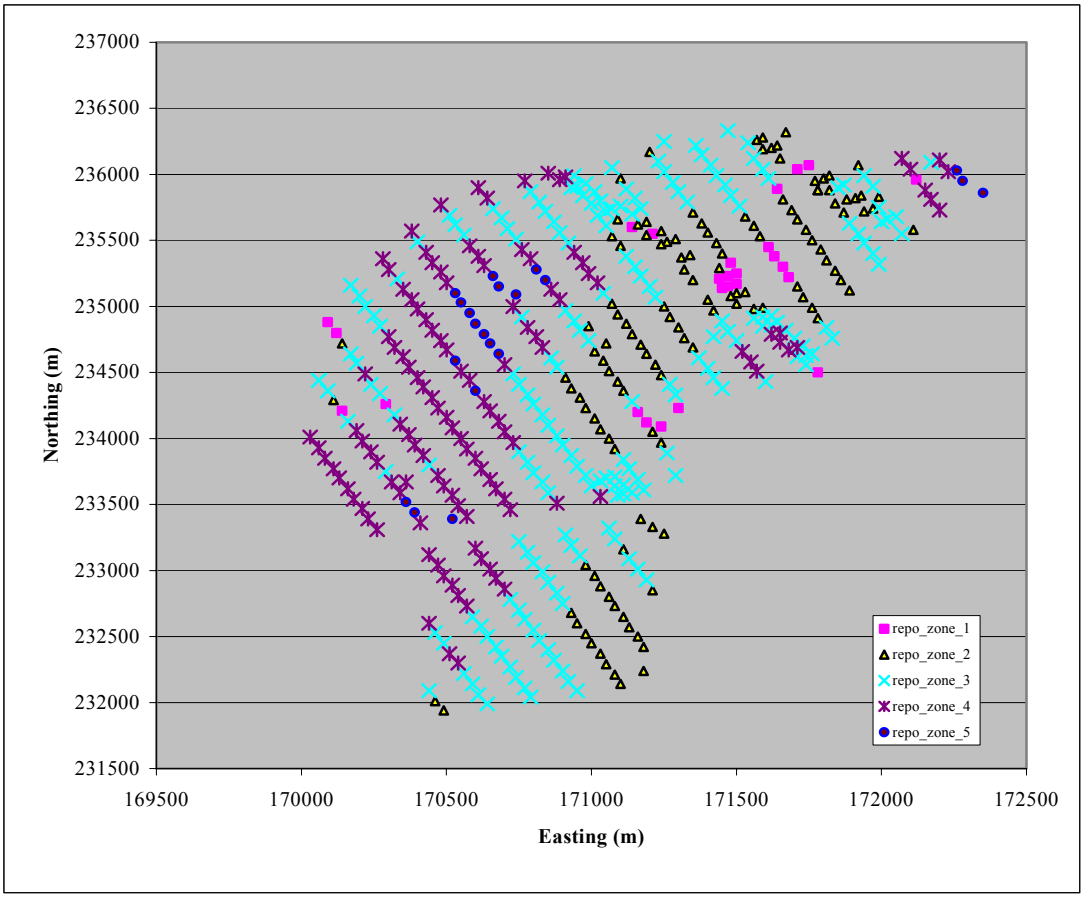

Output-DTN: LA0311BR831371.003

Figure 6-16. FEHM Repository Release Nodes Transformed Based on SMT Release Nodes (Shown in Figure 6-15).

6.5.16 Radionuclide Collecting Bins at UZ/SZ Interface

For the UZ/SZ interface, all nodes at (or below) the highest potential water table elevation of 850 m in the UZ model were grouped into four regions (or bins). The purpose of this process is for increased resolution to be captured in the TSPA model with respect to the arrival location and its impact on travel times in the SZ. Radionuclide mass reaching the water table in one location may have a different SZ travel path and travel time than mass arriving at some other location. The collecting bins are the means by which this potentially significant feature of the system can be quantified. The total radionuclide mass flow rate in each of these four bins will be focused at a random point (within each of the four bins) in the SZ model to reduce the effects of artificial dilution between the model interfaces. The four regions (Figure 6-17) are defined by an east-west boundary at a Universal Transverse Mercator (UTM) easting coordinate of 548500 and a north-south boundary at a UTM northing coordinate at 4078630 m (BSC 2003 [164870], Table 6-8).

All nodes at or beneath the water table in the UZ model were grouped into one of the four regions based on data listed in Table 6-8 in BSC 2003 [164870]. The FEHM water table collecting bins are larger than the SZ source release bins defined in Figure 6-17 to ensure that no particles fall outside of the four SZ release zone and go uncounted. The FEHM water table collecting bin nodes were extracted from the ELEME data from TOUGH2 site scale flow model package (DTN: LB0323DSSCP9I.001 [163044]). This data contains the cell name and coordinates for each node in the site scale UZ flow model. As the UZ transport model uses the Nevada State Plan (NSP) coordinates, the given UTM coordinates are converted into NSP coordinates during the extraction of the water table collect bins. The extraction was done in an Excel spreadsheet through several conditional if statements (See Attachment II for detail). The four collecting bins in FEHM are named 701, 702, 703, and 704, containing SZ source release regions 1, 2, 3, and 4, respectively. Among them, zone 701 contains all nodes beneath the water table with a UTM easting coordinate less than 548500 m (NSP: 171189.79 m) and a UTM northing coordinate greater than 4078630 m (NSP: 233459.87m); zone 702 contains all water table nodes with a UTM easting coordinate greater than 548500 m (NSP: 171189.79 m) and a UTM northing coordinate greater than 4078630 m (NSP: 233459.87m); zone 703 contains all water table nodes with a UTM easting coordinate less than 548500 m (NSP: 171189.79 m) and a UTM northing coordinate less than 4078630 m (NSP: 233459.87m); and zone 704 contains water table nodes with a UTM easting coordinate greater than 548500 m (NSP: 171189.79 m) and a UTM northing coordinate less than 4078630 m (NSP: 233459.87m).

Nodes contained in each of the collection bins were stored in file *wt.zone* and defined in the corresponding FEHM zone file. Once a particle reaches the water table, the particle is removed from the system. Inside FEHM, the code records mass leaving the system within each bin/zone (FEHM V2.21 Users Manual, LANL 2003 [165741]). As climate change can cause water table rise or fall, the defined collection bins/zones contain all nodes between the lowest and the highest water tables, up to an elevation of 850 m (see Section 6.4.9 for details). Note that for the simulations in this Model Report, the present day water table is used for all simulation results to maintain consistency and allow comparison to the process model simulation results.

At the end of each simulation time step, FEHM collects the total radionuclide mass leaving each water table collection bin/zone and then passes the data to GoldSim (BSC 2003 [161572]) for use as input for SZ transport simulations.

6.6 BASE-CASE MODEL

In this Model Report, we set our base case as a case using mean radionuclide transport parameters and present day mean infiltration. The results from this run will not be used by TSPA. This simulation activity illustrates the possible transport behavior of radionuclides within the UZ under the conditions of present day mean infiltration condition and mean transport parameter values. In TSPA-LA, the abstracted model will be used with different parameter combinations to study the uncertainty of parameters and flow fields on radionuclide transport through the UZ and its impacts on system performance.

6.6.1 Overview

The simulation was carried out using FEHM V2.21 (LANL 2003 [165741]). Data used in this simulation are the mean parameter values listed in Section 6.5 Transport Model Inputs. The flow field used in this simulation was for present day mean infiltration.

The objective of this run is to study the movement of radionuclides released from EBS into unsaturated fractured geological media downward to the water table as stated in Section 6.1 Model Objectives.

A total of 36 species (Table 6-25) were simulated to study the transport of radionuclides.

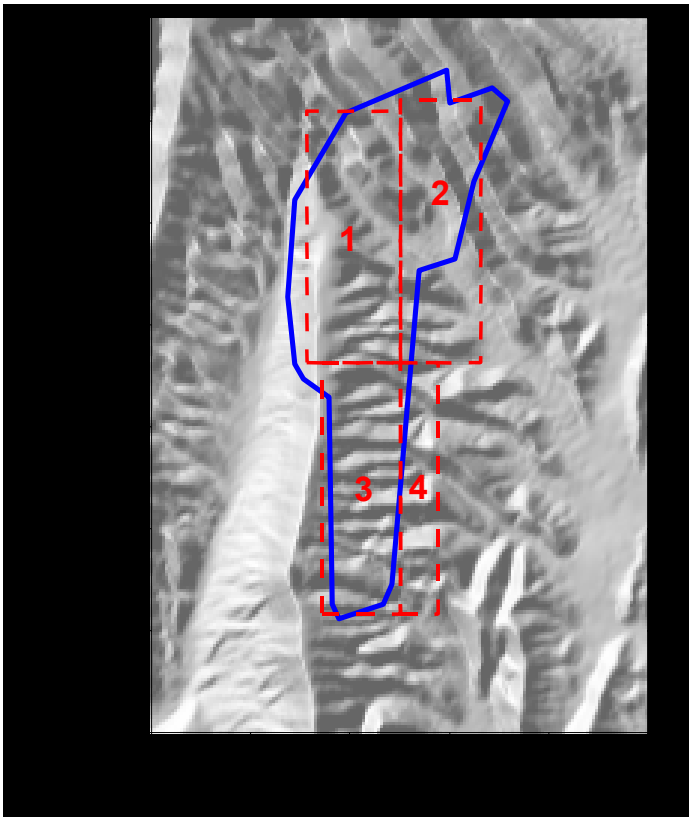

Source: BSC 2003 [164870], Figure 6-26

Figure 6-17. Source Regions for Radionuclide Release in the SZ Transport Abstraction Model. Dashed lines represent the boundaries of the SZ release regions and the solid lines represent the boundary of the repository release region.

6.6.2 Base-Case Model Results

Figure 6-18 shows the normalized cumulative breakthrough curves at water table for the 36 species simulated under the present-day mean infiltration condition. Note that for the colloid simulations, colloid filtration at matrix interfaces (Section 6.5.9) was not included in these calculations. The process model does not have this particular feature, so it was decided that, in order to make comparison with the process model results simpler, the calculations presented here should omit this process as well. However, this mechanism should be included in the TSPA-LA

model. The simulation results reveal that irreversible fast colloids (curves labeled If239, If241, If242, and If243) which are not affected by matrix diffusion and retardation have the shortest breakthrough times and the greatest breakthrough quantities. Within a time period of less than 100 years, over 50 percent of the irreversible fast colloids traveled through the UZ.

Irreversible slow colloids which undergo retardation move more slowly than their corresponding fast colloids but faster than their corresponding dissolved species. The travel time of the irreversible slow colloids depends on their retardation factor. In TSPA-LA simulations, the retardation factors of the slow colloids will be sampled and its impact on system performance will be evaluated.

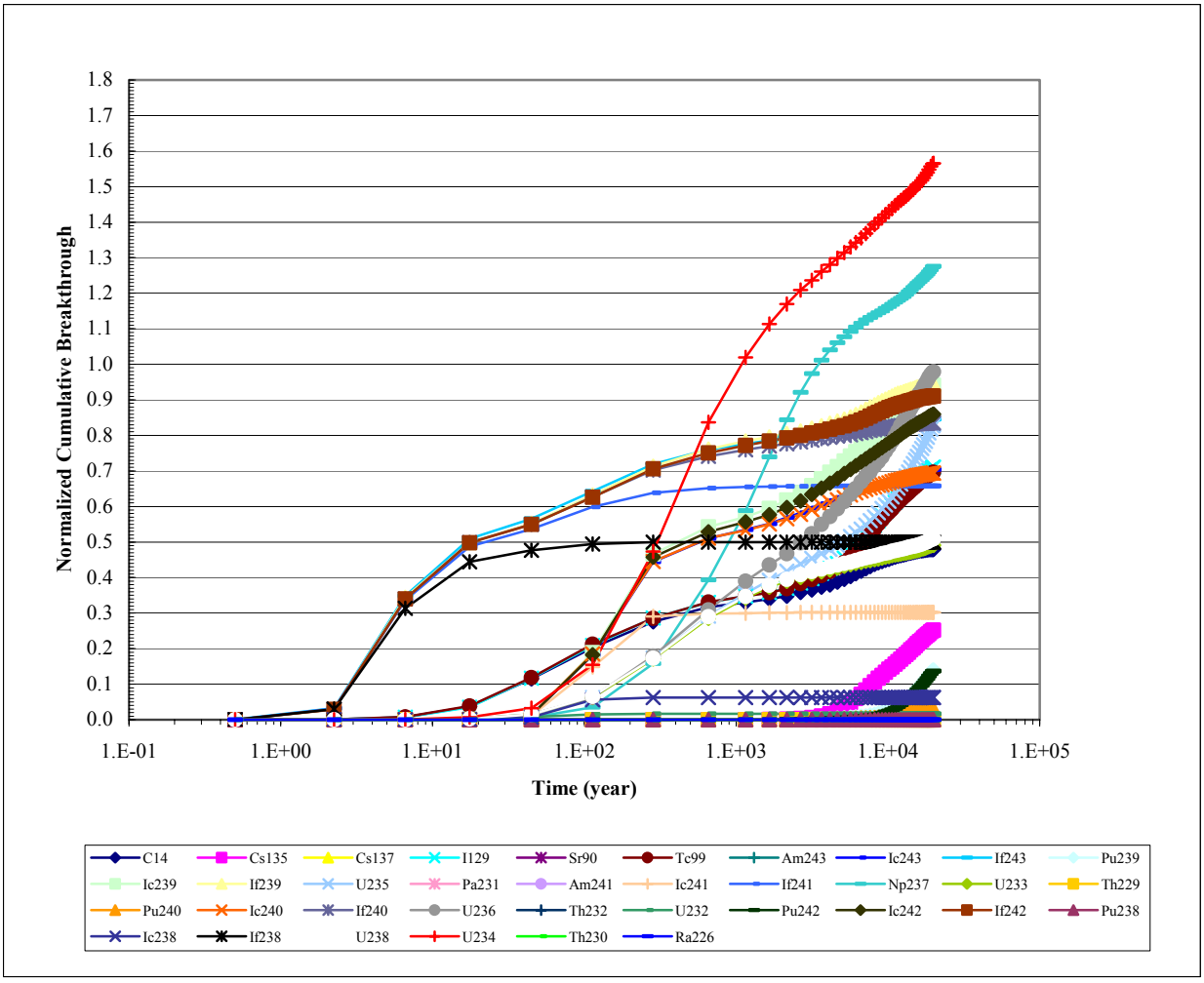

Output-DTN: LA0311BR831371.003

NOTE: These results are for comparison purposes only. Actual radionuclide mass flux reaching the water table will depend on release rates and locations, and will be simulated in the TSPA model.

Figure 6-18. Base Case Model Normalized Breakthrough Curve for 36 Radionuclide Species, Present-day Mean Infiltration Scenario

Dissolved species have the longest breakthrough time among the three transport mechanism (irreversible fast colloids, irreversible slow colloids, and dissolved species) due to matrix diffusion and matrix adsorption. The results show that for non-sorbing species, like Tc-99 and I-129, about 20 percent of the mass travels through fast flow paths and arrives at the water table in less than 100 years. The remainder of the mass traveled at much lower velocities due to matrix diffusion. Dissolved species with moderate matrix adsorption, like the isotopes of Uranium, travel more slowly through the UZ than the non-sorbing species Tc-99 and I-129. Within the first 100 years under the present-day mean infiltration conditions, only about 5% percent of the total U-233 mass passed through the UZ. U-234 exhibits a relatively fast transport process with higher mass output than the other dissolved Uranium radionuclides because it is produced by the decay of a colloid facilitated species (Pu-238). Strongly sorbing species like Pu-242 (median Kd of 100 mL/g in Zeolitic, 70 mL/g in Devitrified, and 100 mL/g in vitric layers) exhibit transport of less than 15% of the input through the UZ within the 20,000 year period. The most strongly sorbing species such as Th-230 (mean Kd of 15500mL/g in Zeolitic, 5500 mL/g in Devitrified, and 5500mL/g in vitric layers) do not break through the UZ within the 20,000 year period. Finally, note that U-234 and Np-237 have normalized cumulative breakthrough values greater than 1 at 20,000 year due to the decay of Pu-238 (Pu238, If238, and Ic238) and Am241 (Am241, If241, and Ic241), respectively.

For comparison, a case was also run under the wetter glacial mean infiltration condition to investigate the influence of higher infiltration on radionuclide transport through the UZ. Figure 6-19 shows the normalized cumulative breakthrough curves of the same 36 species with the same rock and transport properties as for the present day mean infiltration case. As before, normalized cumulative breakthrough values for some Uranium species (U-234, U-235, and U-236) and Np-237 are larger than 1 due to decay of Pu and Am (Am-241, If241, and Ic241, respectively). Under the glacial mean infiltration condition, all species travel much faster and arrive at the water table earlier. A comparison of Figures 6-18 and 6-19 reveals that significantly more Tc-99 breaks through at the water table under the glacial infiltration condition, which indicates increased fast flow in fractures and more modest matrix diffusion effects. The same is true for Np-237, which diffuses and sorbs to the matrix rock. This comparison shows that fast water flow under wetter infiltration conditions can reduce the effect of matrix diffusion and transport radionuclides through the UZ within the simulation time period of 20,000 years.

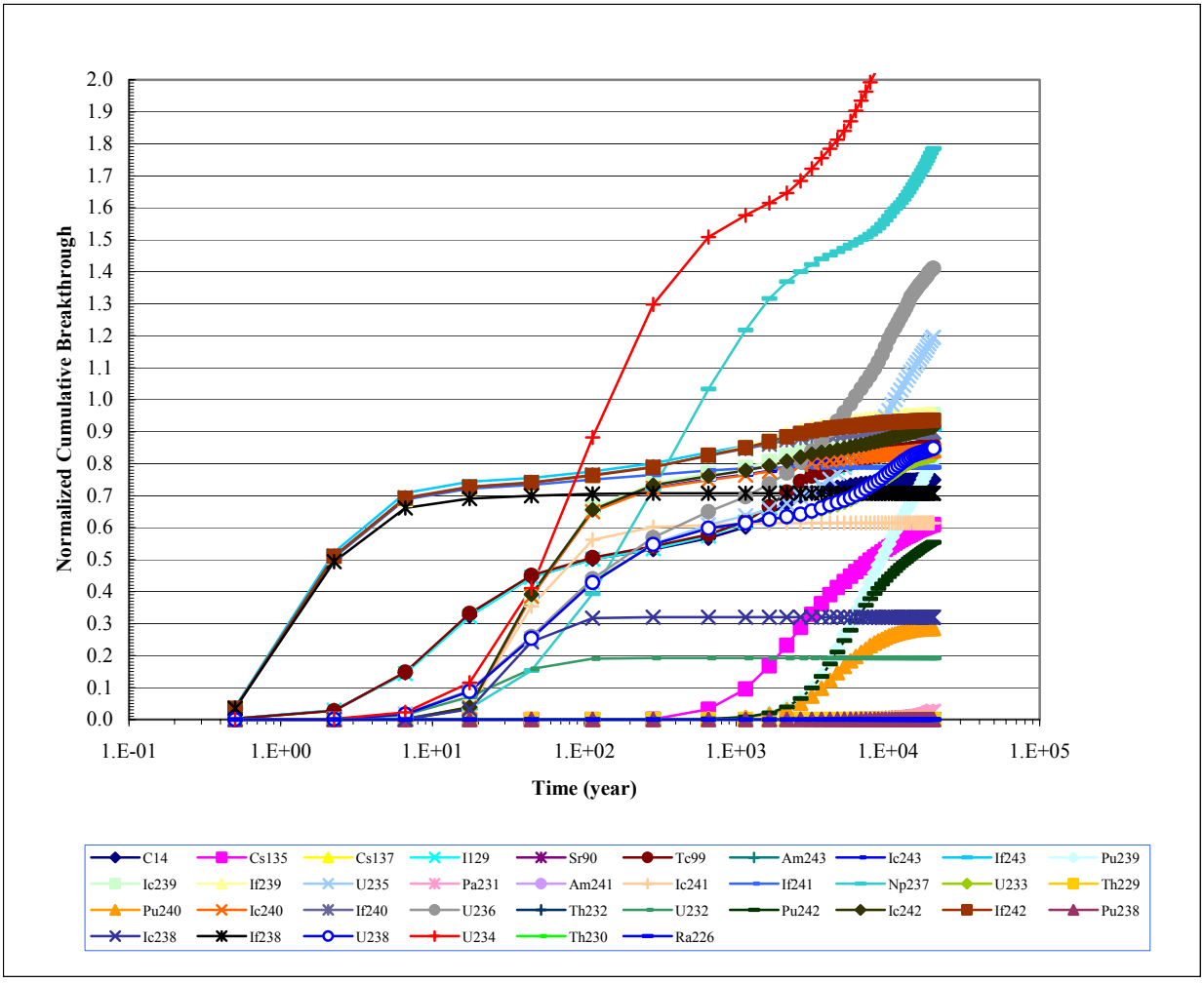

Output-DTN: LA0311BR831371.003

NOTE: These results are for comparison purposes only. Actual radionuclide mass flux reaching the water table will depend on release rates and locations, and will be simulated in the TSPA model.

Figure 6-19. Base Case Model Normalized a Breakthrough Curve for 36 Radionuclide Species, Glacial Mean Infiltration Scenario

With regard to colloid transport, the simulation results show that current conceptualizations suggest that colloids can play an important role in accelerating the transport of radionuclides in the UZ, especially the irreversible fast colloids. Of course, if the quantity of irreversible fast colloids is low, the impact on dose would not be expected to be important. In TSPA-LA calculations, a conservative percentage of irreversible fast colloids will be selected to study its impact on dose. For irreversible slow colloids, the retardation factor should be sampled to investigate parameter uncertainty on system performance.

Matrix diffusion and matrix adsorption can play an important role in retarding the movement of dissolved radionuclides and could significantly impact dose predictions. The strength of fracture-matrix interaction due to matrix diffusion and adsorption depends on matrix diffusion coefficient, matrix adsorption coefficient, fracture spacing, and fracture aperture. In TSPA-LA calculations, those parameters will be sampled based on uncertainty distributions, and the impact

on system performance of these uncertainties will be quantified. Another important factor that controls the transport process is infiltration rate. The impact of climate changes on system performance will be investigated using different flow fields developed in BSC 2003 [163045] and DTN: LB0305TSPA18FF.001 [165625]. These flow fields have different amounts of fracture and matrix flow, and water table elevation changes will also be included (see Section 6.4.9). Based on the results presented here, under the wetter climate conditions, radionuclide transport velocities will increase during the wetter climates due to increased infiltration and greater fracture flow.

Table 6-25. Radionuclides Simulated in Base Case Run

Species	Half-Life (days)	Decay Ingrowth	Species_Name
1	2.09E+06	Simple decay	C14
2	8.4E+08	Simple decay	Cs135
3	1.10E+04	Simple decay	Cs137
4	5.73E+09	Simple decay	I129
5	1.05E+04	Simple decay	Sr90
6	7.78E+07	Simple decay	Tc99
7	2.69E+06	10	Am243
8	2.69E+06	11	Ic243
9	2.69E+06	12	If243
10	8.80E+06	13	Pu239
11	8.80E+06	13	1c239
12	8.80E+06	13	if239
13	2.57E+11	14	U235
14	1.20E+07	Simple decay	Pa231
15	1.58E+05	18	Am241
16	1.58E+05	18	ic241
17	1.58E+05	18	if241
18	7.82E+08	19	Np237
19	5.81E+07	20	U233
20	2.7E+06	Simple decay	Th229
21	2.40E+06	24	Pu240
22	2.40E+06	24	ic240
23	2.40E+06	24	if240
24	8.55E+09	25	U236
25	5.11E+12	Simple decay	Th232
26	2.55E+04	Simple decay	U232
27	1.37E+08	33	Pu242
28	1.37E+08	33	ic242
29	1.37E+08	33	if242
30	3.20E+04	34	Pu238
31	3.20E+04	34	ic238
32	3.20E+04	34	if238
33	1.63E+12	34	U238
34	8.99E+07	35	U234
35	2.75E+07	36	Th230
36	5.84E+05	Simple decay	Ra226

Source: BSC (2002 [160059])

NOTE: Half-life data are from Table 6-23. The 3rd column shows the species index the radionuclide decays into. Species with a name starting as icxxx represents irreversible colloids traveling retarded. Species with a name starting as ifxxx represents irreversible colloids traveling unretarded.

6.7 EVALUATION OF ALTERNATIVE MODELS AND MODEL UNCERTAINTY

Geological, hydrological, and geochemical data have been used to support parameters, used in conceptual models, process-level models, and alternative conceptual models, considered in the abstraction of radionuclide transport in the UZ. These traceable, well-documented data have been used to support the technical bases for FEPs that have been included in the abstraction of radionuclide transport in the UZ (Table 6-1). As discussed in the Radionuclide Transport Process Model (BSC 2003 [163228]) on which this abstraction model is based, analysis demonstrates that the associated burden in implementing complex alternative conceptual or processes models is not commensurate to the benefit in reducing uncertainty in model predictions. Therefore a conservative model approach has been used to address conceptual model or processes uncertainty (Table 6-26). The selected conceptual model of radionuclide transport in the UZ is conservative, and supported by available data and current scientific understanding.

BSC (2003 [163228]) discusses alternative conceptual radionuclide transport models involving:

a) Different representations of the matrix-fracture system - multiple interactive continua, (MINC) versus dual-permeability (dual-k) systems.

b) Different conceptual methods of describing the transport problem (Particle tracking versus conventional representation in control-volume finite element codes).

In the MINC method, the steep gradients at the matrix fracture surface are resolved by including additional grids in the matrix in an appropriate number of nested shells. This is based on the concept that rapid changes at the fracture–matrix interface will propagate rapidly through the fracture system, while invading the tight matrix comparatively slowly (steep gradient to the inside of matrix block). The MINC behavior results in later breakthrough times (as the enhanced fracture/matrix interaction allows for increased diffusion), longer contact times, and more effective sorption (in sorbing media/solute systems). In BSC (2003 [163228]), the MINC model response (using both T2R3D V1.4 (LBNL 1999 [146654]) and TOUGH2 V1.11 MEOS9nTV1.0 (LBNL 1999 [113943]) codes) was compared to UZ transport models employing a particle-tracking–based numerical method (DCPT V2.0; LBNL 2003 [154342]). The results of those simulations are presented in the Validation section of the present Model Report (Figure 7-7). The result with the MINC grid conforms to expectations, resulting in later breakthrough times, when matrix diffusion is significant. However, despite its conceptual appeal, the application of the MINC concept to the 3-D UZ site-scale model would incur a large computational burden because it necessitates replacement of the single matrix block in the current dual permeability system with several MINC sub-domains. The validation conducted in Section 7 shows that the FEHM particle-tracking code replicates behavior similar to that of the MINC model when transfer functions developed using a Discrete Fracture Model (DFM) are used. By contrast, when transfer functions are developed with a dual-k formulation, behavior similar to that of the dual-k process model are obtained. Therefore, these alternate conceptual models can both be examined at the total-system level using the UZ transport abstraction model.

Table 6-26 gives a summary of alternative conceptual models and processes, and the recommended disposition for the TSPA transport abstraction.

Table 6-26. Summary of Alternative Conceptual Model Processes and their Dispositions for TSPA

Alternative Conceptual Model	Key Assumptions	Summary of Subsystem Evaluation	Recommend TSPA Evaluation
MINC model of UZ matrix, alternative to single matrix dual permeability model	More accurately models concentration gradient at fracture-matrix interface, resulting in a more accurate model of matrix diffusion	Results in later break-through times when matrix diffusion is significant for long lived radionuclides. MINC models not directly handled by particle tracking codes.	MINC not directly used in TSPA because of large computation burden, but FEHM particle tracking transport abstraction model reproduces the results predicted by MINC and discrete fracture models.
Finite difference numerical models EOS9nT, T2R3D, and DCPT particle tracking, alternative to FEHM particle tracking	Provide a basis for modeling coupled flow and transport of single (T2R3D) or multiple Radionuclides (EOS9nT).	Used primarily to provide validated models of UZ transport processes that form the basis for the abstraction models. These are calibrated against a variety of experimental and analytical models.	Large computational burden limits use for multiple realizations that can provide uncertainty estimates. FEHM particle tracking transport abstraction model can reproduce the results predicted by dual-k models by using transfer functions developed using a dual-k formulation.
Lateral flow diversion in UZ above repository, alternative to no PTn lateral diversion model flow fields	Lateral flow in the PTn will divert percolating water to the faults and reduce percolation flux at repository.	Used in UZ flow model to provide evaluation of the impact of lateral flow on UZ flux. The steady state flow fields provide basis for transport simulations.	The base case flow fields used provide a basis. Lateral diversion is not significant at infiltrations > 1mm/year and may be important only at lower bounds of infiltration ranges or in areas with low infiltration.
No Radionuclide release into faults, alternative to radionuclide release into all repository level nodes including faults.	High fault permeability leads to fast advective transport of radionuclide directly released into Faults to top of TSw and to water table.	No significant effects on overall transport to water table even for Non-sorbing tracers, except for Np and Pu (which already has a high t_{10}). There is no effect on t_{50}, because lateral diversion redirects advective flow to faults and other fast flow pathways	Conservative estimate of transport times, but has substantial effect on radionuclide arrival at top of CHn (TSw39). TSPA models should consider no release into faults by limiting the nodes into which radionuclides are released.
Include drift shadow, a capillary diversion, alternative to no drift shadow effects	Capillary diversion even under ambient conditions may result in low fracture saturation below the drift (drift shadow) that may persist for years	Drift shadow may develop and remain only under low infiltration. Seepage through fractures may be significant after climate change	Ignoring drift shadow is a conservative assumption of transport in the UZ
Perched water permeability barrier zones below the repository, alternative to no perched water permeability barrier (continuous and well-connected fractures)	Perched water will delay and dilute radionuclide concentration and reduce advective transport	Continuous well connected fractures are used to model transport processes using the particle tracking method. The flow fields from the UZ account for perched water effects.	Perched water may only be present in the northern part of the repository. Ignoring perched water is a conservative treatment.

Table 6-26. Summary of Alternative Conceptual Model Processes and their Dispositions for TSPA (Continued)

Alternative Conceptual Model	Key Assumptions	Summary of Subsystem Evaluation	Recommend TSPA Evaluation
Include TH, THC, and THM effects on UZ on flow and transport	Vaporization due to repository heat will maintain the drift dry for several hundreds to a few thousand years. THC and THM effects may alter flow and transport properties of UZ rocks	TH, THC, and THM effects are insignificant after change to Glacial climate, the period during which transport processes are dominant, following release of radionuclides by corrosion processes.	Ignoring TH, THC THM effects is a conservative assumptions

Source: BSC 2003 [163045]

6.8 DESCRIPTION OF BARRIER CAPABILITY

The unsaturated zone units below the repository are barriers that delay and limit radionuclide movement to the water table due to a variety of natural processes influenced by local hydrological, the intrinsic characteristics of the rocks, and by the repository design. A full treatment of the barrier capability is presented in BSC (2003 [163228]); a condensed summary is given below. The major large-scale processes included in this TSPA abstraction model are:

1. The limited and low rate of flow of water through the unsaturated zone, which limits the rate at which radionuclides can move by advection out of the repository: included through the use of UZ model flow and transport properties and steady state flow fields. (Section 6.5.1)

2. Sorption, which chemically binds radionuclides to minerals in the rock matrix and on fracture walls: included by explicit modeling of sorption processes. (Section 6.5.4)

3. Matrix diffusion, which physically traps and delays radionuclides within the rock matrix: included by explicit modeling of molecular and colloidal diffusion in the abstraction of transport. (Section 6.5.5)

Other processes that operate at a more local scale also contribute to UZ ability to limit water movement and radionuclide transport. Examples include the diversion of flowing water around drift openings in the UZ by capillary suction and the dry-out of the region surrounding repository drifts by heat associated with emplacement waste. These processes are beyond the scope of this Model Report, which treats only Mountain-scale radionuclide transport.

On the other hand, colloidal transport of radionuclides has the potential to offset the effectiveness of both sorption and matrix diffusion by providing a mechanism for transport of radionuclides that have very low solubility limits. Radionuclides can be transported as intrinsic (true) colloids (fine particles 1 to 10,000 nm) of elemental particles e.g., Plutonium. They can also be transported as pseudo colloids i.e., bound to naturally occurring fine particles. The size of the colloids determines their ability to be excluded or filtered by matrix pores, and transported by fracture advection and dispersion processes. The effect of colloidal transport is discussed in

BSC (2003 [163228]) and is accounted for in this TSPA abstraction of UZ transport (Sections 6.5.9 to 6.5.13).

6.8.1 Analyses of Barrier Capability

The breakthrough times provide a quantitative assessment of the ability of the UZ to delay (retard) the transport of radionuclides to the accessible environment. An example set of calculations from the UZ Transport Process Model (BSC 2003 [163228]) is reproduced in Tables 6-27, 6-28, and 6-29, for aqueous and colloidal radionuclide species. The sorption and diffusion parameters used in these simulations are given in Tables 6.5-1 and 6.6-1 of BSC 2003 [163228]. The t_{10} (time for 10% arrival) and t_{50} (time for 50% arrival) values for solute and colloidal transport, are presented for representative radionuclides, and combinations of three climate states, three infiltration cases, and the two release scenarios (instantaneous and continuous). At repository closure, short lived radionuclides such as strontium-90 and cesium-137 will be reduced to a small fraction of their initial inventory long before they could be transported through the UZ. For long lived radionuclides, models provide a means for assessing the effectiveness of the UZ to delay and retard (by slow advection, sorption and diffusion) their transport through the UZ. For strongly sorbing radionuclides like plutonium-239, the rate of movement is retarded so much that there is virtually no breakthrough before 10,000 years for the mean infiltration case. For weakly sorbing radionuclides such as neptunium-237, radionuclide transport is retarded for at least 1,000 years. For the long-lived non-sorbing radionuclides like ^{99}Tc, the rate of transport is dictated by matrix diffusion and advective transport. However, even these require 3,000 to 4,000 years to move through the unsaturated zone (BSC 2003 [163228]).

Table 6-27. Radionuclide Travel Times in Years to the Water Table for Instantaneous Release

	Climate/ Infiltration	Present-Day		Monsoon		Glacial	
Radionuclide	Case	T_{10} (Years)	T_{50} (Years)	T_{10} (Years)	T_{50} (Years)	T_{10} (Years)	T_{50} (Years)
^{241}Am	Lower	-	-	-	-	-	-
	Mean	-	-	-	-	-	-
	Upper	12	-	3	-	1	-
^{237}Np	Lower	33,800	>1,000,000	15	6,160	185	34,400
	Mean	410	25,400	8	2,120	4	1,070
	Upper	4	1,600	2	714	1	336
^{231}Pa	Lower	-	-	-	-	-	-
	Mean	-	-	-	-	-	-
	Upper	13	-	4	-	2	-
^{239}Pu	Lower	-	-	86,000	-	-	-
	Mean	-	-	10,400	-	3,710	-
	Upper	1,530	-	4	-	2	-
^{226}Ra	Lower	-	-	-	-	-	-
	Mean	-	-	-	-	-	-
	Upper	-	-	-	-	3	-
^{90}Sr	Lower	-	-	-	-	-	-
	Mean	-	-	-	-	-	-
	Upper	-	-	-	-	3	-
^{99}Tc	Lower	13,900	>1,000,000	22	1,310	102	8,140
	Mean	83	6,640	9	417	6	164
	Upper	6	230	2	92	1	42
^{229}Th	Lower	-	-	-	-	-	-
	Mean	-	-	-	-	-	-
	Upper	-	-	4	-	2	-
^{233}U	Lower	65,200	>1,000,000	103	6,730	549	36,900
	Mean	433	29,100	34	2,130	16	893
	Upper	12	1,120	3	458	2	208
^{235}U	Lower	55,300	>1,000,000	101	6,480	540	32,600
	Mean	430	26,500	34	2,080	15	882
	Upper	12	1,100	3	450	2	206
^{135}Cs	Lower	>1,000,000	>1,000,000	22,400	>1,000,000	150,000	>1,000,000
	Mean	52,500	>1,000,000	4,690	309,000	2,460	120,000
	Upper	2,170	71,200	753	24,500	305	990

DTN: LB0307MR0060R1.007 [164752]

Source: BSC 2003 [163228]

NOTE: Symbol "-" indicates breakthrough at this relative arrival (i.e. either 10% or 50%) was never achieved in simulations.

Table 6-28. Radionuclide Travel Times in Years to the Water Table for Continuous Release

Case (Mean Infiltration/Present-Day Climate)	Species	t_{10} (years)	t_{50} (years)
Three-Parents	^{99}Tc	74	3,901
	^{237}Np	781	22,940
	^{235}Pu	-	-
^{239}Pu-Chain	$^{239}Pu+^{235}U+^{231}Pa$	[(a)]6,419	[(a)]33,660
^{241}Am-Chain	$^{241}Am+^{237}Np+^{233}U+^{229}Th$	1,027(a)	23,450(a)

DTN: LB0307MR0060R1.007 [164752]

Source: BSC 2003 [163228]

NOTES: [(a)] Corresponds to the sum of the chain members. Symbol "-" indicates breakthrough at this relative arrival (i.e. either 10% or 50%) was never achieved in simulations.

Table 6-29. Colloid Travel Times in Years to the Water Table for Continuous Release

Case (Mean Infiltration/Present-Day Climate)	Colloid Size (nm)	t_{10} (years)	t_{50} (years)
1 (no declogging, in which colloids, once filtered, do not detach from the pore/fracture walls)	450	4.35	-
	200	4.39	-
	100	4.53	-
	6	-	-
2 (strong kinetic declogging, providing an estimate of maximum colloidal transport)	450	4.35	-
	200	4.39	-
	100	4.53	-
	6	-	-
3 (weak kinetic declogging, approaching equilibrium filtration behavior)	450	4.35	-
	200	4.39	-
	100	4.52	-
	6	-	-
4 (same as Case 2, but the fractures have the same colloidal transport properties as the corresponding matrix; provides an estimate of the importance of fractures in the transport of colloids)	450	32.4	243
	200	27.8	251
	100	27.6	-
	6	-	-

DTN: LB0307MR0060R1.007 [164752]

Source: BSC 2003 [163228]

NOTES: [(a)] Corresponds to the sum of the chain members. Symbol "-" indicates breakthrough at this relative arrival (i.e. either 10% or 50%) was never achieved in simulations.

6.8.2 Summary of Barrier Capability

The radionuclide transport processes model (BSC 2003 [163228]) demonstrates that even under the conservative approach in the 3-D site-scale models, the UZ of Yucca Mountain is an effective barrier to the transport of the strongly sorbing radionuclides (^{90}Sr, ^{226}Ra, ^{229}Th, ^{241}Am, ^{221}Pa and ^{239}Pu). The variably sorbing ^{135}Cs (strongly on zeolites, much less on other rocks), the mildly sorbing ^{233}U, ^{235}U, ^{237}Np, and the nonsorbing ^{99}Tc arrive at the water table at times that are fractions of their respective half-lives. However, this is not necessarily an indication of a breached or ineffective UZ barrier, but can be a direct consequence of the conceptual model of UZ flow and of the conservative approach taken to model transport. Eliminating potential sources from the vicinity of the fault fractures appears to have a small effect on transport and arrivals at the water table. For instantaneous release, the breakthrough curves show a small increase in t_{10}, but t_{50} is practically unchanged.

Figures 6-20 and 6-21 are plots of normalized cumulative breakthrough curves for the same 11 species listed in Table 6-27, which were simulated using the base-case abstraction model in this Model Report. A comparison between the base-case results of this Model Report (Figures 6-20 and 6-21) and results from the process model (Table 6-27) reveals similar behavior for radionuclide transport through the UZ. The abstraction model shows that for the base-case model it takes the colloids far less time to travel through the UZ than the corresponding dissolved species. Due to matrix diffusion, the transport process for even non-sorbing species, like Tc-99, are retarded. Under the present day mean infiltration condition, only about 10 percent of the total mass travels through the UZ within the first 40 years. By 6000 years, about 50 percent of the Tc-99 arrives at the water table. Under the high-glacial infiltration scenario, where the matrix diffusion effect is reduced by the fast flow in the fractures, ten percent of the Tc-99 travels through the UZ in the first 5 years, and 50 percent arrives at the water table within slightly greater than 100 years. These travel times are qualitatively similar to those for the process model presented in Table 6-27. The weakly adsorbed Np-237 had a relatively higher breakthrough value than Tc-99 due to the decay of Am-241 traveling in the form of dissolved species (Am-241), colloids with irreversible sorption but retardation (Ic241), and colloids traveling unretarded (If241). Species with short half-life (Sr-90 and Am-241) did not appear within the 10,000 year period. Clearly, these results are similar to the conclusions reached in BSC (2003 [163228]), providing further confirmation that the abstraction model is in substantial agreement with the process model.

The abstraction model results indicate that the UZ can act as an effective barrier to transport of the dissolved radionuclide species because of matrix diffusion and adsorption. Fast fracture flow in the UZ can weaken the UZ barrier's capability by reducing the effectiveness of matrix diffusion. Given the current model assumptions, the UZ system is a weak barrier for the fraction of the radionuclide inventory that travels via colloid facilitated radionuclide transport, especially under the high-infiltration scenarios. Ultimately, the quality of the barrier with respect to colloids will depend on the quantity of colloids in groundwater, the adsorption coefficient, matrix diffusion coefficient, and geological properties of rock layers. Monte Carlo simulations to address the uncertainty of transport process on system performance are intended to be implemented in the TSPA model.

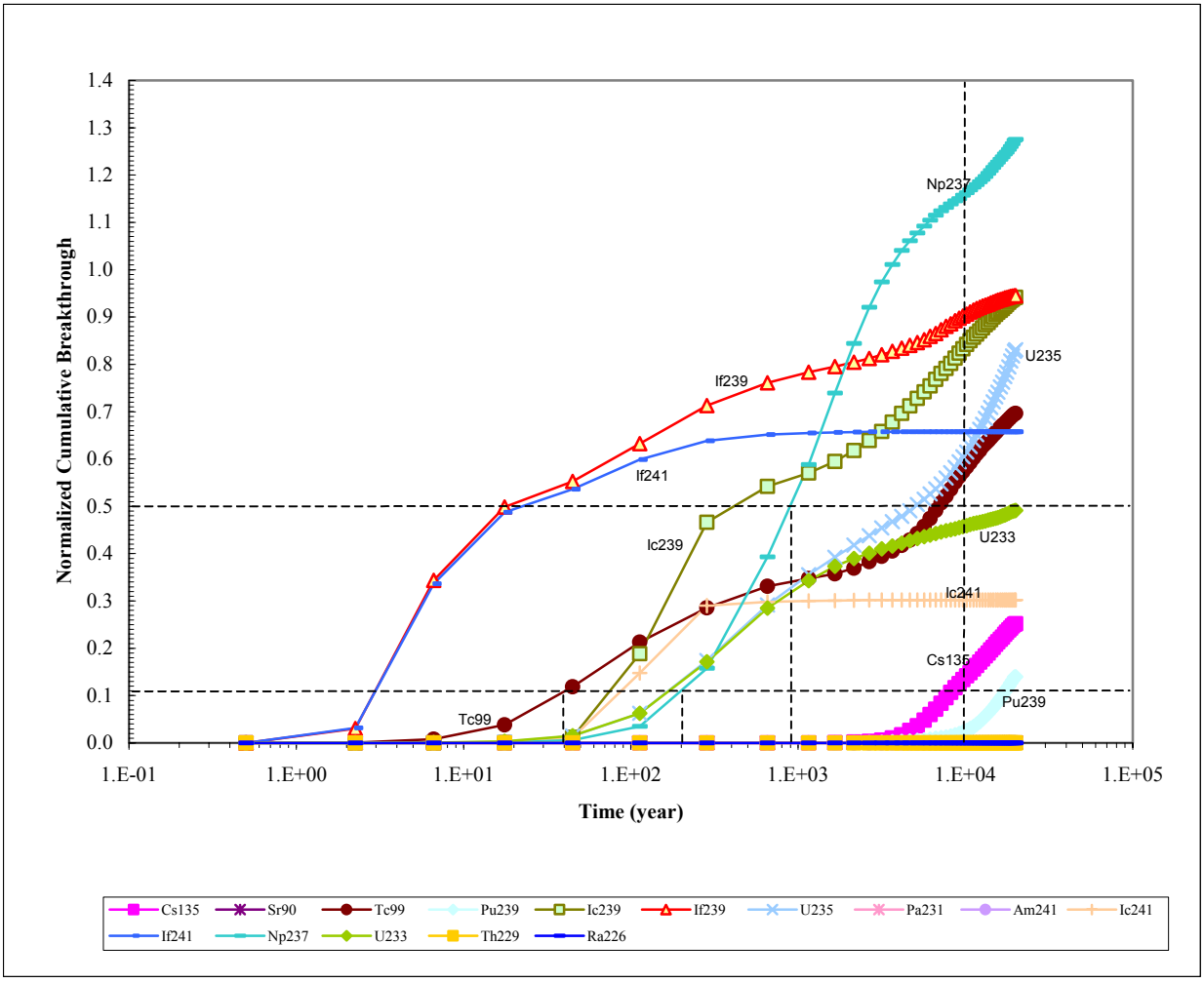

Output DTN: LA0311BR831371.003

NOTE: Ic239 and If239 are colloid species of Pu-239, and Ic241 and If241 are colloid species of Am-241.

Figure 6-20. Normalized Cumulative Breakthrough Curves of the 11 Radionuclides Under Present Day Mean Infiltration Condition. Also shown are four breakthrough curves of colloidal forms of Pu-239 and Am-241.

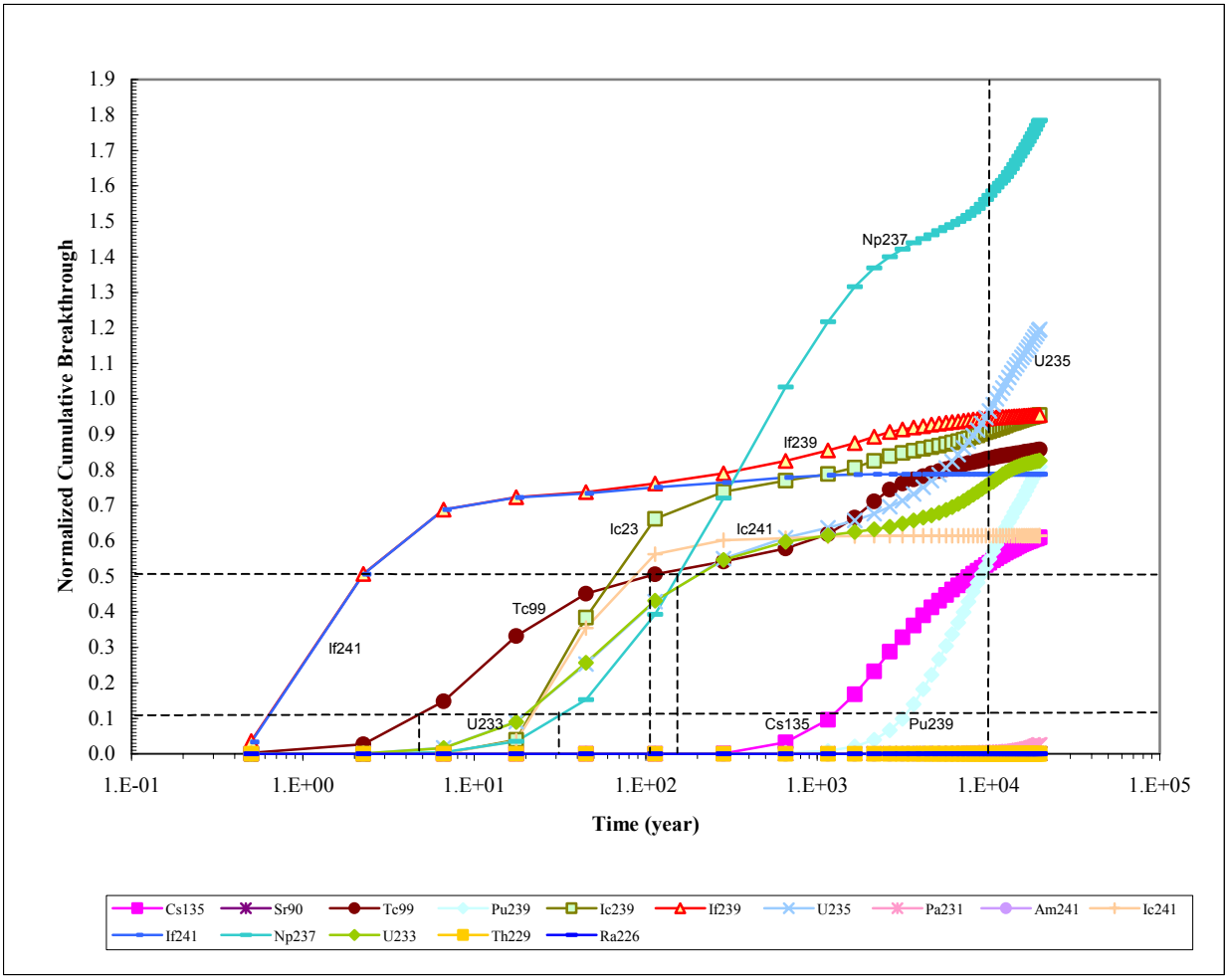

Output DTN: LA0311BR831371.003

NOTE: Ic239 and If239 are colloid species of Pu-239, and Ic241 and If241 are colloid species of Am-241.

Figure 6-21. Normalized Cumulative Breakthrough Curves of the 11 Species Radionuclides Under Glacial Mean Infiltration Condition. Also shown are four breakthrough curves of colloidal forms of Pu-239 and Am-241.

7. VALIDATION

Criteria for validation of this abstraction model have been developed in *Technical Work Plan (TWP) for: Performance Assessment Unsaturated Zone* (BSC 2002 [160819], Section I-2, Work Package [WP] AUZM07) and discussed in general terms in Section 4.2, Acceptance Criterion 5. In essence, validation of this abstraction model consists of a series of visual comparisons of model results with both simple models and a full process model of the UZ. The specific comparisons mentioned in the TWP (BSC 2002 [160819], Section I-2-2-1) are in effect satisfied in this Validation by performing comparisons equivalent to the ones cited in the TWP. For example, the requirement of a comparison to the solution of Sudicky and Frind (1982 [105043]) is satisfied by the comparison to the Discrete Fracture Model (DFM) in Section 7.1.1 below, and the requirement to compare to DCPT V2.0 (LBNL 2002 [154342]) is satisfied in the comparisons to the process model in Sections 7.2 and 7.3. These simulations are designed to summarize and augment the code verification checks that have been performed and documented in the qualification of FEHM V2.21 (see V&V documentation of this code: LANL 2003 [166306]), as well as the individual tests reported in other sections of this Model Report (for example, the decay-chain example of Section 6.4.4). Tests in the V&V documentation but not reproduced here include additional tests for dispersion and matrix diffusion. Validation runs under the more complex situations of interest to TSPA, namely 2-D and 3-D model domains for which process model simulations are available, are also carried out in this report.

Three classes of comparisons are made in this Validation section. The first, presented in Section 7.1, is a series of comparisons of the particle tracking model and a DFM. This comparison focuses on the ability of the model to adequately capture transport in a dual-permeability system under a variety of parameterizations. The series of tests is designed to demonstrate the validity of the underlying particle tracking method on a simple system. Simulations for this suite of runs can be thought of as representing the behavior of transport through an individual layer containing a small number of cells with uniform transport properties. Second, complexity is increased by comparing the particle tracking model with simulations in a 2-D cross sectional model. For comparison purposes, results are available on this cross section from Model Report BSC 2003 [163228] (DTN: LB03093RADTRNS.002 [166071]) assuming both a dual-k and a MINC formulation to capture fracture-matrix interactions. We show that the conceptual model for the fracture/matrix (f/m) interactions has an impact on the predicted behavior, especially for the fastest traveling portion of the solute. By using different transfer function representations (the dual-k and discrete fracture conceptual models) we test the ability of the model to replicate the behavior of the process models employing similar conceptualizations (dual-k and MINC, respectively). Finally, the third class of comparisons uses the full 3-D transport model being used in TSPA-LA, thereby representing the full complexity of the UZ in terms of heterogeneities in fluid flow conditions and properties. The radionuclide Tc-99 is released at the repository horizon, and the breakthrough at the water table is recorded and compared to results from T2R3D, documented in BSC 2003 [163228] (DTN: LB0307MR0060R1.007 [164752]). Results are available at the process model level only for the dual-k f/m interaction conceptualization, so direct comparisons to the particle tracking model are made for the dual-k transfer functions. We then perform a sensitivity analysis to show the effect of employing the DFM conceptualization in the particle tracking model, as well as some

qualitative tests of the implementation of the Active Fracture Model (AFM) in this abstraction model.

7.1 COMPARISONS WITH DISCRETE FRACTURE MODEL

A DFM, in which transport in a dual-permeability medium is simulated directly, is an excellent test case of the computationally simpler transport model employed in the UZ abstraction model. In the most general case, water moves in both media, as well as between the media, and solute communicates between the media as it moves through the system via molecular diffusion and advection. First, a test case for the advective movement between the fracture and matrix in such a system is presented. Then, we focus attention on parallel flow and transport in the two media, with solute introduced into either the fracture or the matrix. To investigate the ability of the model to span a range of hydrologic conditions, a fracture-dominated flow situation (essentially 100% fracture flow) and a case with a 60/40 f/m flow split are used for testing. Figure 6-5 represents the model system simulated with a DFM. Transport between the media occurs via molecular diffusion, so that the breakthrough curve at the outlet of such a model is a function of the relative and absolute velocities, and the degree of diffusive communication of solute between the media. Geometric, flow, and transport parameters, listed in Table 7-1 for this suite of tests, are selected to be representative of transport conditions in the UZ at Yucca Mountain, but do not constitute an actual model of the system, merely a testing setup to enable comparisons to be made. Therefore, data sources for these values are not required.

Table 7-1. Parameter Values for Discrete Fracture Model Test Suite

Parameter	Symbol	Value	
		Case 2 (Sect. 7.1.2)	CASE 3 (Sect. 7.1.3)
Flow Path length (m)	L	300	300
Fracture Half-Spacing (m)	B	0.5	0.5
Fracture Half-Aperture (m)	b	0.5e-3	0.5e-3
Fracture Saturation (unitless)	θ_f	0.2	0.2
Matrix Water Content (unitless)	θ_m	0.4	0.4
Fracture water flux (kg/s)	f_f	1.583e-5 (99% of total)	9.49e-6 (60% of total)
Matrix water flux (kg/s)	f_m	1.583e-7 (1% of total)	6.336e-6 (40% of total)
Diffusion Coefficient (m^2/s)	D_m	1.e-30, 1.e-12, 1.e-11, 1.e-10, 1.e-9	1.e-30, 1.e-12, 1.e-11, 1.e-10, 1.e-9
Matrix sorption coefficient (mL/g)	K_d	0	0 or 5

For this entire set of simulations, a 2-D DFM with these parameters was simulated using FEHM V2.21 (LANL 2003 [165741]) in a manner similar to that used to generate the transfer functions (see Attachment III), and the resulting breakthrough curves at the outlet were processed using the software routine discrete_tf V1.1 (LANL 2003 [165742]). For the simulations using the particle tracking model, a simple one-dimensional pathway is constructed consisting of ten dual-permeability cells (twenty total). The flow conditions (water contents, volumes, flow rates,

etc.) were built into an FEHM restart flow field file by hand. These conditions, along with the grid files and the main FEHM input file, are read directly into the code and the transport particle tracking solution is obtained for the input flow field. This process was chosen to make this test as similar as possible to the way the code is to be used in TSPA calculations, in which flow fields are read in directly and transport is computed. Results are then post-processed using software routine ppptrk V1.0 (LANL 2003 [165753]).

7.1.1 Test of Advective Transport Between Continua

In this initial test case (CASE 1), we examine a situation with parallel flow in the two media, but with 90% fracture flux, 10% matrix flux for the first half of the flow path, transitioning abruptly to 60% fracture flux, 40% matrix flux for the second half of the path. Other geometric and storage parameters are the same as those listed in Table 7-1. Solute mass is input into the fracture. By turning off diffusion (which is tested separately in runs discussed later), it is trivial to determine the arrival times that the particle tracking code should produce. The early arrival represents mass that stays in the fracture, and later arrival represents the fracture transport for half of the path, and matrix transport for the remainder. In the results plotted in Figure 7-1, the vertical lines are the theoretical arrival times that the code should reproduce, and the horizontal line (at 2/3, or 0.67) is the theoretically determined proportion of mass that should take the fracture pathways all the way through the model. The particle tracking code reproduces the theoretical behavior for advective movement between the media, thereby confirming that the code correctly routes particles on the basis of advective flow between the fracture and matrix continua. The two simulation curves in the figure are: a simulation with the diffusion model turned off completely, and a simulation with the diffusion model invoked, but the diffusion coefficient set to a low value. Despite the fact that both means for performing the simulation yield acceptable results, it is advisable to completely turn off the diffusion model if the intention is to model a solute with no diffusion. Nevertheless, this result indicates that if diffusion coefficient is set low, the model yields the correct behavior.

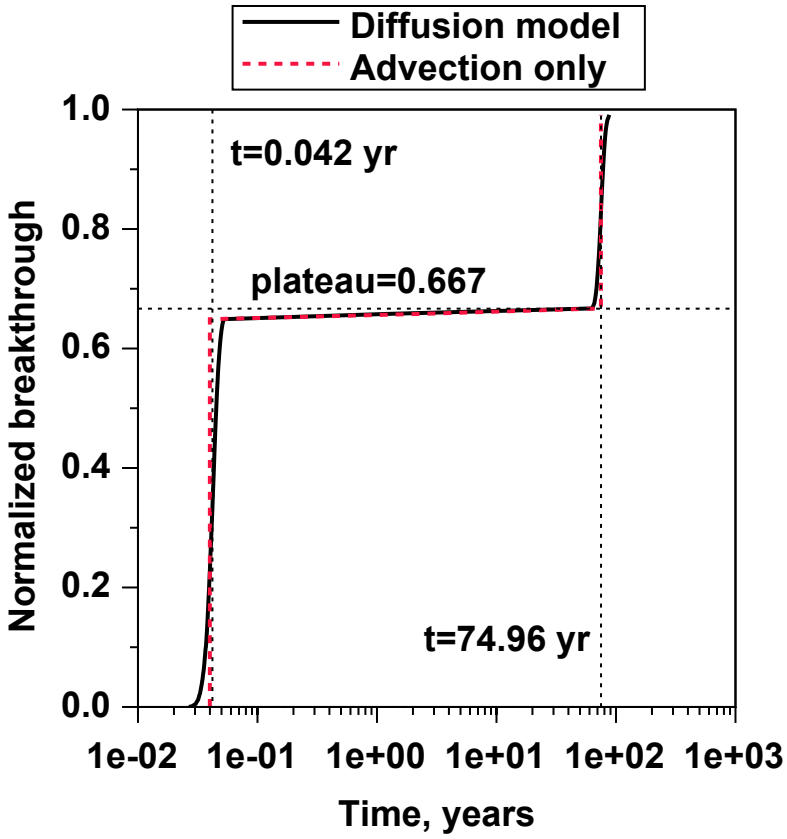

Output DTN: LA0311BR831371.001

Figure 7-1. Particle Tracking Abstraction Model Behavior for Advective Transport Between the Fracture and Matrix Continua: No Diffusion or Sorption, Solute Injected into the Fracture, Compared to Theoretical Results

7.1.2 Comparisons with Diffusion for Fracture-Dominated Flow

Figure 7-2 (Case 2) shows the results of simulations representative of fracture-dominated flow, with 99% of the flow occurring in the fracture. Solute is introduced into the fracture, and the breakthrough at the end of the model is simulated. The simulations show that over the range from fracture-dominated transport (D=1.e-30 m^2/s) to conditions corresponding to complete diffusive interchange between the two media (D=1.e-9 m^2/s), the particle tracking model provides very close agreement with the DFM of the same system. Although it is tempting to assume that the model is simply reproducing the same curve that was provided as input in the form of a transfer function, this is not the case. In the particle tracking model, the code executes a transfer function operation for each of the ten cells of the flow path. Each cell has a fracture travel time of one-tenth the total, meaning that the code correctly seeks the appropriate transfer function for that cell, and then predicts the overall breakthrough curve for a pathway consisting of multiple nodes. Deviations between the particle tracking model and the discrete fracture solution are due to the fact that the exact transfer functions for the test case are not available, and the model must find the curve with parameters closest to the desired values. This approach is therefore approximate, and relies on the code being supplied a family of transfer functions that covers the range of parameters encountered in a given simulation. Despite this limitation, this test demonstrates that the basic process for determining the travel times of individual particles

through a series of connected cells is properly implemented. It also demonstrates the ability of the model to simulate the behavior for an important end-member condition, that of fracture-dominated flow.

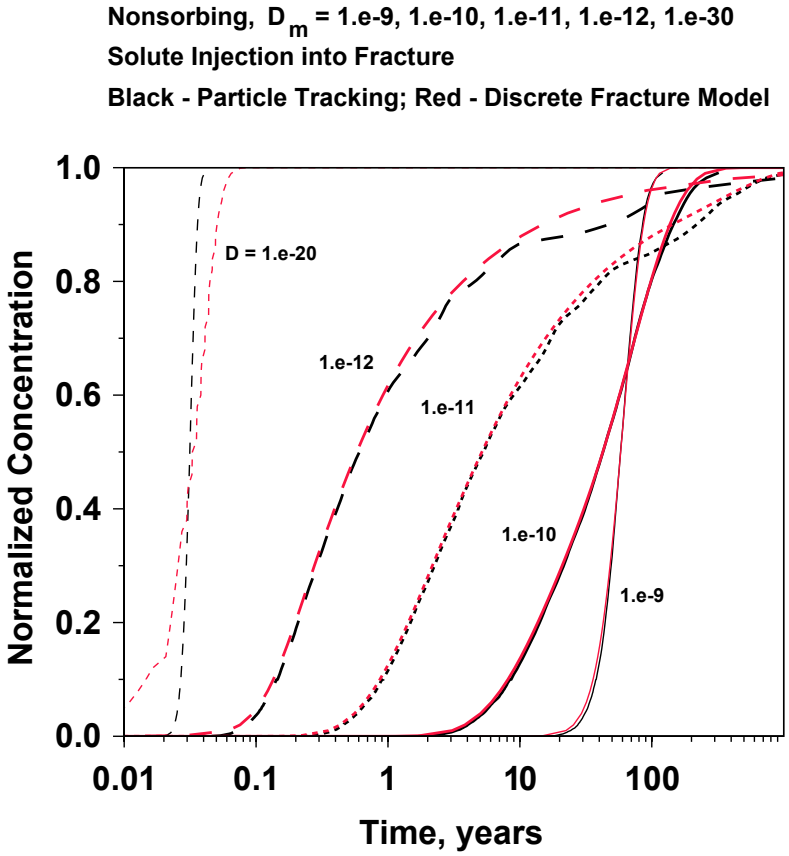

Output DTN: LA0311BR831371.001

Figure 7-2. Comparison of Discrete Fracture Model and Particle Tracking Abstraction Model: Non-Sorbing Solute Injected into the Fracture, for Different Values of Diffusion Coefficient, f_f = 0.99

7.1.3 Comparisons with Diffusion and Sorption for Intermediate Flow Case

Figure 7-3 (Case 3) compares the DFM and the particle tracking model for the case of more evenly divided flow in the two media (60/40 f/m flow split). Different diffusion coefficients are used, spanning the range from fracture-dominated transport to a diffusive regime in which the system is essentially behaving as a single continuum. The particle tracking model replicates the behavior adequately over the entire range of parameters. At the lower diffusion coefficients (1.e-11 and 1.e-12 m^2/s), there is a slight distortion in the breakthrough curve of the particle tracking model at later times caused by the process by which particles are probabilistically shifted from one medium to the other due to the diffusive process. This is explained as follows. Consider the case in which a particle that enters a cell via the fracture is instructed by the algorithm to leave that cell via the matrix. This can occur in a low-diffusion regime for some of the solute mass. When the particle is placed in the matrix in the next cell, it is implicitly assumed to be randomly placed along the width of the matrix. In reality, for low diffusion, solute mass will reside preferentially near the fracture, so that the assumption of it being randomly placed along the

matrix width is somewhat in error. This results in somewhat longer travel times for mass that shifts from fracture to matrix. The result is a tendency to predict longer travel times than is expected from a DFM. Despite this error, the initial breakthrough is captured very well, and the overall trends of the DFM are reproduced. At higher diffusion coefficients, this problem does not occur because the assumption of randomly distributed solute mass along the matrix width is a good one. Therefore, the important end-member of single-continuum behavior, with breakthrough times controlled by the matrix storage volume, is reproduced as well. Finally, this phenomenon is less pronounced for the fracture-dominated flow case of the previous section because fewer particles leave via the matrix for the case of low matrix flow. Although this error is reasonably small compared to the robust fashion in which the model captures the transport behavior over orders of magnitude ranges in diffusion coefficient, and the error is fairly small for either fracture-dominated flow or highly diffusive transport, we perform additional tests at the end of this section to investigate the nature of this error and document its magnitude.

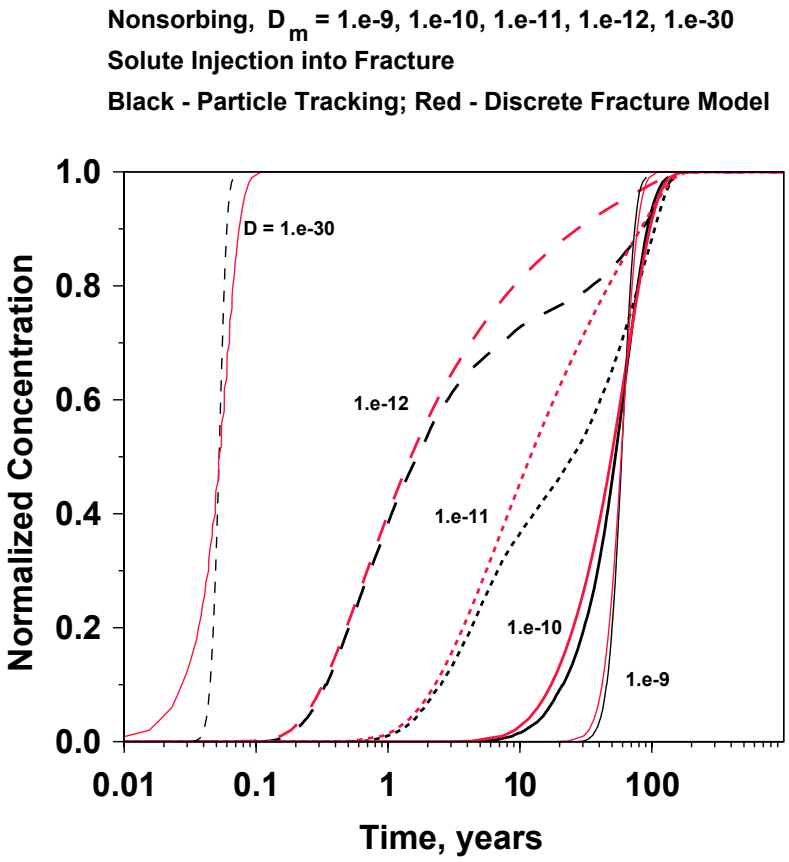

Output DTN: LA0311BR831371.001

Figure 7-3. Comparison of Discrete Fracture Model and Particle Tracking Abstraction Model: Non-Sorbing Solute Injected into the Fracture, for Different Values of Diffusion Coefficient, f_f = 0.6

Figure 7-4 shows a set of breakthrough curves for Case 2 with a sorbing solute of $K_d = 5$ cc/g. Similar behavior is observed, with longer travel times caused by sorption of the mass that diffuses into the matrix. Similar to the nonsorbing solute comparisons, these comparisons

illustrate that the model adequately captures the impact of sorption on the matrix rock. Differences similar to those observed in the non-sorbing cases are present, but the particle tracking model replicates the fracture-matrix interactions in the dual permeability model over a broad range of diffusion coefficients with sorption included. Further verification of the correct implementation of the model for sorption is shown in Figures 7-5 and 7-6, which show the comparisons to the discrete fracture model for high values of K_d. At a diffusion coefficient of 1.e-11 (Figure 7-5) or 1.e-10 (Figure 7-6), the application of high values of K_d in the model are shown to reproduce the expected behavior for the discrete fracture model.

Next, Figure 7-7 replicates the conditions of the nonsorbing simulations, except that the solute mass is introduced into the matrix. Very important features of the transport behavior predicted by the DFM are replicated quite closely in these runs. The generally longer travel times are due to the introduction of mass into the slower moving matrix flow. The nature of these results in terms of first arrivals and mean behavior can be understood as follows. When diffusion is finite but relatively low, the small portion of the solute introduced close to the fracture can diffuse into the fracture and travel rapidly to the outlet, yielding a leading edge of the breakthrough curve at short times. This important aspect of the behavior for releases into the matrix is reproduced very accurately by the particle tracking code, as evidenced by the comparison to the DFM. This leading edge is not present for higher diffusion coefficients because mass diffuses readily between the continua, making the probability of rapid transport along the entire length of the model negligibly small. However, the rise in the breakthrough curve representing the bulk of the mass arrival occurs earlier for the high-diffusion case. This can be understood by recognizing that when diffusion is large enough to allow migration of solute over distances comparable to B, the system becomes essentially a composite medium with an effective flow rate equal to the sum of the fracture and matrix fluxes. By contrast, at low diffusion coefficients, travel times through the matrix are governed by the matrix flux, which in this example is only 40% of the total. Hence, arrival times for the matrix release case and low diffusion is later than for the high-diffusion case.

Of note in these comparisons is that the particle tracking model reproduces these features quite well, with the following caveats. At later arrival times, the particle tracking and discrete fracture models diverge somewhat, with particle tracking breakthroughs occurring somewhat earlier than the DFM breakthrough. The explanation described when explaining the differences for fracture releases applies in reverse for solute releases into the matrix. Nevertheless, the particle tracking simulations compare well overall with the DFM results, capturing the key features and the travel times for matrix releases. This comparison provides important assurance that the mass that enters the UZ transport model via EBS diffusive releases into the matrix will be properly simulated.

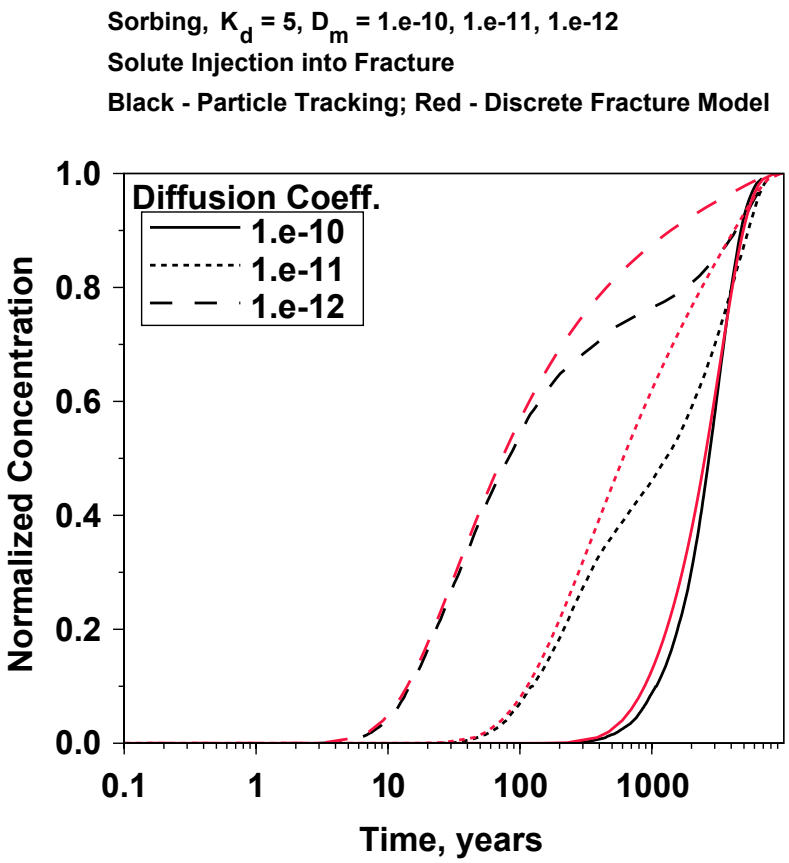

Output DTN: LA0311BR831371.001

Figure 7-4. Comparison of Discrete Fracture Model and Particle Tracking Abstraction Model: Sorbing Solute Injected into the Fracture, for Different Values of Diffusion Coefficient

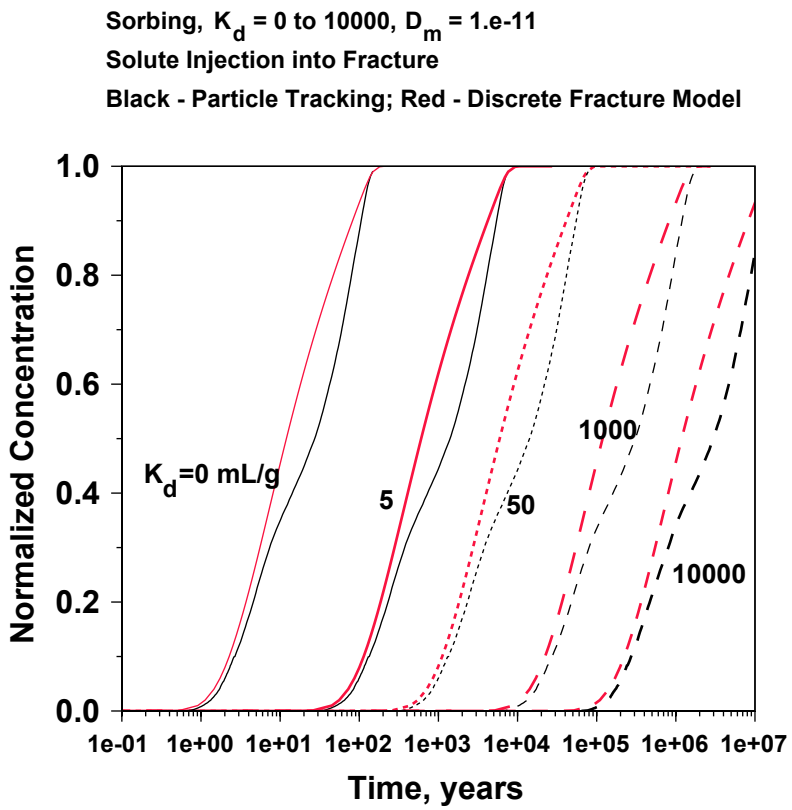

Output DTN: LA0311BR831371.001

Figure 7-5. Comparison of Discrete Fracture Model and Particle Tracking Abstraction Model: Solute Injected into the Fracture, for Different Values of Sorption Coefficient. D_m = 1.e-11.

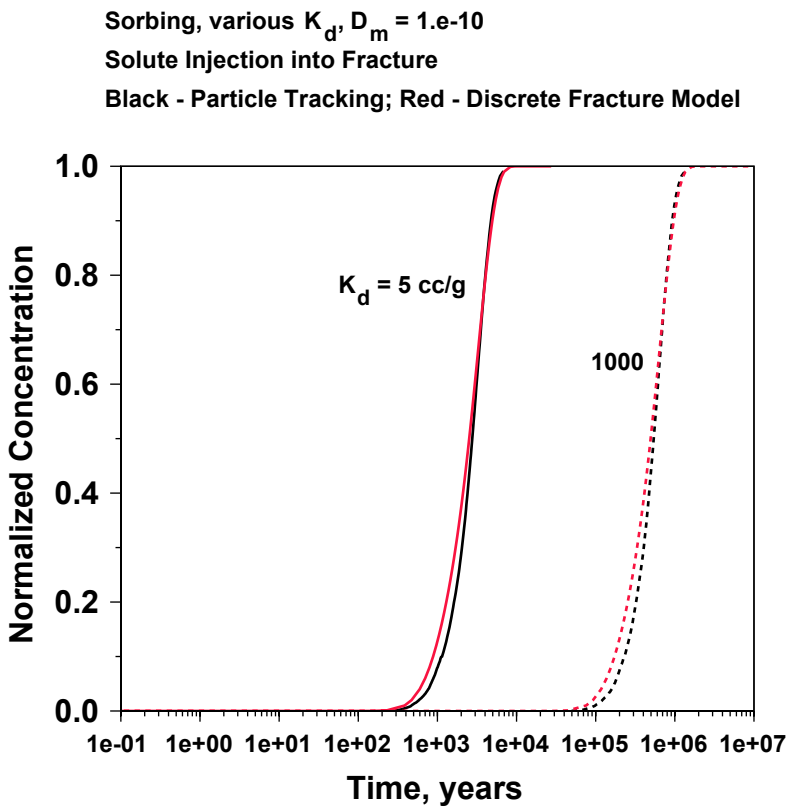

Output DTN: LA0311BR831371.001

Figure 7-6. Comparison of Discrete Fracture Model and Particle Tracking Abstraction Model: Solute Injected into the Fracture, for Different Values of Sorption Coefficient. D_m = 1.e-10.

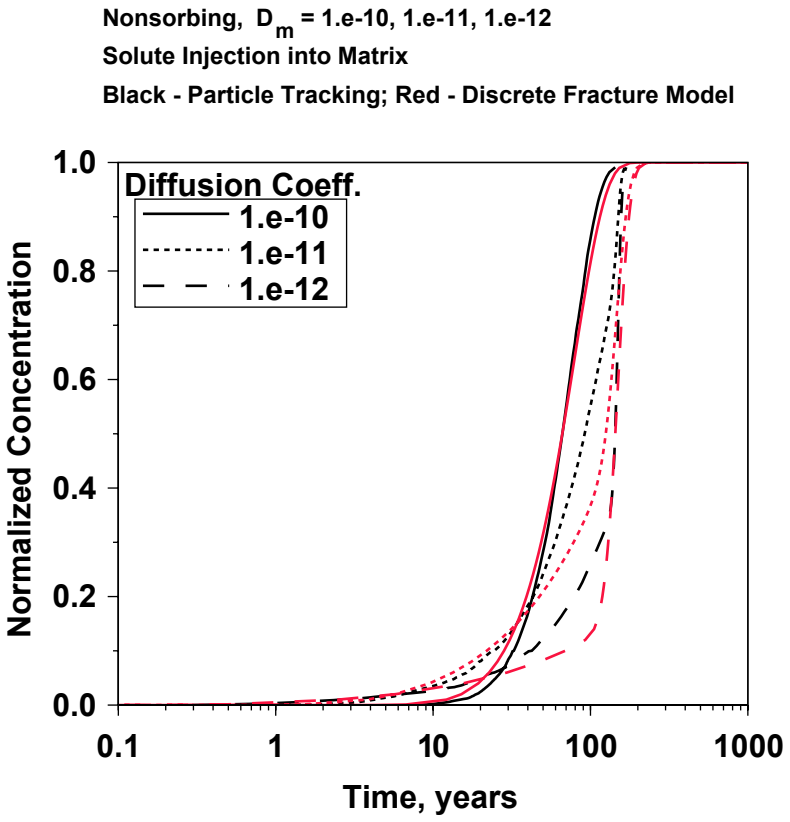

Output DTN: LA0311BR831371.001

Figure 7-7. Comparison of Discrete Fracture Model and Particle Tracking Abstraction Model: Non-Sorbing Solute Injected into the Matrix, for Different Values of Diffusion Coefficient

To further explore the discrepancies for cases with relatively even distribution of flow in the two media, we examine a series of tests in which the number of grid cells in the path are varied. These tests were performed for D=1.e-11 m^2/s, no sorption, and solute introduced in the fracture. Figure 7-8 compares the breakthrough curves for different numbers of cells with the DFM results. In all cases the overall flow path characteristics are the same, but the discretization is varied. For one cell, the discrete fracture model is replicated virtually exactly, because in this case we truly are reproducing a DFM result that was used to generate the transfer function itself. This curve merely shows that for a single cell, the code finds the correct transfer function and the stochastic particle tracking method is implemented properly. As the number of cells in the path is increased to five or ten, the moderate error observed previously appears. An important point to consider in assessing this grid error is the fact that when flow transitions at interfaces of contrasting hydrologic properties, major transitions in particles from one medium to the other due to advection are likely to occur. Therefore, this type of test really replicates the behavior of the model within a single hydrogeologic unit. Since the number of grid cells within a unit tends to be rather small, the error within a unit is also likely to be small, perhaps of the magnitude shown in the five-cell curve.

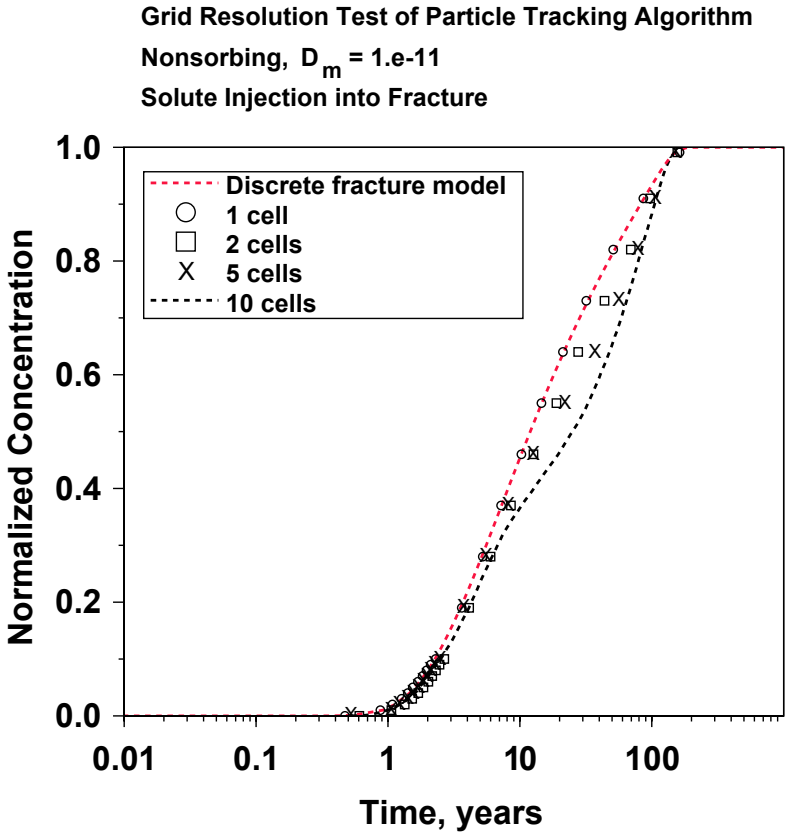

Figure 7-8. Comparison of Discrete Fracture Model and Particle Tracking Abstraction Model: Sorbing Solute Injected into the Fracture, for Different Numbers of Grid Cells in the Flow Path.

7.1.4 Summary of Validation Tests for a Discrete Fracture Model

To summarize the results of this first validation test suite, the behavior of the particle tracking model agrees well with a DFM over a very broad range of transport conditions. The deviations that have been observed between the two models are very unlikely to influence TSPA model predictions, and the cause of these differences is well-understood. Furthermore, fracture-matrix advective transport has been demonstrated to be properly implemented, and the case of releases into the matrix is also shown to be properly implemented. Therefore these comparisons constitute an adequate demonstration of the effectiveness of the particle tracking model for capturing the fracture-matrix interactions that the model is designed to simulate.

7.2 COMPARISON WITH THE DUAL-K AND MINC MODEL FORMULATIONS ON A TWO-DIMENSIONAL CROSS SECTION MODEL

Multi-dimensional benchmarking simulations of the UZ transport system is the next step in the validation of the abstraction model. Of course, the system is too complex to enable comparison to analytical solutions. In fact, selecting a code to benchmark against is also difficult because all available codes formulate the transport problem somewhat differently. BSC (2003 [163228]) showed that these formulations, which constitute alternate conceptual models for transport, can produce significantly different results. These differences must be understood to appreciate the

differences in the benchmarking results, especially for a complex, multi-dimensional model. In this section, we benchmark the particle tracking abstraction model developed here to simulations of the system performed using T2R3D, documented in BSC (2003 [163228]). Two ACMs have been developed on the 2-D cross section model using T2R3D. The simulations called "dual-k" use a finite-volume dual-permeability model formulation in which the fracture-matrix diffusion term is governed by a simple gradient calculated as the difference in concentration between the media divided by a characteristic distance, on the order of the flowing fracture spacing. In addition, in BSC 2003 [163228] the MINC conceptual model employs a series of grid blocks in the matrix. The UZ abstraction model implemented in FEHM is capable of simulating either situation. In the conceptualization we term the DFM f/m interaction model, sharp concentration gradients are captured through use of a transfer function obtained using a DFM with fine discretization in the matrix, analogous to a MINC formulation. These are the transfer functions used in the comparisons to the DFM in Section 7.1. By contrast, a dual-k model can be used to generate transfer functions, and those results might be expected to resemble those of T2R3D when an analogous dual-k formulation is used. These comparisons are performed in this section. A final point on these conceptual models is that in all abstraction model cases, the flow field on which the transport model is run is a dual-k flow field because the particle tracking abstraction model was formulated with the dual-k flow assumption. Therefore, the transport runs with the DFM formulation for the f/m interaction submodel employ a finely discretized matrix block for transport, but a single matrix block for the flow field. This approach should enable sharp gradients likely to be present for solute transport to be captured in the model.

Figure 7-9 plots the comparison results of the particle tracking model and the two ACMs simulated with T2R3D. For the FEHM runs, the 2-D flow fields compatible with FEHM were obtained from the TDMS (DTN: LB0310T2FEHMFF.001 [166060]). In all cases, particles are released uniformly across all nodes designated as repository nodes in the model. First, we examine the case of no diffusion. This comparison is performed to benchmark the particle tracking code in a mode in which particles are routed through the model with dispersion. There is excellent agreement between the particle tracking model and the dual-k, no-diffusion model using T2R3D. Slight differences may be attributable to subtle differences in model formulation, numerical errors for one or the other model, or due to the fact that one of the eleven nodes designated as a repository node in the T2R3D runs was omitted from the particle tracking runs because it was found to be located in the PTn. Even with these possible sources for the difference, the agreement provides confidence that particle routing and transit times are properly implemented. We also note that colloidal species will be simulated with no diffusion, so these results provide confidence in the transport predictions for colloid-facilitated radionuclides.

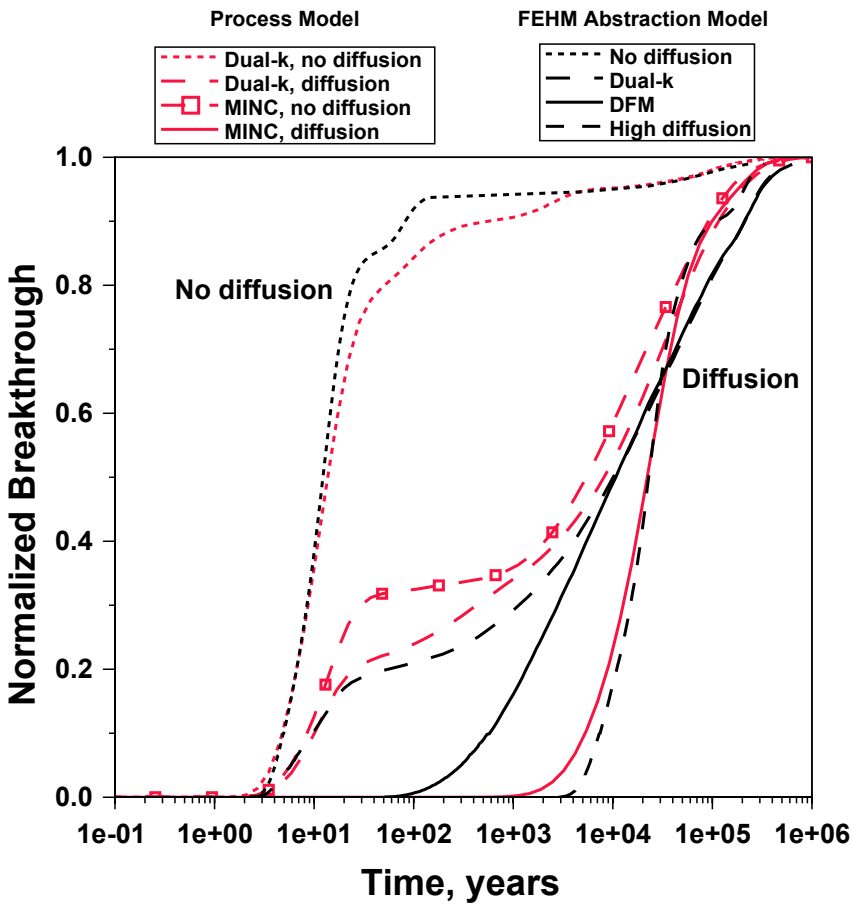

T2R3D Simulations DTN: LB030932RADTRNS.002 [166071]
Output DTN: LA0311BR831371.002

Figure 7-9. Comparison of Particle Tracking Model with Process Models for a 2-D, Mountain-scale Model: With and Without Diffusion, for Dual-k and DFM Formulations for the f/m Interaction Model.

Before proceeding to the results with diffusion, a discussion of the MINC simulation with no diffusion is in order. Since transport runs without diffusion depend only on advective processes, it is apparent that the mismatch between the MINC, no diffusion and the dual-k simulations (both T2R3D and particle tracking) indicates that there are differences in the flow regime for the MINC model. The reasons for this difference stem from the fact that the numerical discretization of this model is different than that of the dual-k model. We raise this issue not to imply that one model is correct and the other is not, but rather to point out that because of differences in the flow regimes of the MINC and dual-k flow models, we do not necessarily expect the particle tracking runs, which input the dual-k flow field rather than the MINC flow field, to match the MINC results precisely. Nevertheless, we would expect similar breakthrough curve features to be predicted by the particle tracking and MINC models, when the former are computed with the DFM conceptual model transfer function curves. By contrast, diffusion in the dual-k transport model is expected to predict much earlier breakthrough of a portion of the solute mass.

The simulations with diffusion in Figure 7-9 confirm this result. In this figure, various FEHM particle tracking simulations are benchmarked against simulations using a dual-k or MINC

formulation for the 2-D cross section. The difference in predicted behavior between the two conceptual models is reflected in the FEHM simulations in a manner similar to that of the process models. Comparing the MINC and FEHM DFM conceptual model, first arrivals in both cases occur much later in time than the dual-k models. For comparison, a high-diffusion case is also presented to illustrate the upper limit of breakthrough times for this flow field. Regarding the dual-k models, the characteristic feature of early arrival of a significant portion of the mass at times similar to that of pure fracture transport is produced in both the process and abstraction models. The fraction of the mass arriving early is somewhat lower in the FEHM model than in the T2R3D model, but qualitatively, the dual-k transfer function curves yield behavior quite similar to the process model result using T2R3D. Also, both the process model and abstraction model results converge at longer travel times, regardless of the formulation of the f/m interaction model or the value of diffusion coefficient used. Finally, the high-diffusion FEHM simulation is shown to bracket the behavior of the breakthrough curves in the figure, with results that are very close to that of the MINC model.

All of these indicators show that the abstraction model compares adequately with the process models, and properly accounts for the role of conceptual model uncertainty in the f/m interaction model. The relatively minor differences of the models employing the dual-k f/m conceptual model are probably attributable to subtle differences in model formulation and mathematical techniques for solving the transport problem.

7.3 COMPARISON WITH T2R3D PROCESS MODEL FOR THE THREE DIMENSIONAL SYSTEM

Full simulation of the 3-D UZ transport system is the last step in the validation of the abstraction model. In Section 7.2 we demonstrated on a system for which the dual-k and MINC f/m interaction model results were available for comparison, the FEHM particle tracking results can provide qualitatively similar behavior for these ACMs simply by choosing transfer functions developed for a given conceptualization. In this section, we benchmark the particle tracking abstraction model developed here to simulations of the system performed using T2R3D, documented in BSC (2003 [163228]). The T2R3D simulations use a finite-volume dual-permeability model formulation in which the fracture-matrix diffusion term is governed by a simple gradient calculated as the difference in concentration between the media divided by a characteristic distance, on the order of the flowing fracture spacing. No results are available using a MINC or other formulation that captures sharp gradients into the matrix. Therefore, our principle benchmarking simulations for FEHM will be those using the dual-k transfer functions. However, we also demonstrate that the code can effectively explore uncertainty associated with this conceptual model.

7.3.1 Comparisons of FEHM and T2R3D for the Dual-k Conceptual Model

In these comparisons, we restrict attention to a non-sorbing radionuclide Tc-99, since simulations in Section 7.1 above showed that sorption is handled appropriately. For all model runs using either FEHM or T2R3D, breakthrough at the water table is simulated for a release function consisting of a pulse of radionuclide introduced uniformly across the entire repository. The comparisons between the models are for the cumulative, normalized arrival time distributions at the water table. Of course, these release functions are not realistic representations of how the

actual engineered system will behave. Such a release function yields the distribution of travel times for the UZ as a whole for releases across the repository, and as such is a useful point of reference for how the UZ behaves, as well as being an appropriate benchmark for comparing the models. Parameters in the abstraction model are uncertain. For this comparison, values documented in BSC 2003 [163228] are used to perform this comparison, and the present-day climate flow fields are used to make the comparison throughout the entire simulation period. This approach allows us to test the model over a significant range of infiltration scenarios, those spanning the uncertainty range for infiltration rate using the three present-day flow fields derived in BSC 2003 [163045].

Figure 7-10 shows the cumulative travel time distributions through the UZ for Tc-99 for the two models for the three flow fields (lower, mean, and upper) developed to capture uncertainty in the present-day infiltration rates. The agreement between FEHM using the dual-k transfer functions and T2R3D is excellent, considering the vast range of infiltration conditions covered in these comparisons. For the lower infiltration scenario, the early arrival of a small fraction of the released mass, and the steepening breakthrough curve after 10,000 years, are observed in both models. The plateau at values between 0.4 and 0.5 at long times is due to radioactive decay of Tc-99. For the mean infiltration flow field, the agreement of the process and abstraction models is also excellent at all travel times. For the upper infiltration scenario, FEHM predicts a somewhat earlier arrival for the fastest moving solute, indicating a difference in the way the two models handle diffusion in rapid fracture flow. Nevertheless, in benchmarking exercises of such a complex model, differences are the norm. In this case, we consider the benchmarking results to be very successful, in that all significant features of the UZ transport system are captured with the abstraction model.

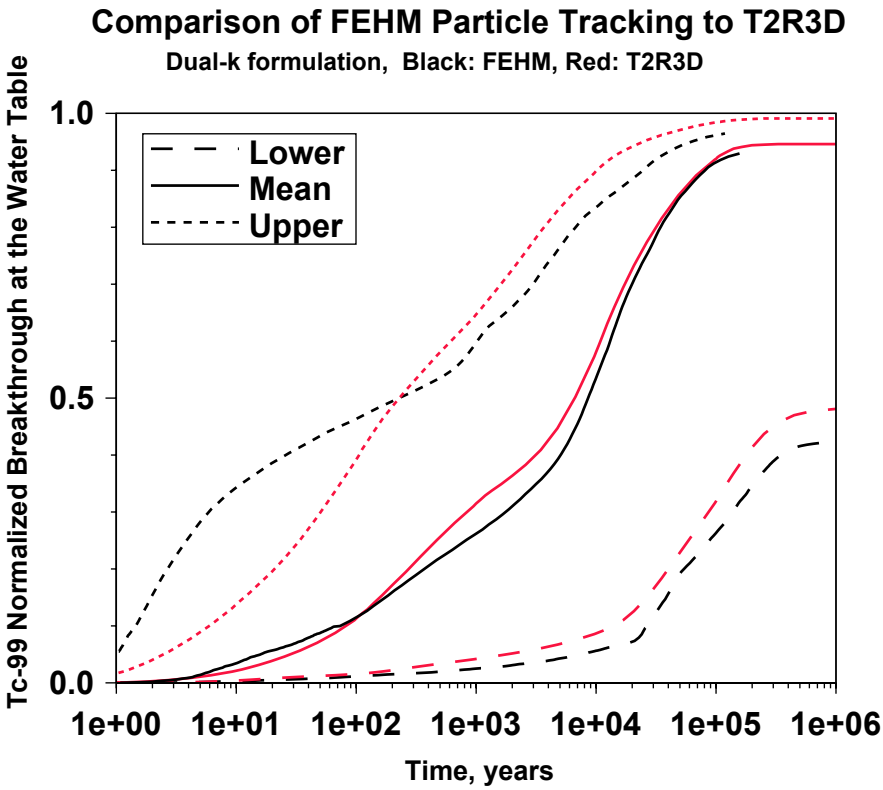

Figure 7-10. Comparison of Breakthrough Curves for Tc-99 for T2R3D and the UZ Transport Abstraction Model: Simulations for Different Present-Day Infiltration Rate Scenarios (Lower, Mean, and Upper)

7.3.2 Influence of Diffusion Coefficient and F/M Interaction ACM

To amplify on the simulations presented in the previous section, in Figure 7-11 we bracket the behavior of the particle tracking model as a function of diffusion. This figure shows the behavior of the FEHM model over the complete range of diffusion coefficients, from no diffusion to a case in which diffusion is set so high that it effectively yields a composite medium behavior (D=1.e-8 m^2/s). The envelope of behavior as a function of diffusion is quite large, whereas the behavior of T2R3D is reproduced when the same parameters and conceptual model for f/m interactions is selected. This result illustrates that the abstraction model yields reasonable results over a wide range of diffusion coefficient, one of the key parameter uncertainties in the TSPA model. Also shown in Figure 7-11 is the predicted behavior using the DFM formulation for the f/m interaction model. No process model results are available for comparison due to the computational limitations of simulating the full 3-D model using a MINC formulation. These limitations are not an issue for the abstraction model, which simply uses a different set of transfer functions as input. The results are reasonable, given our understanding of these models and the comparisons presented in Section 7.2 for the smaller 2-D cross section model. The main differences for these ACMs are at the earliest arrival times, where the dual-k model predicts much faster arrivals at the water table. For later travel times, the two curves track each other closely, showing that the results are insensitive to the conceptual model. Finally, all breakthrough curves with diffusion, including the high-diffusion case, converge at large travel

times. This result is also reasonable, providing additional evidence for the correct functioning of the f/m interaction model.

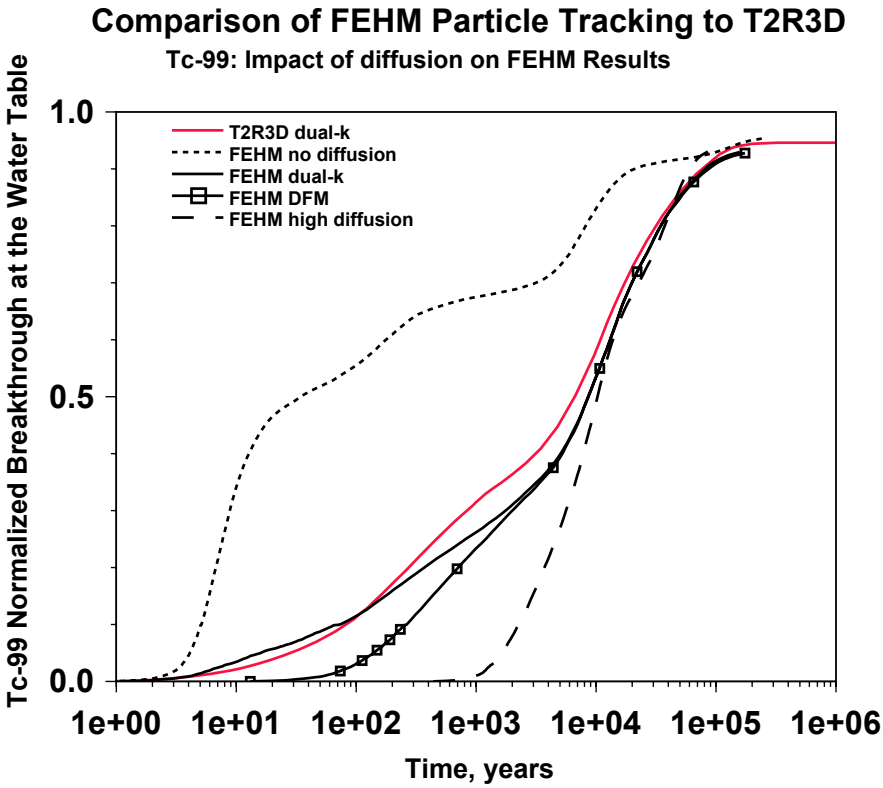

Figure 7-11. Comparison of Breakthrough Curves for Tc-99 for T2R3D and the UZ Transport Abstraction Model: Mean Infiltration Scenario, Diffusion in FEHM Ranging from No Diffusion to High Values.

The influence of f/m conceptual model is explored more fully in Figure 7-12, a comparison, using only the FEHM particle tracking model, of the dual-k and DFM Alternative Conceptual Models (ACMs) for all of the flow scenarios. The choice of ACM is particularly sensitive for the upper infiltration scenario, whereas differences become progressively more subtle for the mean and lower infiltration scenarios, respectively. As the fluid velocity is reduced, the characteristic diffusional distance into the matrix increases. For this situation, the dual-k model becomes more like the DFM in the sense that concentration gradients in the latter are not nearly as steep. With respect to the abstraction model, we conclude that these comparisons have reasonable qualitative explanations. This result illustrates that the abstraction model can propagate conceptual model uncertainties for f/m interactions through the TSPA model.

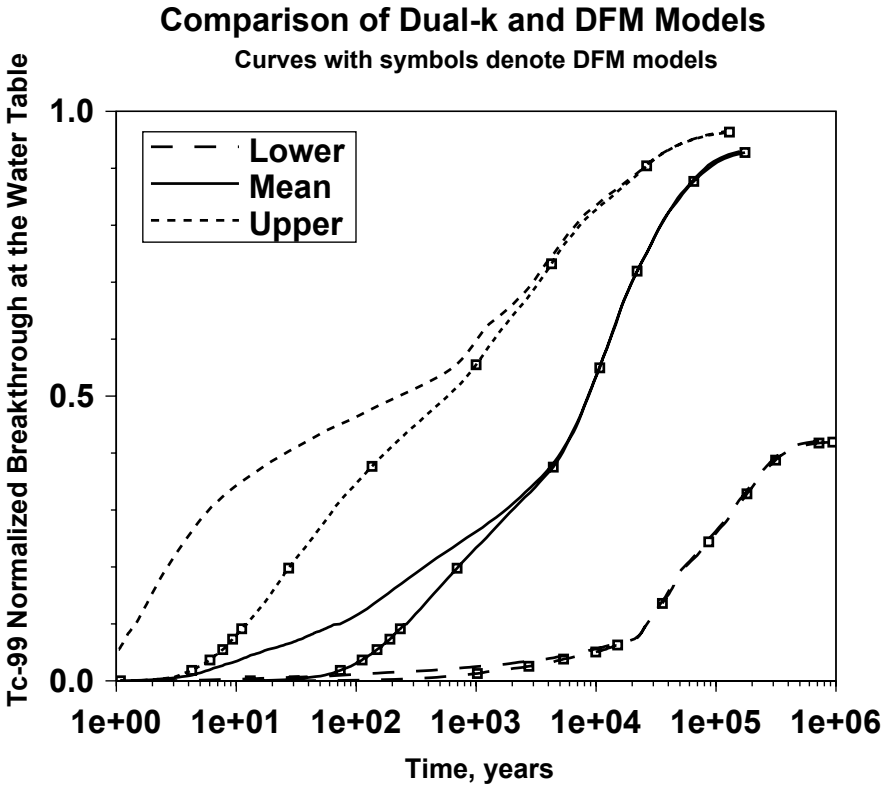

Output DTN: LA0311BR831371.002

Figure 7-12. Breakthrough curves for Tc-99 using the UZ Transport Abstraction Model to Investigate the Role f/m Interaction Conceptual Model: Simulations for Different Present-day Infiltration Rate Scenarios (Lower, Mean, and Upper)

7.3.3 Tests of the Active Fracture Model Implementation

The AFM has been identified in BSC 2003 [163228] and BSC 2003 [163045] as a model whose parameters are quite uncertain, and potentially this uncertainty may significantly influence UZ performance predictions. Therefore, it is important to demonstrate that the sensitivity explored in the process model work can be represented in the abstraction model. In this section we examine the impact of the gamma parameter in the AFM on the results. This set of simulations is intended to confirm that the AFM formulation in FEHM yields results similar to that of the process model, and to extend those results by performing the same analysis for the DFM model for f/m interactions. To be completely rigorous, one would need to regenerate flow fields using the alternate AFM model parameters because the AFM influences both flow and transport processes. However, process flow model results (BSC 2003 [163045], Section 6.8.1) have demonstrated that the AFM parameters have very little influence on the relevant flow model parameters for transport, namely the fluid saturations and flow rates in the fracture and matrix continua. Therefore, it is an excellent approximation to simply apply AFM parameter changes to the transport model using flow model results obtained from the base case flow simulation. Figure 7-13 illustrates the impact of lowering the gamma parameter in the same fashion as was done in Section 6.8.2 of BSC 2003 [163045]. Note the close qualitative similarity of the simulation results with that of Figure 6.8-3 of that report. Lowering the gamma parameter in the TSw in the same manner as in BSC (2003 [163045]) yields a trend toward longer arrival times for the

earliest arriving solute. The curves converge at longer travel times. The fact that the lowering of gamma in additional units below the repository has no further effect indicates that the principle sensitivity is for the AFM parameters in the TSw. For the purposes of the abstraction model validation, this qualitative comparison to the results of BSC (2003 [163045], Figure 6.8-3) provides strong evidence that the implementation in FEHM with respect to the AFM replicates the behavior of the process model.

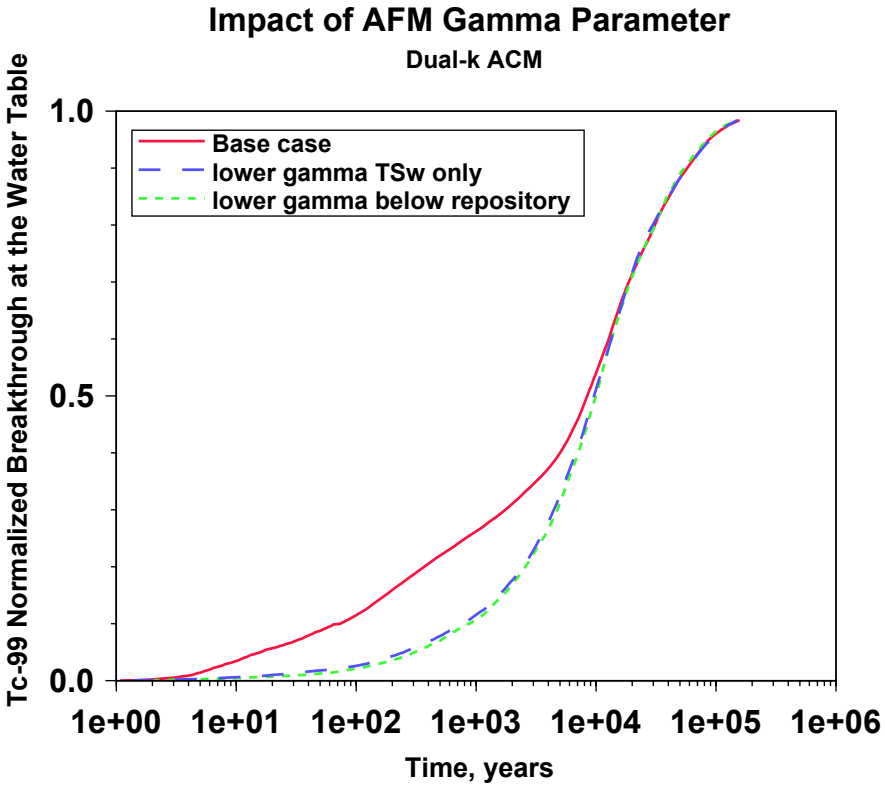

NOTE: The colors, line types, and legend descriptors are chosen to facilitate a direct visual comparison to the simulation results presented in BSC 2003 [163045], Figure 6.8-3.

Figure 7-13. Breakthrough Curves for Conservative Solute Using the UZ Transport Abstraction Model to Investigate the Role of AFM Parameter Gamma: Dual-k ACM, Simulation for Different Values of Gamma in Rock Units Beneath the Repository.

Finally, Figure 7-14 shows a similar investigation of the role of AFM model parameters for the DFM conceptualization. Note that in comparison to the dual-k DFM, gamma has smaller influence on the transport behavior. This result is a consequence of the way in which the two ACMs simulate the early-time behavior of the breakthrough curves. When a more refined grid is used to resolve gradients in the matrix, the role of flowing fracture spacing and interface area is less important than for the case in which a single matrix grid block is used to represent diffusion. The implication of this conclusion is that AFM model parameters will have a relatively smaller influence on predicted UZ behavior for the DFM conceptualization. By contrast, a somewhat larger sensitivity to AFM gamma parameter is predicted for the dual-k conceptual model. These differences must be recognized when interpreting sensitivity studies involving the AFM and the

f/m interaction models. In general, the diffusion coefficient itself, rather than the AFM model parameters, is a much more sensitive parameter controlling the UZ performance.

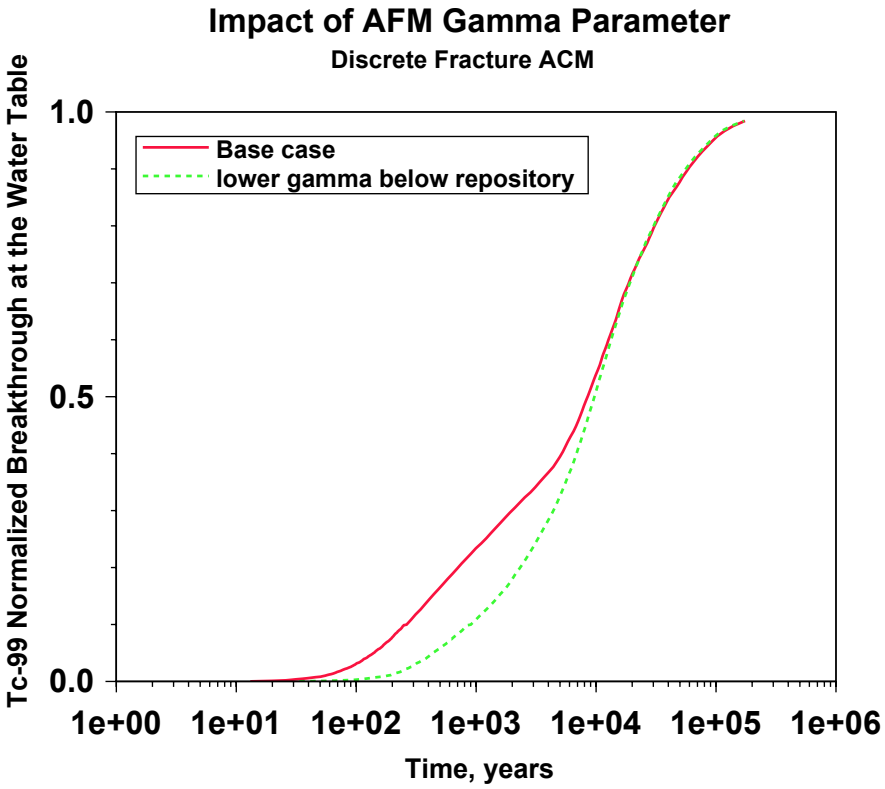

Output DTN: LA0311BR831371.002

NOTE: The colors, line types, and legend descriptors are chosen to facilitate a direct visual comparison to the simulation results presented in BSC 2003 [163045], Figure 6.8-3.

Figure 7-14. Breakthrough Curves for Conservative Solute Using the UZ Transport Abstraction Model to Investigate the Role of AFM Parameter Gamma: DFM ACM, Simulation for Different Values of Gamma in Rock Units Beneath the Repository

7.4 DISCUSSION OF VALIDATION ACTIVITIES

The series of simulations presented in this section, along with additional simulations performed to test the performance of the model in the FEHM V&V documentation, provide assurance that the UZ transport system is adequately captured in the abstraction model that is the subject of this Model Report. Direct numerical comparisons with quantitative criteria would be inappropriate for these comparisons because the modeling approach is designed to capture the essential features of the transport behavior over an extremely broad range of conditions (flow rates, transport parameters, relative flow rates in the two media, and the conceptual model for f/m interactions). Furthermore, analytical solutions do not exist to perform the comparisons made in this study, so the issue of whether the model is "correct" is not answerable by simply comparing to another code. Rather, the sort of benchmarking performed in this section is designed to build confidence in the adequacy of the abstraction model through a series of comparisons designed to probe the key features of the model that will be exercised during its use in TSPA simulations.

Adequate visual comparisons for benchmarking against the DFM simulations illustrate that the algorithms have been implemented to handle upscaling of dual permeability transport processes, for low or high diffusion, sorbing or nonsorbing solutes, and fracture or matrix releases. Discrepancies between the particle tracking and discrete fracture models, though relatively small, were noted and additional investigations were conducted to explain and assess the differences. In this way the robustness of the model was demonstrated, and we conclude that TSPA simulations using the UZ transport abstraction model will be able to propagate uncertainties in the form of parameter distributions through the UZ portion of the TSPA model. After testing the model in a simple particle tracking setup, the complexities of the system were studied in two and three dimensions through comparisons to the T2R3D based process model. These results are also adequate. Good agreement was observed at a variety of infiltration scenarios and diffusion models and parameters. In addition, the abstraction model is set up to enable alternate conceptual models for f/m interaction through the use of a different set of transfer function curves. Finally, the implementation of the AFM in the abstraction model was shown to reproduce the qualitative features of the breakthrough curves documented in the process model reports on which this abstraction is based. Thus, the abstraction model has been compared in the full complexity of the UZ model, and found to be able to represent the system robustly and efficiently for the entire range of parameters and conceptual models required. On this basis we conclude that the UZ transport abstraction model is suitable for use in TSPA analyses.

8. CONCLUSIONS

8.1 SUMMARY OF MODELING ACTIVITY

The principle output from this Model Report is an abstraction model for radionuclide transport in the UZ. It is intended for this model to be used directly in the TSPA system model developed using GoldSim V7.50.100 (BSC 2003 [161572]). The code used to implement the model is FEHM V2.21 (LANL 2003 [165741]), in the form of a dynamic link library (dll) callable from GoldSim. Testing of the operation of the dll in a GoldSim model environment has been developed and tested elsewhere (V&V documentation of FEHM V2.21; LANL 2003 [166306]) and is not repeated here, except to discuss the data structure of the interface between GoldSim and the FEHM dll.

This Model Report pulls together information and data from a variety of sources, creating a simulation model capable of efficiently computing the transport of multiple radionuclides through the UZ. Data sources are listed in Section 4.1, assumptions are discussed in detail in Section 5, and the mathematical formulation and assessment of parameter ranges and distributions are treated in Section 6. The main activity documented in this Model Report is the synthesis of data and models into a simulation tool. The model to be used in TSPA simulations consists of a code (FEHM V2.21, PC dll) and input files to the code that must be present to run the model within GoldSim. Table 8-2 lists the computer files required to run the base-case model, and a brief description of the purpose of each file. Fixed parameters have been inserted into the appropriate FEHM files. Parameter distributions given in Section 6.5 should be used to generate a table of parameters in a text file, which is read using FEHM's capability of reading in parameters from a separate file and inserting those parameters into the simulation at runtime (see the User Documentation for FEHM V2.21 for details). Thus, this set of files provides the template for the TSPA modelers to set up the UZ abstraction model in a multiple-realization GoldSim system model. The table of uncertain parameters itself is not generated in this Model Report: this needs to be done by TSPA system modelers to facilitate parameter correlations and to enable the exploration of parameter sensitivities to be studied systematically at the system level. Table 8-1 lists the UZ transport parameters which should be pre-sampled and assembled into a table and for FEHM to read at run time, in TSPA.

This report is intended to fulfill some of the abstraction model acceptance criteria, listed in the *Yucca Mountain Review Plan (YMRP), Final Report* (NRC 2003 [163274]). Further discussion with respect to the YMRP criteria, and the sections where they are addressed, is provided in Section 4.2.

Table 8-1. List of Uncertain Parameters to be Sampled in TSPA-LA Runs

Uncertain Parameters	Description
matrix adsorption coefficient (mL/g)	Matrix adsorption coefficient will be pre-sampled to based on given distributions for dissolved species in Section 6.5.4, Table 6-5.
matrix diffusion coefficient (m^2/sec)	Matrix water content and effective permeability will first be sampled based on given distribution in Section 6.5.5, Table 6-6. Then, the sampled water content and effective permeability are used in Eq. 6.19 for estimating matrix diffusion coefficients.
fracture porosity, fracture frequency, and fracture aperture (m)	If desired, fracture porosity, fracture frequency, and fracture aperture can be sampled based on given distribution in Table 6-13 and Eq. 6-26.
colloid K_c	Colloid concentration and colloid K_d are sampled based given distribution in Tables 6-19 and 6-20. The sampled colloid concentration and K_d are then used in Section 6.5.12, Eq. 6-27 for calculating colloid K_c.
colloid R_c	Colloid R_c is sampled based on given distribution in Section 6.5.13, Table 6-22.

8.2 MODEL OUTPUTS

8.2.1 Developed Output

Many of the model outputs (FEHM input files to be used by TSPA system modelers) are derived from results of process models or other studies. For a discussion of the uncertainties of those parameters, the reader is referred to the references cited in Table 8-1. For those outputs in Table 8-2 listed as being developed in this Model Report, the development of the parameter values is discussed in this Model Report. The table shows 2 primary output DTNs. In addition to the files listed in the table, there may be auxiliary files that the TSPA modeling group must develop and document to complete the process of incorporating the UZ transport abstraction model into GoldSim V7.50.100 (BSC 2003 [161572]). These files, which are the responsibility of the TSPA modeling group to create, may include files such as batch files to copy files at runtime from one filename to another. They will implement features that are documented in FEHM V2.21, and are discussed in the User Manual for the code. They will contain no data, so are not required to be documented in this Model Report.

Table 8-2. Computer Files Comprising the UZ Transport Process Model

Computer Files comprising the UZ Transport Process Model	Qualitative Description and Intended Use	Data Tracking Number used to Develop	Product Output DTN
Files Developed in other Studies That Feed this Abstraction Model.			
fehmn.grid fehmn.stor	Numerical model grid files required for UZ transport abstraction model.	LB0305TSPA18FF.001 [165625]	N/A
fehmn.zone fehmn.zone2	File that indexes each grid node number to a hydrologic zone. Input zone list file for UZ transport abstraction model. Fehmn.zone2 also contains repository zones.	LB0305TSPA18FF.001 [165625]	N/A
preqla.ini preqma.ini prequa.ini glaqla.ini glaqma.ini glaqua.ini monla.ini monma.ini monua.ini glaqlA_wtrise.ini glaqmA_wtrise.ini glaquA_wtrise.ini monlA_wtrise.ini monmA_wtrise.ini monuA_wtrise.ini	Steady state flow fields used to set the fluid flow rates in the UZ transport abstraction model.	LB0305TSPA18FF.001 [165625] LB0312TSPA06FF.001 [166671]	N/A
Files Developed in this Model Report			
fehm_amr_base.rock	Rock properties for all zones defined in fehm.zone – bulk rock density, heat capacity (placeholder, not used in the model), and porosity. File is part of the UZ transport process model.	LB0305TSPA18FF.001 [165625] LB0210THRMLPRP.001 [160799]	LA0311BR831371.003
fehm_amr_base.dpdp	Dual permeability model parameters – fracture volume fraction, characteristic distance into the matrix between fractures. File is part of the UZ transport process model.	LB0205REVUZPRP.001 [159525] LB0207REVUZPRP.001 [159526]	LA0311BR831371.003
fehm_amr_base.mptr .	All solute transport parameters for the multiple radionuclide simulations. File is part of the UZ transport process model.	LA0302AM831341.002 [162575] LB0302UZDSCPUI.002 [161787] LB0305TSPA18FF.001 [165625] LL000122051021.116 [142973] SN0306T0504103.005 [164132] SN0306T0504103.006 [164131] LA0303HV831352.002 [163558]	LA0311BR831371.003
repo.zon.xls	Zone lists containing node numbers of repository nodes in each infiltration bin. Used in UZ transport abstraction model as part of radionuclide release model in GoldSim (BSC 2003 [161572]) system model.	LL030610323122.029 [164513]	LA0311BR831371.003
wt.zone	Zone lists containing node numbers of grid nodes in each collection node at the water table.	LB03023DSSCP9I.001 [163044]	LA0311BR831371.003
fehm_la.zone2	Zone files containing node numbers in different rock layers and the repository and water table collection bins from repo.zone.xls and wt.zone.	LB0305TSPA18FF.001 [165625] repo.zone.xls and wt.zone	LA0311BR831371.003

Table 8-2. Computer Files Comprising the UZ Transport Process Model (Continued)

Computer Files comprising the UZ Transport Process Model	Qualitative Description and Intended Use	Data Tracking Number used to Develop	Product Output DTN
fracture_pf.doc	File contains developed fracture porosity and frequency distribution data to be used in LA	LB0205REVUZPRP.001 [159525] LB0207REVUZPRP.001 [159526]	LA0311BR831371.003
matrix_ekwc.doc	Matrix water content and effective permeability distributions developed for estimating matrix diffusion coefficient.	LB03023DSSCP9I.001 [163044]	LA0311BR831371.003
uz_tfcurves_nn_3960.in uz_tfcurves_dualk_nn_3960.in	Transfer function curves for implementing the RTTF particle tracking model for upscaling of fracture-matrix interaction process.	N/A, developed output	LA0311BR831229.001
fehm_amr_base.dat	All control parameters for the FEHM simulation. Used as main input file for UZ transport process model.	N/A, developed output	LA0311BR831371.003

8.2.2 Output Uncertainty

The calculation of UZ transport uncertainties in the TSPA model will be performed and documented in the TSPA Model Report because the radionuclide source term is computed using the system model, of which the UZ transport abstraction model is a part. The goal of the present Model Report is to ensure that a computational tool is set up for TSPA to perform the simulation modeling, and that the uncertainties of parameters in the abstraction model are fully justified and documented. Those goals have been accomplished, in that the software and computer files needed to perform the modeling have been completed, allowing parameter and conceptual uncertainties in the UZ transport to be propagated through the TSPA model.

The uncertainties associated with transport in the UZ have been documented in the Model Report for UZ transport (BSC 2003 [163228]), and have been summarized briefly in the present Model Report. Of note is that fact that both parameter and conceptual model uncertainty have been shown to be incorporated into this abstraction. The key ACMs discussed in BSC (2003 [163228]) and Section 6.7 of this Model Report relate to the treatment of fracture-matrix interactions. Model validation simulations presented in Section 7 suggest strongly that the particle tracking formulation in the abstraction model developed in FEHM replicates the behavior of the process model, and does so in a computationally efficient manner. In addition, simulations using transfer function curves implemented with a dual-k or DFM conceptual model for f/m interactions were shown to yield reasonable results. Thus, both f/m interaction models could conceivably be investigated in TSPA simulations. However, due to the fact that Process Model validation activities were performed based on a dual-k model, the dual-k transfer functions (file uz_tfcurves_dualk_nn_3960.in) should be used in TSPA analyses. The transfer functions based on the DFM conceptual model (file uz_tfcurves_nn_3960.in), are provided because the DFM was required to test the implementation of the particle tracking model through comparison to other numerical models. The DFM representation, though perhaps a more physically realistic scenario for diffusion between the media, should only be used for code validation or sensitivity analyses unless a parallel validation effort of the Process Model using a DFM formulation is successfully carried out in the future.

9. INPUTS AND REFERENCES

The following is a list of the references cited in this document. Column 1 represents the unique six-digit numerical identifier (the Document Input Reference System [DIRS] number), which is placed in the text following the reference callout (e.g., BSC 2002 [160819]). The purpose of these numbers is to assist the reader in locating a specific reference in the DIRS database. Within the reference list, multiple sources by the same author (e.g., BSC 2002) are sorted alphabetically by title.

9.1 DOCUMENTS CITED

(Civilian Radioactive Waste Management System Management and Operations)

101378 Akindunni, F.F.; Gillham, R.W.; Conant, B.; and Franz, T. 1995. "Modeling of Contaminant Movement Near Pumping Wells: Saturated-Unsaturated Flow with Particle Tracking." *Ground Water, 33*, (2), 264-274. Worthington, Ohio: National Water Well Association. TIC: 226455.

158204 BSC (Bechtel SAIC Company) 2001. *Multiscale Thermohydrologic Model*. ANL-EBS-MD-000049 REV 00 ICN 02. Las Vegas, Nevada: Bechtel SAIC Company. ACC: MOL.20020123.0279.

160059 BSC (Bechtel SAIC Company) 2002. *Radionuclide Screening*. ANL-WIS-MD-000006 REV 01. Las Vegas, Nevada: Bechtel SAIC Company. ACC: MOL.20020923.0177.

160819 BSC (Bechtel SAIC Company) 2002. *Technical Work Plan for: Performance Assessment Unsaturated Zone*. TWP-NBS-HS-000003 REV 02. Las Vegas, Nevada: Bechtel SAIC Company. ACC: MOL.20030102.0108.

158966 BSC (Bechtel SAIC Company) 2002. *The Enhanced Plan for Features, Events, and Processes (FEPs) at Yucca Mountain*. TDR-WIS-PA-000005 REV 00. Las Vegas, Nevada: Bechtel SAIC Company. ACC: MOL.20020417.0385.

161773 BSC (Bechtel SAIC Company) 2003. *Analysis of Hydrologic Properties* Data. MDL-NBS-HS-000014 REV 00. Las Vegas, Nevada: Bechtel SAIC Company. ACC: DOC.20030404.0004.

160240 BSC (Bechtel SAIC Company) 2003. *Calibrated Properties Model*. MDL-NBS-HS-000003 REV 01. Las Vegas, Nevada: Bechtel SAIC Company. ACC: DOC.20030219.0001.

160109 BSC (Bechtel SAIC Company) 2003. *Development of Numerical Grids for UZ Flow and Transport Modeling*. ANL-NBS-HS-000015 REV 01. Las Vegas, Nevada: Bechtel SAIC Company. ACC: DOC.20030404.0005.

164889 BSC (Bechtel SAIC Company) 2003. *Drift-Scale Radionuclide Transport*. MDL-NBS-HS-000016 REV 00. Las Vegas, Nevada: Bechtel SAIC Company. ACC: DOC.20030902.0009.

164873 BSC (Bechtel SAIC Company) 2003. *Features, Events, and Processes in UZ Flow and Transport*. ANL-NBS-MD-000001 REV 02A. Las Vegas, Nevada: Bechtel SAIC Company. ACC: MOL.20031016.0004.

165179 BSC (Bechtel SAIC Company) 2003. *Q-List*. TDR-MGR-RL-000005 REV 00. Las Vegas, Nevada: Bechtel SAIC Company. ACC: DOC.20030930.0002.

163228 BSC (Bechtel SAIC Company) 2003. *Radionuclide Transport Models Under Ambient Conditions*. MDL-NBS-HS-000008 REV 01. Las Vegas, Nevada: Bechtel SAIC Company. ACC: DOC.20031201.0002.

162729 BSC (Bechtel SAIC Company) 2003. *Saturated Zone Colloid Transport*. ANL-NBS-HS-000031 REV 01. Las Vegas, Nevada: Bechtel SAIC Company. ACC: DOC.20030916.0008.

162415 BSC (Bechtel SAIC Company) 2003. *Saturated Zone In-Situ Testing*. ANL-NBS-HS-000039 REV 00A. Las Vegas, Nevada: Bechtel SAIC Company. ACC: MOL.20030602.0291.

162649 BSC (Bechtel SAIC Company) 2003. *Site-Scale Saturated Zone Flow Model*. MDL-NBS-HS-000011 REV 01A. Las Vegas, Nevada: Bechtel SAIC Company. ACC: MOL.20030626.0296.

164870 BSC (Bechtel SAIC Company) 2003. *SZ Flow and Transport Model Abstraction*. MDL-NBS-HS-000021 REV 00. Las Vegas, Nevada: Bechtel SAIC Company. ACC: DOC.20030818.0007.

163045 BSC (Bechtel SAIC Company) 2003. *UZ Flow Models and Submodels*. MDL-NBS-HS-000006 REV 01. Las Vegas, Nevada: Bechtel SAIC Company. ACC: DOC.20030818.0002.

161620 BSC (Bechtel SAIC Company) 2003. *Waste Form and In-Drift Colloids-Associated Radionuclide Concentrations: Abstraction and Summary*. MDL-EBS-PA-000004 REV 00. Las Vegas, Nevada: Bechtel SAIC Company. ACC: DOC.20030626.0006.

161770 Canori, G.F. and Leitner, M.M. 2003. *Project Requirements Document*. TER-MGR-MD-000001 REV 01. Las Vegas, Nevada: Bechtel SAIC Company. ACC: DOC.20030404.0003.

101384 Chiang, C.Y.; Wheeler, M.F.; and Bedient, P.D. 1989. "A Modified Method of Characteristics Technique and Mixed Finite Elements Method for Simulation of Groundwater Solute Transport." *Water Resources Research, 25*, (7), 1541-1549. Washington, D.C.: American Geophysical Union. TIC: 226452.

101385 Cordes, C. and Kinzelbach, W. 1992. "Continuous Groundwater Velocity Fields and Path Lines in Linear, Bilinear, and Trilinear Finite Elements." *Water Resources Research, 28*, (11), 2903-2911. Washington, D.C.: American Geophysical Union. TIC: 226449.

134732 CRWMS M&O 2000. *Analysis of Base-Case Particle Tracking Results of the Base-Case Flow Fields (ID: U0160)*. ANL-NBS-HS-000024 REV 00. Las Vegas, Nevada: CRWMS M&O. ACC: MOL.20000207.0690.

141418 CRWMS M&O 2000. *Particle Tracking Model and Abstraction of Transport Processes*. ANL-NBS-HS-000026 REV 00. Las Vegas, Nevada: CRWMS M&O. ACC: MOL.20000502.0237.

148384 CRWMS M&O 2000. *Total System Performance Assessment (TSPA) Model for Site Recommendation*. MDL-WIS-PA-000002 REV 00. Las Vegas, Nevada: CRWMS M&O. ACC: MOL.20001226.0003.

153246 CRWMS M&O 2000. *Total System Performance Assessment for the Site Recommendation*. TDR-WIS-PA-000001 REV 00 ICN 01. Las Vegas, Nevada: CRWMS M&O. ACC: MOL.20001220.0045.

154071 CRWMS M&O 2001. *Colloid-Associated Radionuclide Concentration Limits*: *ANL.* ANL-EBS-MD-000020 REV 00 ICN 01. Las Vegas, Nevada: CRWMS M&O. ACC: MOL.20010216.0003.

101386 Desbarats, A.J. 1990. "Macrodispersion in Sand-Shale Sequences." *Water Resources Research, 26*, (1), 153-163. Washington, D.C.: American Geophysical Union. TIC: 236576.

100547 DOE (U.S. Department of Energy) 1998. *Overview - Viability Assessment of a Repository at Yucca Mountain*. DOE/RW-0508. Washington, D.C.: U.S. Department of Energy, Office of Civilian Radioactive Waste Management. ACC: MOL.19981007.0027.

101387 Fabriol, R.; Sauty, J.P.; and Ouzounian, G. 1993. "Coupling Geochemistry with a Particle Tracking Transport Model." *Journal of Contamination Hydrology, 13*, 117-129. New York, New York: Elsevier. TIC: 222395.

109425 Forester, R.M.; Bradbury, J.P.; Carter, C.; Elvidge-Tuma, A.B.; Hemphill, M.L.; Lundstrom, S.C.; Mahan, S.A.; Marshall, B.D.; Neymark, L.A.; Paces, J.B.; Sharpe, S.E.; Whelan, J.F.; and Wigand, P.E. 1999. *The Climatic and Hydrologic History of Southern Nevada During the Late Quaternary*. Open-File Report 98-635. Denver, Colorado: U.S. Geological Survey. TIC: 245717.

154365 Freeze, G.A.; Brodsky, N.S.; and Swift, P.N. 2001. *The Development of Information Catalogued in REV00 of the YMP FEP Database*. TDR-WIS-MD-000003 REV 00 ICN 01. Las Vegas, Nevada: Bechtel SAIC Company. ACC: MOL.20010301.0237.

101173 Freeze, R.A. and Cherry, J.A. 1979. *Groundwater*. Englewood Cliffs, New Jersey: Prentice-Hall. TIC: 217571.

141512 Grathwohl, P. 2000. *Diffusion in Natural Porous Media: Contaminant Transport, Sorption/Desorption and Dissolution Kinetics*. Boston, Massachusetts: Kluwer Academic Publishers. TIC: 247983.

163236 Hogg, R.V. and Craig, A.T. 1978. *Introduction to Mathematical Statistics*. 4th Edition. New York, New York: Macmillan. TIC: 254311.

101400 Johnson, J.A.; Ravi, V.; and Rumery, J.K. 1994. "Estimation of Solute Concentrations Using the Pathline Counting Method." *Ground Water, 32*, (5), 719-726. Worthington, Ohio: National Water Well Association. TIC: 226453.

101402 Kinzelbach, W. 1988. *The Random Walk Method in Pollutant Transport Simulation*. Groundwater Flow and Quality Modelling. Pages 227-245. Norwell, Massachusetts: D. Reidel Publishing Company. TIC: 224064.

166306 LANL (Los Alamos National Laboratory) 2003. *Validation Test Plan (VTP) for the FEHM Application Version 2.21*. 10086-VTP-2.21-00. Los Alamos, [New Mexico]: Los Alamos National Laboratory. ACC: MOL.20031031.0264; MOL.20031031.0265.

101408 Latinopoulos, P. and Katsifarakis, K. 1991. "A Boundary Element and Particle Tracking Model for Advective Transport in Zoned Aquifers." *Journal of Hydrology, 124*, 159-176. Amsterdam, The Netherlands: Elsevier. TIC: 226466.

105729 Liu, H.H.; Doughty, C.; and Bodvarsson, G.S. 1998. "An Active Fracture Model for Unsaturated Flow and Transport in Fractured Rocks." *Water Resources Research, 34*, (10), 2633-2646. Washington, D.C.: American Geophysical Union. TIC: 243012.

101413 Lu, N. 1994. "A Semianalytical Method of Path Line Computation for Transient Finite-Difference Groundwater Flow Models." *Water Resources Research, 30*, (8), 2449-2459. Washington, D.C.: American Geophysical Union. TIC: 211997.

146957 Maloszewski, P. and Zuber, A. 1991. "Influence of Matrix Diffusion and Exchange Reactions on Radiocarbon Ages in Fissured Carbonate Aquifers." *Water Resources Research, 27*, (8), 1937-1945. Washington, D.C.: American Geophysical Union. TIC: 247494.

101148 Neretnieks, I. 1980. "Diffusion in the Rock Matrix: An Important Factor in Radionuclide Retardation." *Journal of Geophysical Research, 85*, (B8), 4379-4397. Washington, D.C.: American Geophysical Union. TIC: 221345.

101463 Neuman, S.P. 1984. "Adaptive Eulerian-Lagrangian Finite Element Method for Advection-Dispersion." *International Journal for Numerical Methods in*

Engineering, 20, 321-337. New York, New York: John Wiley & Sons. TIC: 226440.

101464 Neuman, S.P. 1990. "Universal Scaling of Hydraulic Conductivities and Dispersivities in Geologic Media." *Water Resources Research, 26*, (8), 1749-1758. Washington, D.C.: American Geophysical Union. TIC: 237977.

163274 NRC (U.S. Nuclear Regulatory Commission) 2003. *Yucca Mountain Review Plan, Final Report*. NUREG-1804, Rev. 2. Washington, D.C.: U.S. Nuclear Regulatory Commission, Office of Nuclear Material Safety and Safeguards. TIC: 254568.

103896 Parrington, J.R.; Knox, H.D.; Breneman, S.L.; Baum, E.M.; and Feiner, F. 1996. *Nuclides and Isotopes, Chart of the Nuclides*. 15th Edition. San Jose, California: General Electric Company and KAPL, Inc. TIC: 233705.

101466 Pollock, D.W. 1988. "Semianalytical Computation of Path Lines for Finite-Difference Models." *Ground Water, 26*, (6), 743-750. Worthington, Ohio: National Water Well Association. TIC: 226464.

101474 Reimus, P.W. 1995. *The Use of Synthetic Colloids in Tracer Transport Experiments in Saturated Rock Fractures*. Ph.D. dissertation. LA-13004-T. Los Alamos, New Mexico: Los Alamos National Laboratory. TIC: 240694.

126243 Reimus, P.W.; Adams, A.; Haga, M.J.; Humphrey, A.; Callahan, T.; Anghel, I.; and Counce, D. 1999. *Results and Interpretation of Hydraulic and Tracer Testing in the Prow Pass Tuff at the C-Holes*. Milestone SP32E7M4. Los Alamos, New Mexico: Los Alamos National Laboratory. TIC: 246377.

163008 Reimus, P.W.; Ware, S.D.; Benedict, F.C.; Warren, R.G.; Humphrey, A.; Adams, A.; Wilson, B.; and Gonzales, D. 2002. *Diffusive and Advective Transport of {superscript 3}H, {superscript 14}C, and {superscript 99}Tc in Saturated, Fractured Volcanic Rocks from Pahute Mesa, Nevada*. LA-13891-MS. Los Alamos, New Mexico: Los Alamos National Laboratory. TIC: 253905.

101154 Robinson, B.A. 1994. "A Strategy for Validating a Conceptual Model for Radionuclide Migration in the Saturated Zone Beneath Yucca Mountain." *Radioactive Waste Management and Environmental Restoration, 19*, (1-3), 73-96. Yverdon, Switzerland: Harwood Academic Publishers. TIC: 222513.

101476 Schafer-Perini, A.L. and Wilson, J.L. 1991. "Efficient and Accurate Front Tracking for Two-Dimensional Groundwater Flow Models." *Water Resources Research, 27*, (7), 1471-1485. Washington, D.C.: American Geophysical Union. TIC: 226448.

101477 Scheibe, T.D. and Cole, C.R. 1994. "Non-Gaussian Particle Tracking: Application to Scaling of Transport Processes in Heterogeneous Porous Media." *Water Resources Research, 30*, (7), 2027-2039. Washington, D.C.: American Geophysical Union. TIC: 226446.

105043 Sudicky, E.A. and Frind, E.O. 1982. "Contaminant Transport in Fractured Porous Media: Analytical Solutions for a System of Parallel Fractures." *Water Resources Research, 18*, (6), 1634-1642. Washington, D.C.: American Geophysical Union. TIC: 217475.

101490 Tompson, A.F.B. and Gelhar, L.W. 1990. "Numerical Simulation of Solute Transport in Three-Dimensional, Randomly Heterogeneous Porous Media." *Water Resources Research, 26*, (10), 2541-2562. Washington, D.C.: American Geophysical Union. TIC: 224902.

146961 van Genuchten, M.T. 1985. "Convective-Dispersive Transport of Solutes Involved in Sequential First-Order Decay Reactions." *Computers in Geosciences, 11*, (2), 129-147. New York, New York: Pergamon Press. TIC: 245188.

166070 Wang, J.S. 2003. "Scientific Notebooks Referenced in Model Report U0065, Particle Tracking Model and Abstraction of Transport Process, MDL-NBS-HS-000020 REV 00." Letter from J.S. Wang (BSC) to File, December 4, 2003, with attachment. ACC: MOL.20031208.0348.

101498 Wolfsberg, A.V. and Freyberg, D.L. 1994. "Efficient Simulation of Single Species and Multispecies Transport in Groundwater with Local Adaptive Grid Refinement." *Water Resources Research, 30*, (11), 2979-2991. Washington, D.C.: American Geophysical Union. TIC: 226450.

101499 Yamashita, R. and Kimura, H. 1990. "Particle-Tracking Technique for Nuclide Decay Chain Transport in Fractured Porous Media." *Journal of Nuclear Science and Technology, 27*, (11), 1041-1049. Tokyo, Japan: Nihon Genshryoku Gakkai. TIC: 236573.

101501 Yeh, G.T. 1990. "A Lagrangian-Eulerian Method with Zoomable Hidden Fine-Mesh Approach to Solving Advective-Dispersion Equations." *Water Resources Research, 26*, (6), 1133-1144. Washington, D.C.: American Geophysical Union. TIC: 224067.

101502 Zheng, C. 1993. "Extension of the Method of Characteristics for Simulation of Solute Transport in Three Dimensions." *Ground Water, 31*, (3), 456-465. Worthington, Ohio: Water Well Publishing Company. TIC: 226465.

101503 Zheng, C. 1994. "Analysis of Particle Tracking Errors Associated with Spatial Discretization." *Ground Water, 32*, (5), 821-828. Dublin, Ohio: Water Well Publishing Company. TIC: 226463.

100614 Zimmerman, R.W.; Chen, G.; Hadgu, T.; and Bodvarsson, G.S. 1993. "A Numerical Dual-Porosity Model with Semianalytical Treatment of Fracture/Matrix Flow." *Water Resources Research, 29*, (7), 2127-2137. Washington, D.C.: American Geophysical Union. TIC: 236571.

101026 Zyvoloski, G.; Dash, Z.; and Kelkar, S. 1992. *FEHMN 1.0: Finite Element Heat and Mass Transfer Code*. LA-12062-MS, Rev. 1. Los Alamos, New Mexico: Los Alamos National Laboratory. ACC: NNA.19910625.0038.

100615 Zyvoloski, G.A.; Robinson, B.A.; Dash, Z.V.; and Trease, L.L. 1997. *User's Manual for the FEHM Application–A Finite-Element Heat- and Mass-Transfer Code*. LA-13306-M. Los Alamos, New Mexico: Los Alamos National Laboratory. TIC: 235999.

Software Cited:

161572 BSC (Bechtel SAIC Company) 2003. *Software Code: GoldSim*. V7.50.100. PC. 10344-7.50.100-00.

165742 LANL (Los Alamos National Laboratory) 2003. *Software Code: discrete_tf*. V1.1. SUN, SunOS 5.8; PC, Windows 2000 and Linux 7.1. 11033-1.1-00.

165741 LANL (Los Alamos National Laboratory) 2003. *Software Code: FEHM*. V2.21. SUN, SunOS 5.8; PC, Windows 2000 and Linux 7.1. 10086-2.21-00.

165754 LANL (Los Alamos National Laboratory) 2003. *Software Code: fehm2post*. V1.0. SUN, SunOS 5.8 and 5.7; PC, Windows 2000 and Redhat Linux 2.4.18. 11031-1.0-00.

165753 LANL (Los Alamos National Laboratory) 2003. *Software Code: ppptrk*. V1.0. SUN, SunOS 5.8 and 5.7; PC, Windows 2000 and Linux 7.1. 11030-1.0-00.

146654 LBNL (Lawrence Berkeley National Laboratory) 1999. *Software Code: T2R3D*. V1.4. FORTRAN 77, SUN, DEC/ALPHA. 10006-1.4-00.

113943 LBNL (Lawrence Berkeley National Laboratory) 1999. *Software Code: TOUGH2*. V1.11 MEOS9nTV1.0. MAC, SUN, DEC/Alpha, PC. 10065-1.11MEOS9NTV1.0-00.

154342 LBNL (Lawrence Berkeley National Laboratory) 2002. *Software Code: DCPT*. V2.0. PC, Windows. 10078-2.0-00.

163453 LBNL (Lawrence Berkeley National Laboratory) 2003. *Software Code: WTRISE*. V2.0. PC/WINDOWS 2000/98; DEC ALPHA/OSF1 V5.1. 10537-2.0-00.

9.2 CODES, STANDARDS, REGULATIONS, AND PROCEDURES

156671 66 FR 55732. Disposal of High-Level Radioactive Wastes in a Proposed Geologic Repository at Yucca Mountain, NV. Final Rule 10 CFR Part 63. Readily available.

AP-2.22Q, REV 1, ICN 0. *Classification Analyses and Maintenance of the Q-List.* Washington, D.C.: U.S. Department of Energy, Office of Civilian Radioactive Waste Management. ACC: DOC.20030807.0002.

AP-SI.1Q, REV 5 ICN 2. *Software Management*. Washington, D.C.: U.S. Department of Energy, Office of Civilian Radioactive Waste Management. ACC: DOC.20030902.0003.

9.3 SOURCE DATA, LISTED BY DATA TRACKING NUMBER

144462 LA0002PR831231.003. Probabilities from C-Wells Microsphere Data. Submittal date: 02/17/2000.

149557 LA0003JC831362.001. Preliminary Matrix Diffusion Coefficients for Yucca Mountain Tuffs. Submittal date: 4/10/2000.

147285 LA0003MCG12213.002. Cumulative Probabilities for Colloid Transport Between One Matrix and Another Calculated from Interpolation of Pore Volume Data from Yucca Mountain Hydrologic (Stratigraphic) Samples. Submittal date: 03/10/2000.

153251 LA0007MCG12213.001. Colloid Size Distribution. Submittal date: 07/31/2000.

162575 LA0302AM831341.002. Unsaturated Zone Distribution Coefficients (KDS) for U, NP, PU, AM, PA, CS, SR, RA, and TH. Submittal date: 02/04/2003.

163558 LA0303HV831352.002. Colloid Retardation Factors for the Saturated Zone Fractured Volcanics. Submittal date: 03/31/2003.

165624 LA0303HV831352.003. Fraction of Colloids that Travel Unretarded. Submittal date: 03/31/2003.

159525 LB0205REVUZPRP.001. Fracture Properties for UZ Model Layers Developed from Field Data. Submittal date: 05/14/2002.

159526 LB0207REVUZPRP.001. Revised UZ Fault Zone Fracture Properties. Submittal date: 07/03/2002.

160799 LB0210THRMLPRP.001. Thermal Properties of UZ Model Layers: Data Summary. Submittal date: 10/25/2002.

163044 LB03023DSSCP9I.001. 3-D Site Scale UZ Flow Field Simulations for 9 Infiltration Scenarios. Submittal date: 02/28/2003.

161787 LB0302UZDSCPUI.002. Drift-Scale Calibrated Property Sets: Upper Infiltration Data Summary. Submittal date: 02/05/2003.

165625 LB0305TSPA18FF.001. Eighteen 3-D Site Scale UZ Flow Fields Converted from TOUGH2 to T2FEHM Format. Submittal date: 05/09/2003.

164752 LB0307MR0060R1.007. Ambient Radionuclide Transport - TSPA Deliverable Extractions. Submittal date: 07/19/2003.

166071 LB03093RADTRNS.002. Three Way Transport Model Comparison: Data Summaries. Submittal date: 09/24/2003.

166060 LB0310T2FEHMFF.001. 1-D and 2-D Site Scale UZ Flow Fields Converted from TOUGH2 to T2FEHM Format. Submittal date: 10/20/2003.

166671 LB0312TSPA06FF.001. Six Flow Fields with Raised Water Tables. Submittal date: 12/23/2003.

142973 LL000122051021.116. Summary of Analyses of Glass Dissolution Filtrates. Submittal date: 01/27/2000.

164513 LL030610323122.029. Multiscale Thermohydrologic Model Output to TSPA and WAPDEG for the Mean Infiltration Case. Submittal date: 06/27/2003.

164132 SN0306T0504103.005. Revised Groundwater Colloid Mass Concentration Parameters for TSPA (Total System Performance Assessment). Submittal date: 06/30/2003.

164131 SN0306T0504103.006. Revised Sorption Partition Coefficients (KD Values) for Selected Radionuclides Modeled in the TSPA (Total System Performance Assessment). Submittal date: 06/30/2003.

9.4 OUTPUT DATA, LISTED BY DATA TRACKING NUMBER

LA0311BR831229.001. UZ Transport Abstraction Model, Transfer Function Calculation Files. Submittal date: 11/17/2003.

LA0311BR831371.001. UZ Transport Abstraction Model, Validation Simulations for the Discrete Fracture Comparison Problem. Submittal date: 11/202003.

LA0311BR831371.002. UZ Transport Abstraction Model, Validation Simulations for the Comparison to T2R3D. Submittal date: 11/202003.

LA0311BR831371.003. UZ Transport Abstraction Model, Transport Parameters and Base Case Simulation Results. Submittal date: 11/25 /2003.

INTENTIONALLY LEFT BLANK

ATTACHMENT I
DERIVATION OF THE DISTRIBUTION OF WATER CONTENT AND EFFECTIVE PERMEABILITY FOR SAMPLING MATRIX DIFFUSION COEFFICIENT

INTENTIONALLY LEFT BLANK

ATTACHMENT I

DERIVATION OF THE DISTRIBUTION OF WATER CONTENT AND EFFECTIVE PERMEABILITY FOR SAMPLING MATRIX DIFFUSION COEFFICIENT

Matrix diffusion is linked through the correlation given by Reimus et al. 2002 [163008] to porosity and permeability. For unsaturated conditions, this relationship is extended to water content and effective permeability. This is done in segments from the output file from rows 61001-122000, 122001-184000, and 184001-245506, and repeated for each of the nine flow fields. Rows 1-61000 are not needed because none of these cells lie within the repository footprint.

Starting with the flow output for file for saturation and relative permeability discussed earlier, the file is first sorted on column T to sort out the cells not in the repository footprint. This approximation is made to simplify the procedure, and is a reasonable approach since, for the most part, transport is vertically downward. After sorting the matrix data is copied into a new file. The rock types in column K are compared with the rock types that exist in or beneath the proposed repository horizon. This is done using the following formulas:

Urn = IF(Krn="bf3Md",1,IF(Krn="tr3Md",1,0))

Vrn = IF(Krn="pp2Md",2,IF(Krn="pp1Mz",2,IF(Krn="pp4Mz",2,0)))

Wrn =
IF(Krn="ch2Mz",3,IF(Krn="ch3Mz",3,IF(Krn="ch4Mz",3,IF(Krn="ch5Mz",3,IF(Krn="ch6Mz",3,0)))))

Xrn =
IF(Krn="pcM1z",3,IF(Krn="pcM2z",3,IF(Krn="pcM39",3,IF(Krn="pcM4p",3,IF(Krn="pcM5z",3,IF(Krn="pcM6z",3,0))))))

Yrn = IF(Krn="ch2Mv",4,IF(Krn="ch3Mv",4,IF(Krn="ch4Mv",4,IF(Krn="ch5Mv",4,0))))

Zrn = IF(Krn="tswMv",5,IF(Krn="ch1Mv",5,IF(Krn="ch6Mv",5,IF(Krn="pp3Md",5,0))))

AArn = IF(Krn="tswMz",6,IF(Krn="ch1Mz",6,IF(Krn="bf2Mz",6,0)))

ABrn = IF(Krn="tswM8",7,IF(Krn="pcM38",7,0))

ACrn = IF(Krn="tswM4",8,IF(Krn="tswM6",8,IF(Krn="tswM7",8,0)))

ADrn = IF(Krn="tswM3",9,IF(Krn="tswM5",9,0))

AErn = SUM(U1:AD1)

The sum of the columns in column AE identifies, by number, the rock group from 1 to 9. Here is a table of the rock groups:

Rock Group	Hydrogeologic Units
1	bf3Md, tr3Md
2	pp2Md, pp1Mz, pp4Mz
3	ch2Mz, ch3Mz, ch4Mz, ch5Mz, ch6Mz, pcM1z, pcM2z, pcM39, pcM4p, pcM5z, pcM6z
4	ch2Mv, ch3Mv, ch4Mv, ch5Mv
5	tswMv, ch1Mv, ch6Mv, pp3Md
6	tswMz, ch1Mz, bf2Mz
7	tswM8, pcM38
8	tswM4, tswM6, tswM7
9	tswM3, tswM5

The groupings are based on similarities in porosity and permeability, as shown here:

Model Unit	Porosity	Permeability m^2	Rock Group
bf3Md	0.175	3.55E-14	1
pp2Md	0.221	1.7E-15	2
pp1Mz	0.297	2.57E-15	2
pp4Mz	0.321	1.02E-15	2
ch6Mz	0.271	8.2E-19	3
pcM39	0.275	6.2E-18	3
pcM1z	0.285	9.3E-20	3
pcM2z	0.322	2.4E-18	3
ch5Mz	0.322	5.2E-18	3
ch4Mz	0.322	5.2E-18	3
ch3Mz	0.322	5.2E-18	3
ch2Mz	0.322	5.2E-18	3
ch5Mv	0.346	4.9E-11	4
ch4Mv	0.346	4.9E-11	4
ch3Mv	0.346	4.9E-11	4
ch2Mv	0.346	4.9E-11	4
tswMv	0.229	2.24E-13	5
pp3Md	0.318	1.26E-13	5
ch1Mv	0.331	1.39E-12	5
tswMz	0.275	3.5E-17	6
ch1Mz	0.285	3.5E-17	6
pcM38	0.043	3E-19	7
tswM8	0.043	7.4E-18	7
tswM7	0.103	7.41E-19	8
tswM6	0.103	7.41E-19	8
tswM4	0.111	2.96E-19	8
tswM5	0.131	8.55E-18	9
tswM3	0.155	2.39E-179	9

The rock type identification files are stored as

gt upper rock type identification 61001-122000.xls
gt upper rock type identification 122001-184000.xls
gt upper rock type identification 184001-245506.xls

gt mean rock type identification 61001-122000.xls
gt mean rock type identification 122001-184000.xls
gt mean rock type identification 184001-245506.xls

gt lower rock type identification 61001-122000.xls
gt lower rock type identification 122001-184000.xls
gt lower rock type identification 184001-245506.xls

ms upper rock type identification 61001-122000.xls
ms upper rock type identification 122001-184000.xls
ms upper rock type identification 184001-245506.xls

ms mean rock type identification 61001-122000.xls
ms mean rock type identification 122001-184000.xls
ms mean rock type identification 184001-245506.xls

ms lower rock type identification 61001-122000.xls
ms lower rock type identification 122001-184000.xls
ms lower rock type identification 184001-245506.xls

pd upper rock type identification 61001-122000.xls
pd upper rock type identification 122001-184000.xls
pd upper rock type identification 184001-245506.xls

pd mean rock type identification 61001-122000.xls
pd mean rock type identification 122001-184000.xls
pd mean rock type identification 184001-245506.xls

pd lower rock type identification 61001-122000.xls
pd lower rock type identification 122001-184000.xls
pd lower rock type identification 184001-245506.xls

Columns U through AD are deleted and the file is sorted on column U (Rock Type) in descending order. Those with rock type "0" are deleted.

These files are saved as

gt upper sort by rock type 61001-122000.xls
gt upper sort by rock type 122001-184000.xls
gt upper sort by rock type 184001-245506.xls

gt mean sort by rock type 61001-122000.xls
gt mean sort by rock type 122001-184000.xls
gt mean sort by rock type 184001-245506.xls

gt lower sort by rock type 61001-122000.xls
gt lower sort by rock type 122001-184000.xls
gt lower sort by rock type 184001-245506.xls

ms upper sort by rock type 61001-122000.xls
ms upper sort by rock type 122001-184000.xls
ms upper sort by rock type 184001-245506.xls

ms mean sort by rock type 61001-122000.xls
ms mean sort by rock type 122001-184000.xls
ms mean sort by rock type 184001-245506.xls

ms lower sort by rock type 61001-122000.xls
ms lower sort by rock type 122001-184000.xls
ms lower sort by rock type 184001-245506.xls

pd upper sort by rock type 61001-122000.xls
pd upper sort by rock type 122001-184000.xls
pd upper sort by rock type 184001-245506.xls

pd mean sort by rock type 61001-122000.xls
pd mean sort by rock type 122001-184000.xls
pd mean sort by rock type 184001-245506.xls

pd lower sort by rock type 61001-122000.xls
pd lower sort by rock type 122001-184000.xls
pd lower sort by rock type 184001-245506.xls

The results for each climate scenario are compiled into a single file and ordered by column V in descending order. The files are stored as:

gt upper composite by rock type.xls
gt mean composite by rock type.xls
gt lower composite by rock type.xls

ms upper composite by rock type.xls
ms mean composite by rock type.xls
ms lower composite by rock type.xls

pd upper composite by rock type.xls
pd mean composite by rock type.xls
pd lower composite by rock type.xls

Similarities between rock groups 1, 2, 4, 5, and 6 led to making this a single group. The same was also found for groups 7, 8, and 9. This reduces the groupings to 3 composite groups:

1, 2, 4, 5, and 6
3
7, 8, and 9

The first analysis, for the glacial-transition upper climate scenario, was conducted on the individual rock groups 1-9. Porosity was randomly sampled because the flow fields and resulting saturations and effective permeabilities are independent of porosity under steady-flow conditions. Porosity sampling was conducted for each model unit according to the mean and standard deviation for the model unit and a minimum and maximum of 9 and 1, respectively, using a beta distribution. The sampling methodology is described on pages 55 through 59 of Wang (2003 [166070], SN-LBNL-SCI-236-V1). Once the sampled porosities were generated on separate worksheets in the same file, the porosities were copied and pasted into column T on the main worksheet. Water content for each cell is generated by multiplying column D by column T as follows:

Urn = Drn*Trn

After generating the water content for each model unit, the combined units were assembled and the main worksheet was ordered by rock type (descending order) and secondarily by cell name (ascending order).

Statistics for the water content and effective permeability were assembled from the data based on a volume-weighted average. The cell volumes are given in column L. The total sum of cell volumes are computed as follows:

X1 = SUM(L1:Lre)

Where “re” stands for the last row of data on the worksheet. The statistics for water content are derived from the following:

Yrn = Urn*Lrn/W$1
Zrn = ((Urn-Z$1)^2)*Lrn/W$1
AA1 = SUM(X1:Xre)
AB1 = SQRT(SUM(Y1:Yre))
AC1 = MAX(U1:Ure)
AD1 = MIN(U1:Ure)

where Yrn and Zrn are the sums to determine the volume weighted mean and variance of the water content. AA1 is then the mean water content, AB1 is the standard deviation of water content, AC1 is the maximum water content, and AD1 is the minimum water content.

Statistics for the effective permeability are based on a log-normal distribution. The statistics are derived through the following formulas:

AFrn = LOG(Frn*Srn)*Lrn/W$1

AGrn = ((LOG(Frn*Srn)-AG$1)^2)*Lrn/W$1

AH1 = SUM(AF1:AFre)

AI1 = SQRT(SUM(A1:AGre))

Where AFrn and AGrn are the sums to determine the volume weighted mean and variance of the logarithm of the effective permeability. AH1 is then the mean of the logarithm of the effective permeability and AI1 is the standard deviation of the logarithm of the effective permeability.

This was carried out for each of the nine flow fields. The files containing the results are stored as:

gt upper group 6-5-4-2-1 diffusion parameters.xls

gt upper group 3 diffusion parameters.xls

gt upper group 9-8-7 diffusion parameters.xls

gt mean group 6-5-4-2-1 diffusion parameters.xls

gt mean group 3 diffusion parameters.xls

gt mean group 9-8-7 diffusion parameters.xls

gt lower group 6-5-4-2-1 diffusion parameters.xls

gt lower group 3 diffusion parameters.xls

gt lower group 9-8-7 diffusion parameters.xls

ms upper group 6-5-4-2-1 diffusion parameters.xls

ms upper group 3 diffusion parameters.xls

ms upper group 9-8-7 diffusion parameters.xls

ms mean group 6-5-4-2-1 diffusion parameters.xls

ms mean group 3 diffusion parameters.xls

ms mean group 9-8-7 diffusion parameters.xls

ms lower group 6-5-4-2-1 diffusion parameters.xls

ms lower group 3 diffusion parameters.xls

ms lower group 9-8-7 diffusion parameters.xls

ps upper group 6-5-4-2-1 diffusion parameters.xls

ps upper group 3 diffusion parameters.xls

ps upper group 9-8-7 diffusion parameters.xls

ps mean group 6-5-4-2-1 diffusion parameters.xls

ps mean group 3 diffusion parameters.xls

ps mean group 9-8-7 diffusion parameters.xls

ps lower group 6-5-4-2-1 diffusion parameters.xls

ps lower group 3 diffusion parameters.xls

ps lower group 9-8-7 diffusion parameters.xls

Summary files for each climate were created. These are stored as:

Summary of matrix diffusion for glacial-transition climate.xls

Summary of matrix diffusion for monsoon climate.xls

Summary of matrix diffusion for present day climate.xls

Averages were conducted across the climate/infiltration scenarios to create categories based on rock type only. Simple arithmetic averages of the results from each climate infiltration scenario were computed for the mean and variance of water content and logarithm of the effective permeability. Composite Distributions for all climate scenarios segregated only by the higher level rock groupings (6-5-4-2-1, 3, 9-8-7) are given in the following file:

Matrix diffusion summary with averages by rock type.xls

And a summary file with only the results is given in:

Matrix diffusion - summary values only.xls

INTENTIONALLY LEFT BLANK

ATTACHMENT II
DERIVATION OF WATER TABLE COLLECTING BINS

INTENTIONALLY LEFT BLANK

ATTACHMENT II

DERIVATION OF WATER TABLE COLLECTING BINS

The water table bins were calculated starting with the ELEME data from TOUGH2 available in DTN: LB03023DSSCP9I.001 [163044]. This data contains the cell name and coordinates for each node in the site-scale UZ flow model. Because the number of elements is 245506, the file is split into 4 groups as follows such that the data fits onto an excel worksheet:

Group A
1-62000.xls
62001-124000.xls
124001-186000.xls
186001-245506.xls

The "BT" cells in the UZ flow model comprise the bottom boundary of the model at the present-day water table. These are cells in the file 186001-245506.xls from row 57465 to row 59506. The "BT" cell coordinates were put into columns I, J, and K of the following files:

Group B
1-62000 with exact WT picks.xls
62001-124000 with exact WT picks.xls
124001-186000 with exact WT picks.xls
186001-245506 with exact WT picks.xls

Columns L and M were generated using the following relationship:

Lrn = Ern&Frn
Mrn = Irn&Jrn

where the "rn" subscripts stand for "row number". The character strings in columns L and M represent, respectively, a unique x-y coordinate character for the grid nodes and for the "BT" cells. Each grid node was then checked for a match with a "BT" cell. The index for the match was recorded in Column N,

Nrn = MATCH(Lrn,M$1:M$end,0)

where M$end represents the last occupied cell in column M.

The index in column N is then used to extract the local water table elevation in column H as follows:

Hrn = INDEX(K:K,Nrn)

In roughly 10% of the cells, no match was found, in which case a value of #N/A was returned. To evaluate a value of the local water table for these cells, columns A through H were copied into a second worksheet in the files listed above. A column was inserted into column A for a sequential number for each cell. Therefore, the local water table resided in column I. The

worksheet was sorted on column I to group the cells without local water table values. The cells without local water table values were copied into the following file:

Stragglers.xls

Cells without local water table values were found for each of the following cell ranges:

1-62000

62001-124000

186001-245506

and these cells were kept on separate worksheets in the Straggles.xls file.

To identify an appropriate local water table elevation for these cells, the following file was developed:

WT identification for stragglers.xls

Columns A, B, and C, from row 3 to row 4086 contain the coordinates of the "BT" cells. Up to 250 x-y coordinates for cells without an exact water table value were put in rows 1 and 2, columns D through IS. Then the square of the distance between each cell and each "BT" cell was computed for each x-y coordinate as follows:

COLrn = (COL$1-$Arn)^2+(COL$2-$Brn)^2

where COL represents a column label and rn the row number. Each column represents the x-y distance from a cell without an exact local water table value to each of the "BT" cells. The minimum distance was determined in row 4087 using the following formula:

COL4087 = MIN(COL3:COL4086)

The index of the "BT" cell associated with the minimum distance was determined in row 4088 as follows:

COL4088 = MATCH(COL4087,COL3:COL4086,0)

And the water table elevation associated with the index is determined in row 4089 as follows:

COL4089 = INDEX($C3:$C4086,COL4088)

These water table elevations were included in the third worksheet of the Group B files.

Files "62001-124000 wt bins.xls", "124001-186000 wt bins.xls, and "186001-245506 wt bins.xls contain the extracted water table collection cells in TOUGH2 columns using conditional if statements and the definition of the collection bin boundary data.

File “62001-124000 wt bins with fehm nodes .xls”, “124001-186000 wt bins with fehm nodes.xls”, and “124001-186000 wt bins with fehm nodes.xls” contain extracted collection bin nodes in FEHM grid format.

The final extracted water table collection bins are stored in file collect_zone which only contains the fracture nodes as required by FEHM.

All the files used in the extraction of water table collection bins are included in zip file wtbin.zip. The file names are listed below.

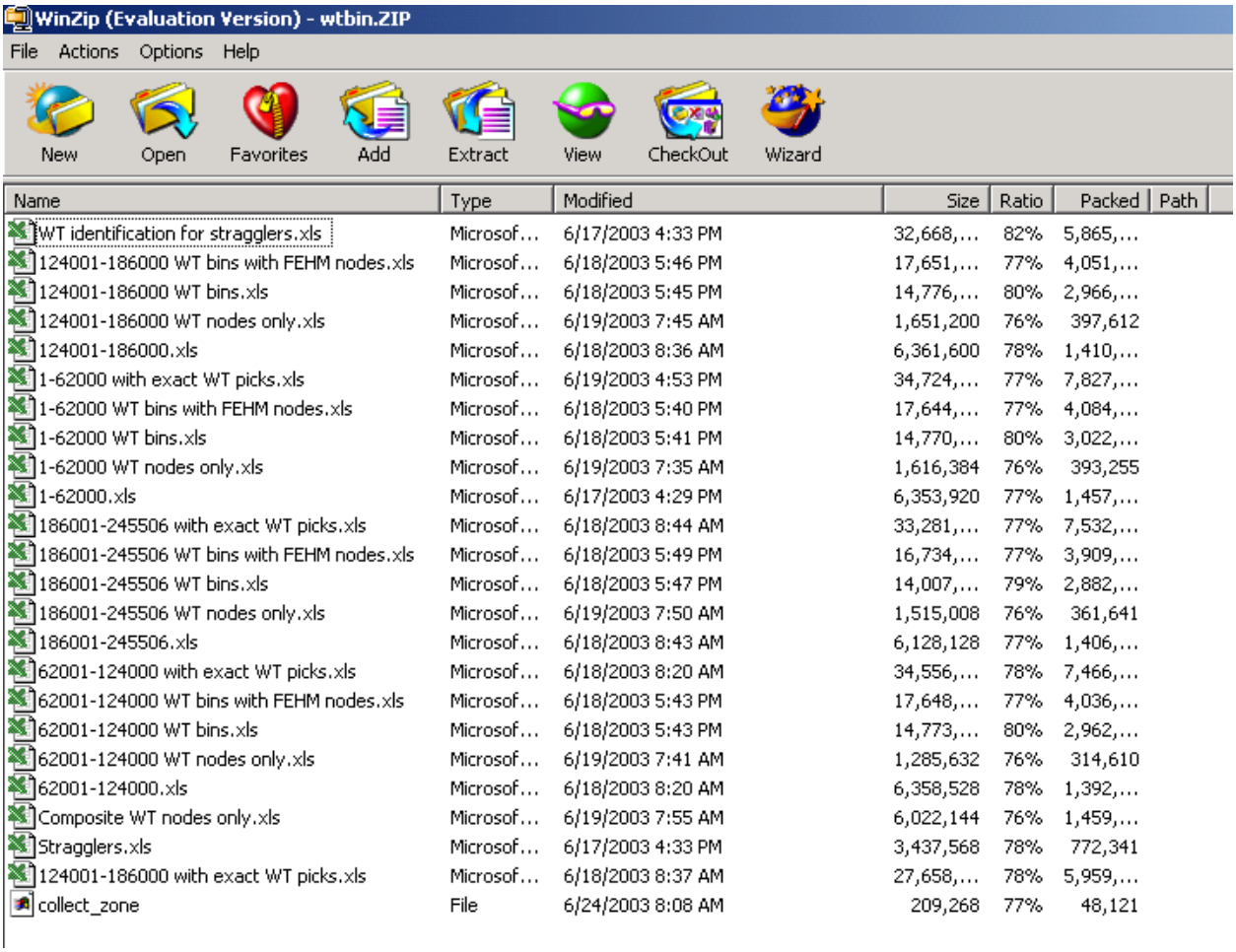

Name	Type	Modified	Size	Ratio	Packed	Path
WT identification for stragglers.xls	Microsof...	6/17/2003 4:33 PM	32,668,...	82%	5,865,...	
124001-186000 WT bins with FEHM nodes.xls	Microsof...	6/18/2003 5:46 PM	17,651,...	77%	4,051,...	
124001-186000 WT bins.xls	Microsof...	6/18/2003 5:45 PM	14,776,...	80%	2,966,...	
124001-186000 WT nodes only.xls	Microsof...	6/19/2003 7:45 AM	1,651,200	76%	397,612	
124001-186000.xls	Microsof...	6/18/2003 8:36 AM	6,361,600	78%	1,410,...	
1-62000 with exact WT picks.xls	Microsof...	6/19/2003 4:53 PM	34,724,...	77%	7,827,...	
1-62000 WT bins with FEHM nodes.xls	Microsof...	6/18/2003 5:40 PM	17,644,...	77%	4,084,...	
1-62000 WT bins.xls	Microsof...	6/18/2003 5:41 PM	14,770,...	80%	3,022,...	
1-62000 WT nodes only.xls	Microsof...	6/19/2003 7:35 AM	1,616,384	76%	393,255	
1-62000.xls	Microsof...	6/17/2003 4:29 PM	6,353,920	77%	1,457,...	
186001-245506 with exact WT picks.xls	Microsof...	6/18/2003 8:44 AM	33,281,...	77%	7,532,...	
186001-245506 WT bins with FEHM nodes.xls	Microsof...	6/18/2003 5:49 PM	16,734,...	77%	3,909,...	
186001-245506 WT bins.xls	Microsof...	6/18/2003 5:47 PM	14,007,...	79%	2,882,...	
186001-245506 WT nodes only.xls	Microsof...	6/19/2003 7:50 AM	1,515,008	76%	361,641	
186001-245506.xls	Microsof...	6/18/2003 8:43 AM	6,128,128	77%	1,406,...	
62001-124000 with exact WT picks.xls	Microsof...	6/18/2003 8:20 AM	34,556,...	78%	7,466,...	
62001-124000 WT bins with FEHM nodes.xls	Microsof...	6/18/2003 5:43 PM	17,648,...	77%	4,036,...	
62001-124000 WT bins.xls	Microsof...	6/18/2003 5:43 PM	14,773,...	80%	2,962,...	
62001-124000 WT nodes only.xls	Microsof...	6/19/2003 7:41 AM	1,285,632	76%	314,610	
62001-124000.xls	Microsof...	6/18/2003 8:20 AM	6,358,528	78%	1,392,...	
Composite WT nodes only.xls	Microsof...	6/19/2003 7:55 AM	6,022,144	76%	1,459,...	
Stragglers.xls	Microsof...	6/17/2003 4:33 PM	3,437,568	78%	772,341	
124001-186000 with exact WT picks.xls	Microsof...	6/18/2003 8:37 AM	27,658,...	78%	5,959,...	
collect_zone	File	6/24/2003 8:08 AM	209,268	77%	48,121	

INTENTIONALLY LEFT BLANK

ATTACHMENT III
DERIVATION OF FRACTURE-MATRIX INTERACTION SUBMODEL AND GENERATION OF TRANSFER FUNCTIONS

INTENTIONALLY LEFT BLANK

ATTACHMENT III

DERIVATION OF FRACTURE-MATRIX INTERACTION SUBMODEL AND GENERATION OF TRANSFER FUNCTIONS

III-1. DERIVATION OF FRACTURE-MATRIX INTERACTION SUBMODEL

The governing equations required for the fracture-matrix interaction submodel is a solute transport system in a domain consisting of parallel flow in a fracture and adjacent matrix, with fracture-matrix solute interaction via molecular diffusion in the rock matrix. This model is therefore an extension of the model of Sudicky and Frind 1982 [105043], which assumed the water in the matrix is stagnant. For simplicity, longitudinal dispersion is not considered in either medium, advection is considered only in the z direction, and diffusion is considered only normal to the flow direction. The rationales for these simplifications are as follows. With regard to longitudinal dispersion, this submodel is intended only to capture the impact of diffusion because dispersion is captured separately in the particle tracking algorithm. Likewise, the advection from fracture to matrix (or the reverse) is implemented in the particle tracking algorithm separately. Therefore, the remaining processes to be included as part of the transfer functions are advection and diffusion in the z-direction only.

We begin with a derivation of the transport equation for the fracture. A variant of this equation with longitudinal dispersion and decay was presented by Sudicky and Frind (1982 [105043], Eq. 1). We rederive the equation from first principles to demonstrate the means by which terms in the dimensionless groups must be altered to include the effects of the Active Fracture Model (AFM). Taking a control volume in the fracture of width b (half of the full aperture), depth d, and length Δz, we write the following terms of the transient solute mass balance (units of each of these terms are solute mass per time):

$$\text{Accumulation: } bd\Delta z\theta_f R_f \frac{(C - C_{prev})}{\Delta t} \qquad \text{(Eq. III-1)}$$

where C_{prev} represents the concentration at the previous time step, θ_f is the volumetric water content in the fracture, and R_f is the fracture retardation factor.

$$\text{Advection: } bd\overline{V}_z(C_{z+\Delta z} - C_z) \qquad \text{(Eq. III-2)}$$

where $\overline{V}_z$ is the Darcy velocity in the fracture, equal to volumetric flow rate divided by the total cross sectional area in the fracture.

$$\text{Diffusion into Matrix: } d\Delta z\theta_m D_m \left.\frac{\partial C_m}{\partial x}\right|_{x=b} \qquad \text{(Eq. III-3)}$$

where D_m is the effective diffusion coefficient in the matrix and θ_m is the matrix volumetric water content. These terms form the overall solute mass balance equation:

$$bd\Delta z\theta_f R_f \frac{(C - C_{prev})}{\Delta t} = -bd\overline{V}_z (C_{z+\Delta z} - C_z) + d\Delta z\theta_m D_m \left.\frac{\partial C_m}{\partial x}\right|_{x=b} \quad \text{(Eq. III-4)}$$

Dividing by $bd\Delta z\theta_f$, making use of the relation for the fracture interstitial pore-water velocity $V_f = \overline{V}_z / \theta_f$, and taking the limit as Δz and Δt go to 0, we obtain:

$$R_f \frac{\partial C_f}{\partial t} = -V_f \frac{\partial C_f}{\partial z} + \left.\frac{\theta_m D_m}{\theta_f b}\frac{\partial C_m}{\partial x}\right|_{x=b} \quad \text{(Eq. III-5)}$$

Note also that we have adopted the subscript "f" on the concentration to denote the fracture.

Given the assumptions listed at the beginning of this derivation, the differential equation governing transport in the matrix is:

$$R_m \frac{\partial C_m}{\partial t} = D_m \frac{\partial^2 C_m}{\partial x^2} - V_m \frac{\partial C_m}{\partial z} \quad \text{(Eq. III-6)}$$

where V_m is the interstitial pore-water velocity in matrix, and D_m is the matrix retardation factor. The initial and boundary conditions for the system are:

$$C_f(z,0) = 0 \quad \text{(Eq. III-7)}$$

$$C_m(x,z,0) = 0 \quad \text{(Eq. III-8)}$$

$$C_f(0,t) = C_{o,f} \quad \text{(Eq. III-9)}$$

$$C_m(x,0,t) = C_{o,m} \quad \text{(Eq. III-10)}$$

$$C_m(b,z,t) = C_f(z,t) \quad \text{(Eq. III-11)}$$

$$\frac{\partial C_m}{\partial x}(B,z,t) = 0 \quad \text{(Eq. III-12)}$$

Here the terms $C_{o,f}$ and $C_{o,m}$ for the fracture and matrix, respectively, are nonzero if mass is being introduced into that medium, and 0 if mass is being introduced in the other medium.

Non-dimensionalization of these equations can be accomplished by introducing the following dimensionless variables:

$$\hat{C}_f = C_f / C_o \quad \text{(Eq. III-13)}$$

$$\hat{C}_m = C_m / C_o \quad \text{(Eq. III-14)}$$

$$\hat{z} = z / L \quad \text{(Eq. III-15)}$$

$$\hat{x} = x / B \quad \text{(Eq. III-16)}$$

$$\hat{t} = \frac{V_f t}{R_f L} = \frac{t}{\tau_f R_f} \quad \text{(Eq. III-17)}$$

where L is the length of the flow path. Eq. III-19 uses the definition of $\tau_f = L / V_f$; a corresponding relation is also used for the matrix fluid travel time ($\tau_m = L / V_m$). Note that because the equations are nondimensionalized with respect to travel times through the fracture and matrix, the physical dimensions of the flow path, including the length, is unimportant to the final implementation in the code. Next, we substitute Eqs. III-15 to III-19 into Eq. III-7 and III-8, which yields

$$\frac{\partial \hat{C}_f}{\partial \hat{t}} = -\frac{\partial \hat{C}_f}{\partial \hat{z}} + \frac{\theta_m D_m \tau_f}{\theta_f b B} \frac{\partial \hat{C}_m}{\partial \hat{x}}\bigg|_{\hat{x}=b/B} \quad \text{(Eq. III-18)}$$

$$\frac{\partial \hat{C}_m}{\partial \hat{t}} = \frac{D_m \tau_f R_f}{B^2 R_m} \frac{\partial^2 \hat{C}_m}{\partial \hat{x}^2} - \frac{\tau_f R_f}{\tau_m R_m} \frac{\partial \hat{C}_m}{\partial \hat{z}} \quad \text{(Eq. III-19)}$$

The boundary and initial conditions (Eqs. III-3 to III-8) are transformed to

$$\hat{C}_f(\hat{z},0) = 0 \quad \text{(Eq. III-20)}$$

$$\hat{C}_m(\hat{x},\hat{z},0) = 0 \quad \text{(Eq. III-21)}$$

$$\hat{C}_f(0,\hat{t}) = 1 \text{ (or 0 if injection is into the matrix)} \quad \text{(Eq. III-22)}$$

$$\hat{C}_m(\hat{x},0,\hat{t}) = 1 \text{ (or 0 if injection is into the fracture)} \quad \text{(Eq. III-23)}$$

$$\hat{C}_m(b/B,\hat{z},\hat{t}) = \hat{C}_f(\hat{z},\hat{t}) \quad \text{(Eq. III-24)}$$

$$\frac{\partial \hat{C}_m}{\partial \hat{x}}(1,\hat{z},\hat{t}) = 0 \quad \text{(Eq. III-25)}$$

The end result is that Eqs. III-20 and III-21 illustrate that a when non-dimensional form of the model equations are produced, the system is fully characterized by three dimensionless parameters (Eq. 6-9 to 6-11 of the main document):

$$p_1 = \frac{D_m \tau_f R_f}{B^2 R_m} \quad \text{(Eq. III-26)}$$

$$p_2 = \frac{D_m \tau_f \theta_m}{bB\theta_f} \quad \text{(Eq. III-27)}$$

$$p_3 = \frac{\tau_f R_f}{\tau_m R_m} \quad \text{(Eq. III-28)}$$

where the retardation factor R_m is related to the sorption coefficient K_d using Eq. 6-2. This derivation shows that a series of transfer function curves generated based on a model with parallel flow in the fractures and matrix can capture the range of behavior of the UZ transport fracture-matrix interaction submodel as long as the curves span the ranges of the parameters in the vector (p_1, p_2, p_3). The documentation for the FEHM V2.21 (LANL 2003 [165741]) contains information on the formatting of the input files to invoke this portion of the particle tracking transport model.

III-2. GENERATION OF TRANSFER FUNCTIONS

This section describes the process for generating the transfer function curves. This is accomplished through a numerical solution of the model domain depicted in Figure 6-5. As described in Section 6.4.3, both a Discrete Fracture Model (DFM) and a dual-k model conceptualization is implemented as part of the abstraction. For the DFM, a 2-D DFM was set up to perform transport simulations using the advection-dispersion module of FEHM V2.21 (LANL 2003 [165741]). The model consists of a regular grid domain consisting of regular spacing of 6 m in the z direction (51 grid points in this direction for a total length of 300 m), and increasing grid spacing into the matrix in the x direction, starting with the first column of nodes of width equal to that of a fracture (22 grid points in this direction). In the model simulations, fracture properties are given to the nodes of the first column, and the remaining nodes are given matrix properties. To ensure that parallel flow occurs in the fracture and matrix in the z direction, a flow permeability barrier is established between the fracture and matrix. Furthermore, for injection into the matrix, water is input and output from the boundary nodes in proportion to the volume of that cell. This model design ensures that flow streamlines remain completely in the z direction. Finally, note that although the transfer functions being used are for unsaturated transport, there is no requirement that this submodel use unsaturated flow to generate them, as long as the water content values are known. Therefore, for simplicity, these simulations were performed for saturated flow conditions, with the fracture and matrix porosities used instead of water contents. For the dual-k model, a simple grid was constructed with identical spacings in the x direction, but only one matrix cell in the y direction. Aside from the different grid, cell numbering, and application of boundary conditions, the process for generating the breakthrough curves and transfer functions is the same for the dual-k model. Furthermore, the use of these curves in an FEHM particle tracking simulation is completely transparent, requiring only a choice of which transfer function file to use.

In the simulations to generate the transfer functions, parameter p_3 is varied systematically from fracture-dominated to matrix-dominated flow by varying the relative water flux values in the fractures and matrix. Ranges of other parameter values consistent with the span of those parameters required for the UZ transport model are also selected. Table III-1 lists the variations

of each parameter that were used in the formulation of the transfer function curves. Note that for the sorption coefficient K_d, the fact that the range of values only goes to 100 does not imply that the model is incapable of accurately simulating transport behavior for higher values of K_d. In Section III-4 below, a procedure for normalizing the transfer function curves is described whereby higher values of K_d are properly handled. This procedure allows the code to cover arbitrarily large values of K_d without the need to include transfer function curves that extend to such large values.

A four-dimensional matrix of parameters were established with the parameter values listed in the table, and the transfer function curves for each were computed, for a total of 11x12x3x10=3960 values of the parameter vector (p_1, p_2, p_3).

Table III-1. List of parameter values used to compute transfer function curves

Parameter	# of values	List of values
$F_f = f_f/(f_f + f_m)$	11	0.01, 0.1, 0.2, 0.3, 0.4, 0.5, 0.6, 0.7, 0.8, 0.9, 0.99
D_m	12	1.e-8, 3.e-9, 1.e-9, 3.e-10, 1.e-10, 3.e-11, 1.e-11, 3.e-12, 1.e-12, 3.e-13, 1.e-13, 1.e-20
θ_f	3	0.01, 0.1, 0.5
K_d	10	0., 0.3, 0.5, 1., 3., 5., 10., 30., 50., 100.
Total: 11x12x3x10	3960	(p_1, p_2, p_3) in excel spreadsheet *parameter runs.xls*

Note: K_d range of 0-100 does not mean that the model is limited to K_d values of 100 or less. See Section III-4 for details on the normalization procedure for handling higher values of K_d.

Two runs of the model are performed for each parameter set: one where solute mass is injected in the fracture, and another where mass is injected in the matrix. The list of parameter values (p_1, p_2, p_3) are given in the Excel spreadsheet *parameter runs 3960.xls*, along with the underlying fehm input parameters for each simulation. The code fehm2post V1.0 (LANL 2003 [165754]) was used to execute the multiple realizations and to post-process the results to obtain the transfer functions. The post-processing itself (executed by fehm2post) was performed using the software discrete_tf V1.1 (LANL 2003 [165742]). The resulting output from these runs is then concatenated by hand and the appropriate header information inserted by hand to conform to the input required by FEHM. The file called *uz_tfcurves_nn_3960.in* is the transfer function file for the DFM formulation, whereas the corresponding file for the dual-k formulation is *uz_tfcurves_dualk_nn_3960.in*. These files, along with the excel spreadsheet mentioned above, and the control files required for execution of these runs is available as DTN: LA0311BR831229.001.

III-3. DISCUSSION OF FRACTURE-MATRIX SUBMODEL BEHAVIOR

In this section we explore the behavior of the fracture-matrix submodel for the two alternate formulations, DFM and dual-k. In contrast to the discrete fracture based transfer function model, the dual-k formulation has a single matrix block for each fracture block. All other aspects of the

parameterization are kept the same. Figures III-1 and III-2 compare the DFM and dual-k transport models for a flow situation consisting of 60% fracture flow, 40% matrix flow, over a range of diffusion coefficients given in Table III-2. Breakthrough curves from the fracture are presented for solute injection into the fracture at the inlet. Also shown are vertical, dotted red lines representing the limiting behavior expected for fracture transport and no diffusion (dimensionless time of 1) and composite medium behavior for the case of infinitely large diffusion. Composite medium behavior is attained when the time for diffusion across the model domain B is of that same order or smaller than transport time along the flow path. Under these conditions, the travel time through the system reduces to

$$\tau_{comp} = \frac{R_f m_f + R_m m_m}{f_f + f_m} \tag{III-29}$$

where m_f and m_m are the fluid masses in a cell for the fracture and matrix, respectively, and f_f and f_m are the fluid mass fluxes for the fracture and matrix, respectively. Intuitively, Eq. III-29 is derived by picturing a solute molecule traveling with fluid of total flux given by the denominator, with total storage volume (including sorption sites) given by the numerator. The time τ_{comp} is an important characteristic time for this system, and serves as a reference for understanding the behavior and deriving the detailed method for using transfer function, described in the next section.

Table III-2. Diffusion coefficients used in simulations

Curve Label	Diffusion Coefficient (m^2/s)
a	1.e-8
b	1.e-10
c	1.e-11
d	1.e-12
e	1.e-13
f	1.e-20

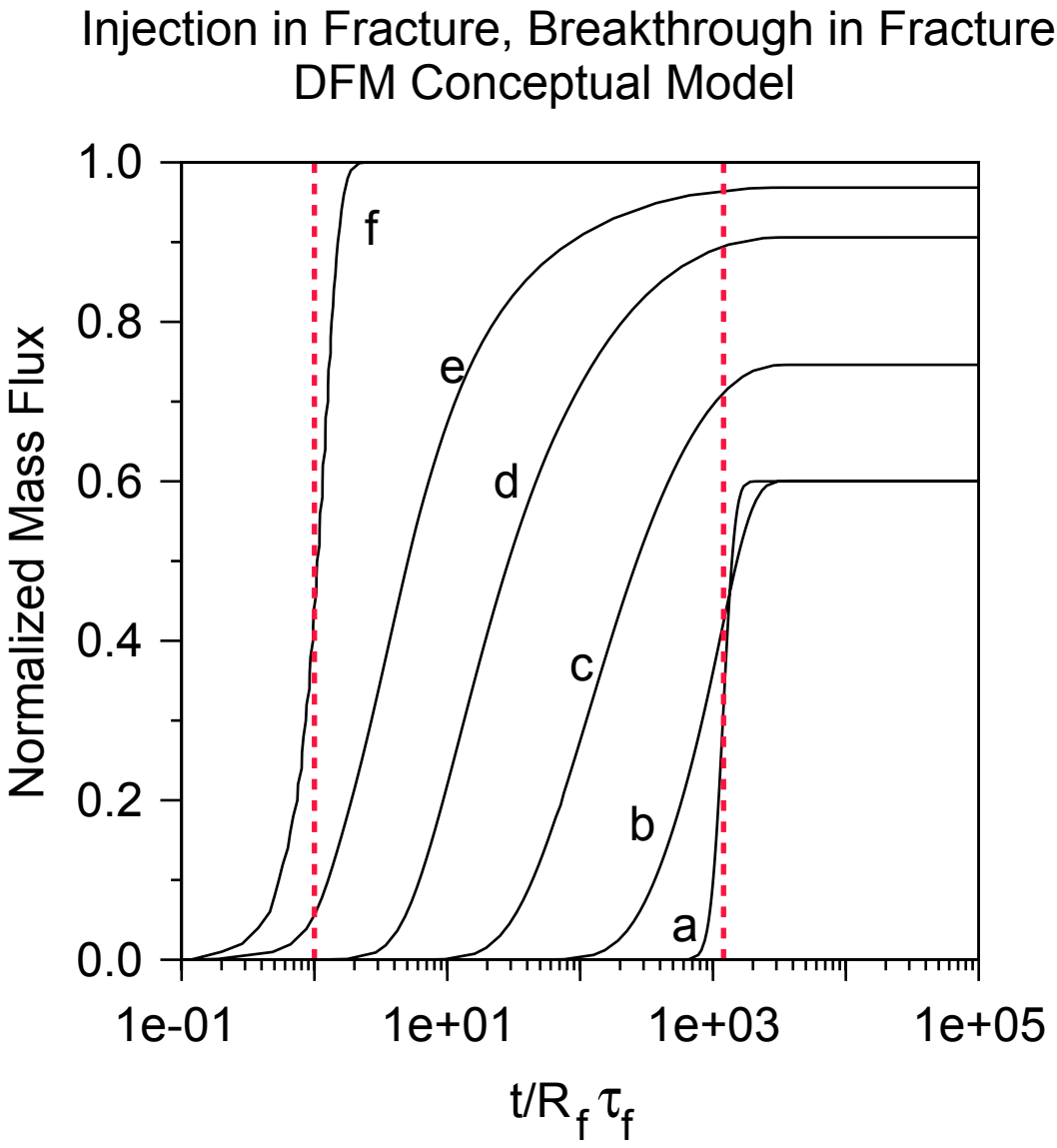

Output DTN: LA0311BR831229.001

Figure III-1. Transfer Function Computed for the Discrete Fracture Model Formulation: Solute Injection in Fracture, Breakthrough in Fracture, Diffusion Coefficients Given in Table III-2

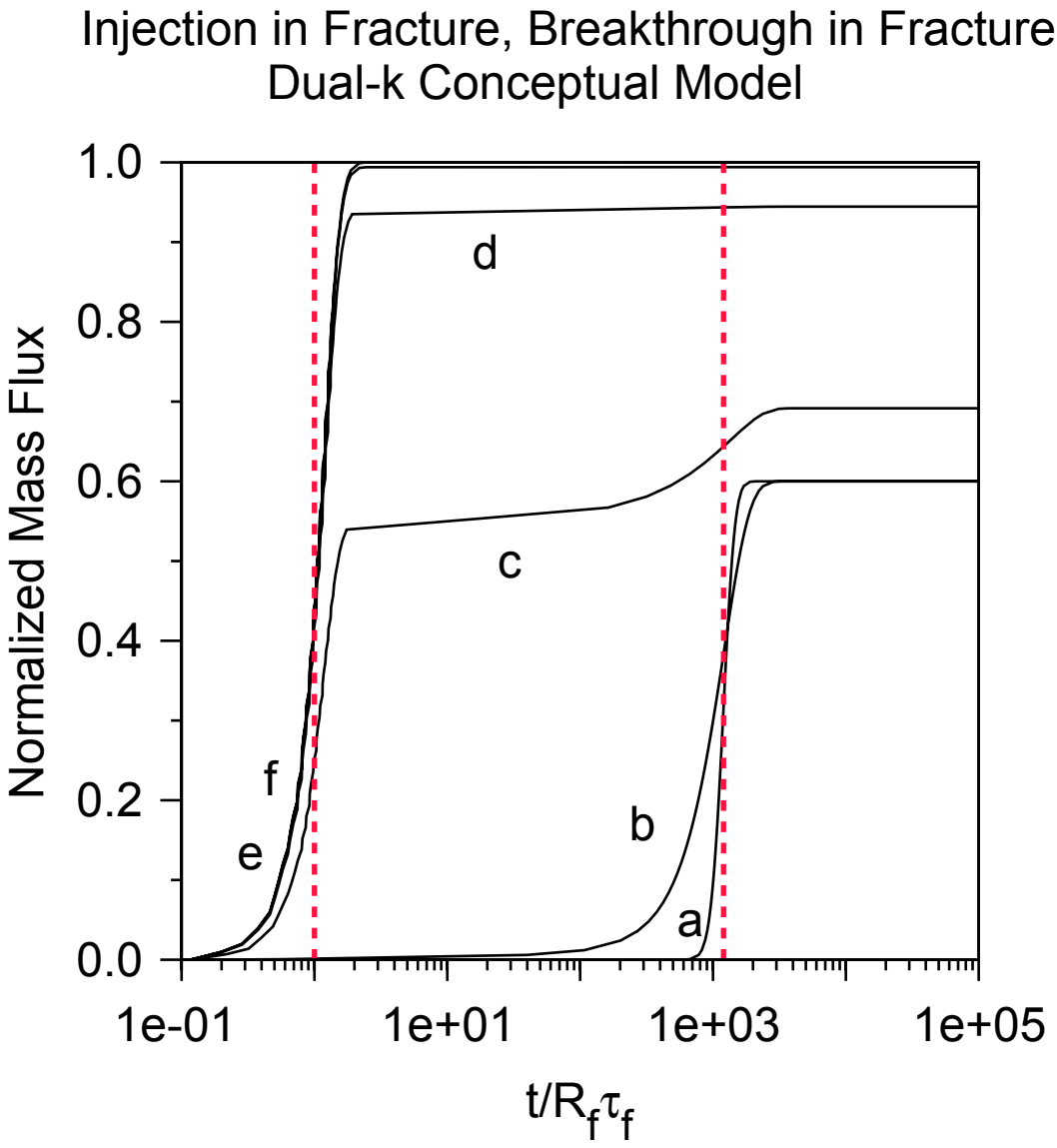

Output DTN: LA0311BR831229.001

Figure III-2. Transfer Function Computed for the Dual-k Model Formulation: Solute Injection in Fracture, Breakthrough in Fracture, Diffusion Coefficients Given in Table III-2

For each model, the behavior at the extremes of low and high diffusion are similar. For negligible diffusion, travel times approach a dimensionless time of 1, and the normalized mass flux attains a plateau at 1, which is to say that all mass injected in the fracture leaves via the fracture. By contrast, at high diffusion, travel times approach τ_{comp}, and the plateau of normalized mass flux approaches a value of F_f (0.6 in this example), meaning that at this extreme, the probability of mass in the fracture leaving via the fracture equals the fraction of the total flow traveling through the fracture. It is at the intermediate values of diffusion coefficient that the two models diverge. Specifically, the dual-k formulation tends to predict early breakthrough due to rapid transport through the fracture for a significant portion of the mass, compared to the DFM formulation, for which smooth breakthrough curves at progressively

longer travel times are predicted for increasing diffusion coefficients. This means that the dual-k formulation ought to predict earlier breakthrough for the first-arriving mass if the parameter ranges of our model are in this intermediate range. Conversely, the models should be similar behavior for high diffusion or low diffusion.

III-4. ADDITIONAL IMPLEMENTATION CONSIDERATIONS

In this section we address some additional details concerning the implementation of the transfer function methodology. These considerations concern the nondimensionalization of the transfer function curves, and the method by which the model handles cases in which some parameters are selected that fall at or outside the range of values assumed when generating the transfer function curves.

In Figures III-1 and III-2, we demonstrated that, in addition to the fracture travel time $R_f\tau_f$ used to nondimensionalize time in the transfer function curves, the composite travel time τ_{comp} is a natural parameter for bracketing the behavior of the f/m interaction submodel. Time in the transfer functions supplied to FEHM is $t/R_f\tau_f$, which contains no information relevant to the extreme of long travel times, which approach τ_{comp}. To make the method more robust, we have found that an improved nondimensionalization for time can be made as follows:

$$\bar{t} = \frac{t - R_f\tau_f}{\tau_{comp} - R_f\tau_f} \qquad \text{(Eq. III-30)}$$

Assuming, as is the case for the UZ transport model, that $\tau_{comp} >> R_f\tau_f$, Eq. III-26 normalizes the breakthrough times to values in the approximate range of 0 and 1 in Figures III-1 and III-2. Because FEHM reads in time values of $t/R_f\tau_f$, we need a means for converting these to dimensionless times given by Eq. III-30. This is done by first dividing the top and bottom of Eq. III-30 by $R_f\tau_f$:

$$\bar{t} = \frac{t/R_f\tau_f - 1}{\tau_{comp}/R_f\tau_f - 1} \qquad \text{(Eq.III-31)}$$

The FEHM input time $t/R_f\tau_f$ minus 1 is the numerator, so we simply need to determine a relation involving the dimensionless parameters (p_1, p_2, p_3) that can be used to express the denominator. For this we first recognize the following relation (obtained from simple algebra from Eqs. III-26 to III-28:

$$\frac{p_2 p_3}{p_1} = \left(\frac{\tau_f}{b\theta_f}\right)\left(\frac{\theta_m B}{\tau_m}\right) \qquad \text{(Eq. III-32)}$$

Alternatively, recognizing that $b\theta_f$ and $\theta_m B$ are proportional to the fluid mass in the fracture and matrix, respectively, then this expression reduces to:

$$\frac{p_2 p_3}{p_1} = \frac{f_m}{f_f} \qquad \text{(Eq. III-33)}$$

An equivalent expression using the definition $F_f = f_f /(f_f + f_m)$ is

$$F_f = \frac{p_1}{p_1 + p_2 p_3} \qquad \text{(Eq. III-34)}$$

Returning to the definition of τ_{comp} (Eq. III-29), we perform the following algebraic manipulations:

$$\tau_{comp} = \frac{R_f m_f + R_m m_m}{f_f + f_m} = F_f (R_f \tau_f + R_m \tau_m \frac{f_m}{f_f}) = F_f R_f \tau_f (1 + \frac{R_m \tau_m}{R_f \tau_f} \frac{p_2 p_3}{p_1}) = F_f R_f \tau_f (1 + \frac{p_2}{p_1})$$

(Eq. III-35)

As a guide to this series of steps, we use Eqs. III-30, III-33, and III-28, along with the definitions $F_f = f_f /(f_f + f_m)$, $\tau_f = m_f / f_f$, and $\tau_m = m_m / f_m$. Finally, the denominator $\tau_{comp} / R_f \tau_f - 1$ in Eq. III-33 is obtained through further algebra and the use of Eq. III-34:

$$\tau_{comp} / R_f \tau_f - 1 = \frac{p_2 (1 - p_3)}{p_1 + p_2 p_3} \qquad \text{(Eq. III-36)}$$

The important point here is that the transformation of Eq. III-31 can be made by subtracting 1 from the input dimensionless time and dividing by the expression in Eq. III-36. This operation is performed by FEHM upon reading in the transfer function curves. Then, after the normalized time for a particle $\bar{t}$ is obtained in the particle tracking algorithm, Eq. III-30 is used to back out the dimensional value of time of the particle. By using this approach, we are taking advantage of the self-similarity of the family of curves such as those in Figures III-1 or III-2. That is, even if the parameters (p_1, p_2, p_3) at a given location in the model are not exactly those used to generate the transfer function, the use of the times $R_f \tau_f$ and τ_{comp} from the model at a given grid cell provide a means for scaling the transfer function accordingly. Also, because we generate a relatively large number of transfer function curves (3960), it is likely that in most instances a curve fairly close to the parameters used in the transfer function will be found.

Despite the effectiveness of this method, we have found that there are a few cases for which special consideration needed to be made. This is because of the extraordinarily wide range of parameter values required to be covered in the TSPA model. As a result, the way in which the model handles some of the extreme values of certain parameters is through the use of special rules designed to achieve accuracy. These methods, described below, all call for the adjustment

of one or more of the parameters (p_1, p_2, p_3) at a given location in the model so as to yield the desired behavior. Details are given below.

Low Diffusion Coefficient: It is often desirable to lower the diffusion coefficient to extremely low values to examine this end-member case. Furthermore, colloids are low-diffusion species that require accuracy at low values of D_m. The most fool-proof way to do this is to not use the transfer function model all, but instead to simply route the particles through the model with advection and dispersion only. However, if this option is not chosen, we still require that the model perform properly at the low end of diffusion. The diffusion coefficient only affects parameters p_1 and p_2, so in the search algorithm we need to account for the fact that below a minimum value of D_m (10^{-18} m^2/s in the code), the precise values of these parameters are not important. To ensure that the search algorithm locates a curve with the correct value of p_3, p_1 and p_2, are assigned values that were actually used in the generation of the low- diffusion transfer function curves (see Table III-1), so that during the search, p_1 and p_2, are de-emphasized and p_3 is in essence the only parameter considered. In doing so, we are ensuring that the code finds the portion of the parameter space with the correct values for p_3. If this is not done, the least squares method for selecting the correct transfer function curve can sometimes compensate for the extreme parameters chosen by selecting an undesirable part of the parameter space. With the approach just described, the method is forced to select a low-diffusion regime while obtaining the correct ratio of travel times in the fracture and matrix.

High Matrix Sorption: Similar to the case just described, an extremely large value of R_m beyond the range used in the transfer functions causes problems for the search algorithm. When searching for the closest transfer function, the uncorrected method compensates for a large R_m by selecting a fracture-dominated flow case to attain as low a value of p_3 as possible. Similarly, the calculation of p_1 is also affected. Thus, to correct for this case, the maximum value of R_m used in the transfer function curve generation (1000) is used as an upper limit when searching for the correct transfer function curve. However, note that this does *not* mean that the matrix retardation is limited to that value in the particle tracking travel time calculation. Recall that the transfer function curves themselves are normalized using Eq. III-30, which includes τ_{comp}. In contrast to the determination of the closest transfer function curve, the actual value of R_m is used in computing τ_{comp}, which results in a determination of travel time that is scaled by the actual sorption set in the matrix. Thus the correction is applied only to find an appropriate transfer function curve, and the method for nondimensionalizing those curves ensures that an appropriately large travel time is reproduced for the case of high matrix sorption.

Fracture-Dominated Flow: The parameterization of the transfer function curves is based on a model that has some flow both the fracture and matrix. When the flow is fracture dominated ($F_f > 0.99$), the details of the actual fraction of flow should be unimportant, since advective transport in the matrix should be negligible. However, without correction for cases where $F_f > 0.99$, the algorithm for finding the transfer function will inappropriately attempt to select

curves with high R_m to compensate for the fact that transfer functions with extremely large F_f are not included. To correct for this problem, the code makes use of the following rearranged form of Eq. III-30:

$$p_3 = \frac{p_1}{p_2}\frac{(1-F_f)}{F_f} \qquad \text{(Eq. III-37)}$$

When $F_f > 0.99$, the code uses 0.99 and the values of p_1 and p_2 to compute p_3 for the purposes of selecting the transfer function curve. This assures that a fracture-dominated transfer function is chosen with appropriate values for the other diffusion and sorption parameters.

Matrix-Dominated Flow: For this extreme, it is desirable to bypass the transfer function method altogether, since the travel time is trivially found to be $R_m\tau_m$. Allowing the transfer function algorithm to be used for this case causes problems because the normalization procedure implicitly assumes that the matrix travel time is longer than the fracture travel time. To cover the special case of essentially no flow in the fracture, the travel time is assigned a value of τ_{comp}, which reduces to $R_m\tau_m$ under these conditions.

III-5. ADAPTING THE ACTIVE FRACTURE MODEL FOR TRANSPORT

The AFM of Liu et al. (1998 [105729]) is formulated on the basis that only a fraction of the fractures flow. This requires that adjustments be applied to the interface area and the mean spacing between flowing fractures. These adjusted parameters can then be used in the transport model calculations. Examining the individual terms of the mass balance for the fracture derived in Section III-1, the accumulation term (Eq. III-1) is unchanged by the AFM, because it is based on the storage volume in the fracture, as well as sorption parameters. Storage volumes in the dual-k flow fields are fully defined by the fracture volume fractions and the fluid saturations in the fracture continuum. Fluid saturations are model output from the flow simulations, and no further correction for transport is required for the accumulation term. Likewise, the Darcy velocity in the advection term (Eq. III-2) is fully defined by the flux through the fracture continuum, so no AFM corrections are required for advection either. The diffusion term (Eq. III-3) consists of a flux $\theta_m D_m \left.\frac{\partial C_m}{\partial x}\right|_{x=b}$ times an interfacial area, which on geometrical grounds for the simple geometry of our transfer function model is $d\Delta z$. This interfacial area term, according to the AFM, should be reduced to account for the fact that not all fractures are flowing. Liu et al. (1998 [105729], Eq. 12), gives the following reduction factor for correcting the advective flux term (note: nomenclature from Liu et al. 1998 [105729] is used in this equation):

$$R = \left(\frac{A_{fm,a}}{A_{fm}}\right)\left(\frac{n_{f,a}}{n_f}\right)\left(\frac{d}{d_a}\right) \qquad \text{(Eq. III-38)}$$

Although Liu et al. (1998 [105729]) refers to R as the F-M interface area reduction factor, it is clear from their derivation that the term represents the ratio of the fluxes for the uncorrected and

corrected cases, correcting for both the interface area and the transport length scale associated with the distance between the flowing fractures (the third term on the right hand side of this equation). Therefore, in the FEHM simulations, AFM-based adjustments should be applied to both the interface area and the spacing B. The term d/d_a is the adjustment to the fracture spacing, and is accounted for by adjusting the spacing B in the FEHM transport simulations using the following relation (Liu et al. 1998 [105729], Eq. 17):

$$\frac{d}{d_a} = S_e^{\gamma} \qquad \text{(Eq. III-39)}$$

Thus, the geometric spacing is divided by S_e^{γ} to obtain the spacing between flowing fractures. The interface-area portion of the adjustment consists of the first two terms on the right hand side of Eq. III-38, the first to account for the reduction in wetted area within an individual fracture, and the second to account for the reduction in area associated with a smaller number of wetted fractures. This term can be related to the AFM parameters using Eqs. 13 and 14 of Liu et al. 1998 [105729]:

$$\left(\frac{A_{fm,a}}{A_{fm}}\right)\left(\frac{n_{f,a}}{n_f}\right) = S_e^{1-\gamma} S_e^{\gamma} = S_e \qquad \text{(Eq. III-40)}$$

To implement this area reduction term in FEHM, we divide the geometrically defined aperture b by S_e. The adjustment to b is for convenience, and actually arises from the need to adjust the interface area in the fracture transport equation. These adjustment factors have been incorporated into FEHM so that for given AFM model parameters, B and b, input as geometrically defined parameters, are converted to hydrologic parameters for use in the transfer function methodology.

INTENTIONALLY LEFT BLANK